

Spin Anisotropy Effects in Dimer Single Molecule Magnets

Dmitri V. Efremov^{1,*} and Richard A. Klemm^{2,†}

¹*Institut für Theoretische Physik, Technische Universität Dresden, 01062 Dresden, Germany*

²*Department of Physics, Kansas State University, Manhattan, KS 66506 USA*

(Dated: September 14, 2018)

We present a model of equal spin s_1 dimer single molecule magnets. The spins within each dimer interact via the Heisenberg and the most general set of four quadratic anisotropic spin interactions with respective strengths J and $\{J_j\}$, and with the magnetic induction \mathbf{B} . We solve the model exactly for $s_1 = 1/2, 1$, and $5/2$, and for antiferromagnetic Heisenberg couplings ($J < 0$), present $\mathbf{M}(\mathbf{B})$ curves at low T for these cases. Low- T $C_V(\mathbf{B})$ curves for $s_1 = 1/2$ and electron paramagnetic susceptibility $\chi(\mathbf{B}, \omega)$ for $s_1 = 1$ are also provided. For weakly anisotropic dimers, the Hartree approximation yields rather simple analytic formulas for $\mathbf{M}(\mathbf{B})$ and $C_V(\mathbf{B})$ at arbitrary s_1 that accurately fit the exact solutions at sufficiently low T or large B . Low- T , large- B formulas for the inelastic neutron scattering cross-section $S(\mathbf{B}, \mathbf{q}, \omega)$ and $\chi(\mathbf{B}, \omega)$ with arbitrary s_1 and \mathbf{B} in an extended Hartree approximation are also given. We show that the various anisotropy interactions give rise to new, detectable electron paramagnetic resonances and to new peaks in $S(\mathbf{q}, \omega)$, which can provide precise determinations of the particular set of microscopic anisotropy interaction strengths. For antiferromagnetic Heisenberg couplings ($J < 0$) and weak anisotropy interactions ($|J_j/J| \ll 1$), we provide analytic formulas for the $2s_1$ level-crossing magnetic inductions $B_{s,s_1}^{lc}(\theta, \phi)$, at which the low- T magnetization $\mathbf{M}(\mathbf{B})$ exhibits steps and the low- T specific heat $C_V(\mathbf{B})$ exhibits zeroes, surrounded by double peaks of uniform height. Strong anisotropy interactions drastically alter these behaviors, however. Our results are discussed with regard to existing experiments on $s_1 = 5/2$ Fe₂ dimers, suggesting the presence of single-ion anisotropy in one of them, but apparently without any sizeable global spin anisotropy. Further experiments on single crystals of these and some $s_1 = 9/2$ [Mn₄]₂ dimers are therefore warranted, and we particularly urge electron paramagnetic resonance and inelastic neutron scattering experiments to be performed.

PACS numbers: 05.20.-y, 75.10.Hk, 75.75.+a, 05.45.-a

I. INTRODUCTION

Single molecule magnets (SMM's) have been under intense study recently, due to their potential uses in magnetic storage and quantum computing.[1, 2, 3] The materials consist of insulating crystalline arrays of identical SMM's 1-3 nm in size, each containing two or more magnetic ions. Since the magnetic ions in each SMM are surrounded by non-magnetic ligands, the intermolecular magnetic interactions are usually negligible. Although the most commonly studied SMM's are the high-spin Mn₁₂ and Fe₈,[1, 2, 3, 4, 5] such SMM's contain a variety of ferromagnetic (FM) and antiferromagnetic (AFM) intramolecular interactions, rendering unique fits to a variety of experiments difficult.[6]

In addition, there have been many studies of AFM Fe_n ring compounds, where $n = 6, 8, 10, 12$, etc.[7, 8, 9, 10] In these studies, analyses of inelastic neutron diffraction data and the magnetic induction \mathbf{B} dependence of the low-temperature T specific heat C_V and magnetization \mathbf{M} steps were made, using the isotropic Heisenberg near-neighbor exchange interaction, the Zeeman interaction, and various near-neighbor spin anisotropy interactions.[7, 8, 9, 10] However, the rings were so complicated that analyses of the data using those simple models were inaccessible to present day computers.[8, 9] Thus, those authors used either simulations or phe-

nomenological fits to a first-order perturbation expansion with different spin anisotropy values for each global ring spin value.[8, 9, 10]

Here we focus on the simpler cases of equal spin $s_1 = s_2$ magnetic dimers, for which the full spin anisotropy effects can be evaluated analytically, investigated in detail numerically, and compared with experiment. AFM dimers with $s_1 = 1/2, 3/2$, [11, 12, 13, 14] and various forms of Fe₂ with $s_1 = 5/2$ were studied recently.[15, 16, 17, 18, 19, 20] Several Fe₂ dimers and effective $s_1 = 9/2$ dimers of the type [Mn₄]₂, [21, 22] have magnetic interactions weak enough that their effects can be probed at $T \approx 1$ K with presently available \mathbf{B} . A comparison of our results with $\mathbf{M}(\mathbf{B})$ step data on a Fe₂ dimer strongly suggests a substantial presence of local spin anisotropy.[17]

The paper is organized as follows. In Section II, we present the model in the crystal representation and give exact formulas for the matrix elements. The general thermodynamics are presented in Section III, along with the universal behavior of the $M(B)$ and $C_V(B)$ behavior associated with the energy level crossing. In Section IV, we solve the model exactly for $s_1 = 1/2$, giving analytic expressions for \mathbf{M} and the specific heat C_V . In Section V, we discuss the exact solution for $s_1 = 1$, present the equations from which the eigenvalues are readily obtained, and give examples of the low- T $\mathbf{M}(\mathbf{B})$ curves. In Section VI, we present examples of the low- T $s_1 = 5/2$ $\mathbf{M}(\mathbf{B})$ curves. In Section VII, we present our induction

representation results for the eigenstates to first order in the anisotropy energies. These are used to obtain the asymptotic Hartree expressions for the thermodynamic quantities \mathbf{M} and C_V , and for the inelastic neutron scattering cross-section $S(\mathbf{B}, \mathbf{q}, \omega)$ and the electron paramagnetic resonance susceptibility $\chi(\mathbf{B}, \omega)$ for arbitrary s_1 , that are accurate at sufficiently low T and/or large B . In addition, an analytic formula accurate to second order in the four independent anisotropy exchange energies is provided for $B_{s,s_1}^{\text{lc}}(\theta, \phi)$, the \mathbf{B} values at which the s th energy level crossing occurs. In Section VIII, we consider FM anisotropic interactions sufficiently strong as to remove the level crossing effects. Finally, in Section IX, we summarize our results and discuss them with regard to experiments on Fe_2 dimers.

II. THE MODEL IN THE CRYSTAL REPRESENTATION

We represent the $s_1 = s_2$ dimer quantum states, $|\psi_s^m\rangle$ in terms of the global (total) spin and magnetic quantum numbers s and m , where $\mathbf{S} = \mathbf{S}_1 + \mathbf{S}_2$ and $S_z = \mathbf{S} \cdot \hat{\mathbf{z}}$ satisfy $\mathbf{S}^2|\psi_s^m\rangle = s(s+1)|\psi_s^m\rangle$ and $S_z|\psi_s^m\rangle = m|\psi_s^m\rangle$, where $s = 0, 1, \dots, 2s_1$, $m = -s, \dots, s$, and we set $\hbar = 1$. We also have $S_\pm|\psi_s^m\rangle = A_s^{\pm m}|\psi_s^{m\pm 1}\rangle$, where $S_\pm = S_x \pm iS_y$ and

$$A_s^m = \sqrt{(s-m)(s+m+1)}. \quad (1)$$

For an arbitrary \mathbf{B} , we assume the Hamiltonian has the form $\mathcal{H} = \mathcal{H}_0 + \mathcal{H}_a + \mathcal{H}_b + \mathcal{H}_d + \mathcal{H}_e$, where

$$\mathcal{H}_0 = -J\mathbf{S}^2/2 - \gamma\mathbf{S} \cdot \mathbf{B} \quad (2)$$

contains the Heisenberg exchange and Zeeman interactions, the gyromagnetic ratio $\gamma = g\mu_B$, $g \approx 2$ and μ_B is the Bohr magneton. The global axial and azimuthal anisotropy terms

$$\mathcal{H}_b = -J_b S_z^2 \quad (3)$$

and

$$\mathcal{H}_d = -J_d(S_x^2 - S_y^2), \quad (4)$$

respectively, only involve components of \mathbf{S} , but have been the main anisotropy terms discussed in the SMM literature,[5, 21] so we have included them for comparison. Such terms have been commonly studied as an effective Hamiltonian for a singlet orbital ground state, in which the tensor global spin interaction with a fixed spin quantum number s has the form $\mathbf{S} \cdot \overleftrightarrow{\mathbf{A}} \cdot \mathbf{S}$, resulting in the principal axes x, y and z . [23] For a dimer, we take $\overleftrightarrow{\mathbf{A}}$ to be diagonal in the orientation pictured in Fig. 1. Then $J = -(\Lambda_{xx} + \Lambda_{yy})/2$, $J_b = -\Lambda_{zz} + (\Lambda_{xx} + \Lambda_{yy})/2$, and $J_d = (\Lambda_{yy} - \Lambda_{xx})/2$. Taking $|J_d/J| \ll 1$ and $|J_b/J| \ll 1$

still leaves J_d/J_b unrestricted. The single-ion axial and azimuthal anisotropy terms,

$$\mathcal{H}_a = -J_a \sum_{i=1}^2 S_{iz}^2 \quad (5)$$

and

$$\mathcal{H}_e = -J_e \sum_{i=1}^2 (S_{ix}^2 - S_{iy}^2), \quad (6)$$

respectively, arise from spin-orbit interactions of the local crystal field with the individual spins. These terms have usually been neglected in the SMM literature, but have been studied with regard to complexes containing a single magnetic ion, such as Ni^{+2} , [23] and with regard to clusters of larger numbers of identical magnetic ions. [23, 24]

The local axially and azimuthally anisotropic exchange interactions

$$\mathcal{H}_f = -J_f S_{1z} S_{2z}, \quad (7)$$

$$\mathcal{H}_c = -J_c (S_{1x} S_{2x} - S_{1y} S_{2y}), \quad (8)$$

satisfy

$$2\mathcal{H}_f/J_f = \mathcal{H}_b/J_b - \mathcal{H}_a/J_a, \quad (9)$$

$$2\mathcal{H}_c/J_c = \mathcal{H}_d/J_d - \mathcal{H}_e/J_e, \quad (10)$$

so we need only include either either \mathcal{H}_a or \mathcal{H}_f and \mathcal{H}_e or \mathcal{H}_c , respectively. [23] That is, if we stick to the Hamiltonian \mathcal{H} , we may incorporate the effects of \mathcal{H}_f and \mathcal{H}_c by letting $J_b \rightarrow J_b + J_f/2$, $J_a \rightarrow J_a - J_f/2$, and $J_d \rightarrow J_d + J_c/2$, $J_e \rightarrow J_e - J_c/2$, respectively. Since \mathcal{H}_a and \mathcal{H}_e describe the axial and azimuthal anisotropy each single ion attains from its surrounding environment, they are the physically relevant local anisotropy interactions. We note that \mathcal{H}_b and \mathcal{H}_a are symmetric under $\hat{\mathbf{x}} \leftrightarrow \hat{\mathbf{y}}$, whereas \mathcal{H}_d and \mathcal{H}_e are antisymmetric under $\hat{\mathbf{x}} \leftrightarrow \hat{\mathbf{y}}$, independent of s_1 .

For the case of Fe_2 , [15] a constituent of the high-spin SMM Fe_8 and the AFM Fe_n rings, [4, 8, 9] the exchange between the Fe^{+3} $s_1 = 5/2$ spins occurs via two oxygen ions, and these four ions essentially lie in the same (xz) plane. [15, 18] We set the z axis parallel to the dimer axis, as pictured in Fig. 1. Since the quantization axis is along the dimer axis, which is fixed in a crystal, we denote this representation as the crystal representation.

We generally expect each of the J_j for $j = a, b, d, e$ to satisfy $|J_j/J| \ll 1$, but there are not generally any other restrictions upon the various magnitudes of the J_j . Since all dimers known to date have predominantly AFM couplings ($J < 0$), and also because their magnetizations and specific heats are particularly interesting, we shall only consider AFM dimers. In addition, since no studies on unequal-spin dimers have been reported to our knowledge, we shall only treat the equal-spin $s_1 = s_2$ case. We note that for equal spin dimers, the group symmetry

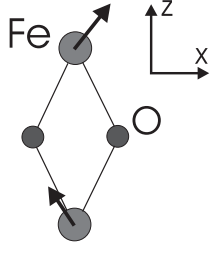


FIG. 1: Sketch of an Fe_2 dimer, with two bridging O^{-2} ions (O). Ligands (not pictured) are attached to the Fe^{+3} ions (Fe). The arrows signify spins.

of the dimer environment is C_{2v} , so that Dzaloshinskiĭ-Moriya interactions do not arise.[23] Hence, our Hamiltonian \mathcal{H} is the most general quadratic anisotropic spin Hamiltonian of an equal-spin dimer.

For $\mathbf{B} = B(\sin \theta \cos \phi, \sin \theta \sin \phi, \cos \theta)$, we have

$$\mathcal{H}_0|\psi_s^m\rangle = E_s^m|\psi_s^m\rangle + \delta E \sum_{\sigma=\pm 1} e^{-i\sigma\phi} A_s^{\sigma m} |\psi_s^{m+\sigma}\rangle, \quad (11)$$

$$\mathcal{H}_b|\psi_s^m\rangle = -J_b m^2 |\psi_s^m\rangle, \quad (12)$$

and

$$\mathcal{H}_d|\psi_s^m\rangle = \frac{-J_d}{2} \sum_{\sigma=\pm 1} F_s^{\sigma m} |\psi_s^{m+2\sigma}\rangle, \quad (13)$$

where

$$E_s^m = -J_s(s+1)/2 - mb \cos \theta, \quad (14)$$

$$\delta E = -\frac{1}{2}b \sin \theta, \quad (15)$$

$$b = \gamma B. \quad (16)$$

and

$$F_s^{\sigma m} = A_s^{\sigma m} A_s^{1+\sigma m}. \quad (17)$$

\mathcal{H}_a and \mathcal{H}_c contain the individual spin operators S_{iz} and $S_{i\pm}$ for $i = 1, 2$. After some Clebsch-Gordan algebra involving the Wigner-Eckart theorem, for arbitrary (s_1, s, m) ,

$$S_{i\pm}|\psi_s^m\rangle = \frac{1}{2}A_s^{\pm m}|\psi_s^{m\pm 1}\rangle \mp \frac{1}{2}(-1)^i \left(C_{s,s_1}^{\pm m} |\psi_{s-1}^{m\pm 1}\rangle - C_{s+1,s_1}^{-1\mp m} |\psi_{s+1}^{m\pm 1}\rangle \right), \quad (18)$$

$$S_{iz}|\psi_s^m\rangle = \frac{m}{2}|\psi_s^m\rangle - \frac{1}{2}(-1)^i \left(D_{s,s_1}^m |\psi_{s-1}^m\rangle + D_{s+1,s_1}^m |\psi_{s+1}^m\rangle \right), \quad (19)$$

where

$$C_{s,s_1}^m = \eta_{s,s_1} \sqrt{(s-m)(s-m-1)}, \quad (20)$$

$$D_{s,s_1}^m = \eta_{s,s_1} \sqrt{(s^2-m^2)}, \quad (21)$$

and

$$\eta_{s,s_1} = \sqrt{[(2s_1+1)^2 - s^2]/(4s^2 - 1)}. \quad (22)$$

The generalizations of these results to dimers with general s_1, s_2 are given in Appendix A.

For $s = 0$, we require $m = 0$, for which $C_{0,s_1}^0 = D_{0,s_1}^0 = 0$. We then find

$$\mathcal{H}_a|\psi_s^m\rangle = \frac{-J_a}{2} \left(G_{s,s_1}^m |\psi_s^m\rangle + \sum_{\sigma'=\pm 1} H_{s,s_1}^{m,\sigma'} |\psi_{s+2\sigma'}^m\rangle \right), \quad (23)$$

$$\mathcal{H}_e|\psi_s^m\rangle = -\frac{J_e}{4} \sum_{\sigma=\pm 1} \left(L_{s,s_1}^{\sigma m} |\psi_s^{m+2\sigma}\rangle + \sum_{\sigma'=\pm 1} K_{s,s_1}^{\sigma m,\sigma'} |\psi_{s+2\sigma'}^{m+2\sigma}\rangle \right), \quad (24)$$

$$\begin{aligned} G_{s,s_1}^m &= m^2 + (D_{s,s_1}^m)^2 + (D_{s+1,s_1}^m)^2 \\ &= s(s+1) - 1 \\ &\quad + [2m^2 + 1 - 2s(s+1)]\alpha_{s,s_1}, \end{aligned} \quad (25)$$

$$H_{s,s_1}^{m,\sigma'} = D_{s+(\sigma'+1)/2,s_1}^m D_{s+(3\sigma'+1)/2,s_1}^m, \quad (26)$$

$$K_{s,s_1}^{x,\sigma'} = C_{s+(\sigma'+1)/2,s_1}^{-\sigma'x-(1+\sigma')/2} C_{s+(3\sigma'+1)/2,s_1}^{-\sigma'x-(3\sigma'+1)/2}, \quad (27)$$

$$L_{s,s_1}^x = 2F_s^x \alpha_{s,s_1}, \quad (28)$$

and

$$\alpha_{s,s_1} = \frac{3s(s+1) - 4s_1(s_1+1) - 3}{(2s-1)(2s+3)}. \quad (29)$$

We note that $2\alpha_{s,s_1} = 1 - \eta_{s,s_1}^2 - \eta_{s+1,s_1}^2$ and that Eq. (29) holds for $s \geq 0$. Equations (18) and (19) allow for an exact solution to the most general Hamiltonian of arbitrary order in the individual spin operators. In all previous treatments of more complicated spin systems with similar anisotropic interactions, it was only possible to obtain numerical solutions, and therefore the full anisotropy of the magnetization and specific heat was not calculated.[23, 24] The operations of \mathcal{H}_0 , \mathcal{H}_b and \mathcal{H}_d satisfy the selection rules $\Delta s = 0$, $\Delta m = 0, \pm 1, \pm 2$. The local anisotropy interactions \mathcal{H}_a and \mathcal{H}_e allow transitions satisfying $\Delta s = 0, \pm 2$, $\Delta m = 0$, and $\Delta s = 0, \pm 2$, $\Delta m = \pm 2$, respectively, so in the presence of either of these interactions, s is no longer a good quantum number, unless $s_1 = 1/2$.

III. GENERAL THERMODYNAMICS

In order to obtain the thermodynamic properties, we first calculate the canonical partition function, $Z = \text{Tr} \exp(-\beta \mathcal{H})$. Since \mathcal{H} is not diagonal in the (s, m) representation, we must construct the wave function from all possible spin states. We then write

$$Z = \text{Tr} \langle \Psi_{s_1} | e^{-\beta \mathcal{H}} | \Psi_{s_1} \rangle, \quad (30)$$

where $|\Psi_{s_1}\rangle$ is constructed from the $\{|\psi_s^m\rangle\}$ basis as

$$\langle\Psi_{s_1}| = \left(\langle\psi_{2s_1}^{2s_1}|, \langle\psi_{2s_1}^{2s_1-1}|, \dots, \langle\psi_1^0|, \langle\psi_1^{-1}|, \langle\psi_1^0|\right), \quad (31)$$

where $\beta = 1/(k_B T)$ and k_B is Boltzmann's constant. To evaluate the trace, it is useful to diagonalize the $\langle\Psi_{s_1}|\mathcal{H}|\Psi_{s_1}\rangle$ matrix. To do so, we let $|\Psi_{s_1}\rangle = \mathbf{U}|\Phi_{s_1}\rangle$, where

$$\langle\Phi_{s_1}| = \left(\langle\phi_{n_{s_1}}|, \langle\phi_{n_{s_1}-1}|, \dots, \langle\phi_1|\right), \quad (32)$$

is constructed from the new orthonormal basis $\{|\phi_n\rangle\}$, and \mathbf{U} is a unitary matrix of rank $n_{s_1} = (2s_1 + 1)^2$. Choosing \mathbf{U} to diagonalize \mathcal{H} , $\mathbf{U}\mathcal{H}\mathbf{U}^\dagger = \tilde{\mathcal{H}}$, we generally obtain $\tilde{\mathcal{H}}|\phi_n\rangle = \epsilon_n|\phi_n\rangle$ and the partition function for a SMM dimer,

$$Z = \sum_{n=1}^{n_{s_1}} \exp(-\beta\epsilon_n). \quad (33)$$

The specific heat $C_V = k_B\beta^2\partial^2 \ln Z/\partial\beta^2$ is then easily found at all T, \mathbf{B} ,

$$C_V = \frac{k_B\beta^2}{Z^2} \left[Z \sum_{n=1}^{n_{s_1}} \epsilon_n^2 e^{-\beta\epsilon_n} - \left(\sum_{n=1}^{n_{s_1}} \epsilon_n e^{-\beta\epsilon_n} \right)^2 \right]. \quad (34)$$

The magnetization

$$\mathbf{M} = -\frac{1}{Z} \sum_{n=1}^{n_{s_1}} \nabla_{\mathbf{B}}(\epsilon_n) \exp(-\beta\epsilon_n), \quad (35)$$

requires $\nabla_{\mathbf{B}}(\epsilon_n)$ for each \mathbf{B} . As $T \rightarrow 0$, at most two eigenstates are relevant. For most B values, only one ϵ_n is important. But near the reduced sth level-crossing induction $b_s^* = \gamma B_{s,s_1}^{\text{lc}}(\theta, \phi)$ at which $\epsilon_s = \epsilon_{s-1}$, two eigenstates are relevant. We then obtain for these two energies

$$C_V(b)/k_B \approx \frac{(\beta\Delta\epsilon_s/2)^2}{\cosh^2(\beta\Delta\epsilon_s/2)}, \quad (36)$$

$$M(b) \approx \frac{1}{2}(M_s + M_{s-1}) + \frac{1}{2}(M_s - M_{s-1}) \tanh(\beta\Delta\epsilon_s/2), \quad (37)$$

where

$$\Delta\epsilon_s = \epsilon_s(b) - \epsilon_{s-1}(b), \quad (38)$$

and $M_s = \gamma\nabla_b\epsilon_s(b)$ is the magnetization of the sth eigenstate only. We then expand in powers of $b - b_s^*$,

$$\epsilon_s(b) = \epsilon_s(b_s^*) + (b - b_s^*)a_{1,s} + \frac{1}{2}(b - b_s^*)^2 a_{2,s} + \dots, \quad (39)$$

and we find

$$C_V(b_s^*) \xrightarrow{T \rightarrow 0} 0, \quad (40)$$

$$C_V \left[b_s^* \pm \frac{2c}{\beta(a_{1,s} - a_{1,s-1})} \right] \xrightarrow{k_B T \ll |J|} C_V^{\text{peak}} \quad (41)$$

$$C_V^{\text{peak}}/k_B = \left(\frac{c}{\cosh c} \right)^2 \approx 0.439229, \quad (42)$$

and

$$M(b_s^*)/\gamma \xrightarrow{T \rightarrow 0} \frac{1}{2}(a_{1,s} + a_{1,s-1}) = s - 1/2 + \mathcal{O}(J_j/J)^2, \quad (43)$$

$$\frac{dM}{\gamma^2 db} \Big|_{b_s^*} \xrightarrow{T \rightarrow 0} \frac{\beta}{4}(a_{1,s} - a_{1,s-1})^2 = \frac{\beta}{4}(1 + \mathcal{O}(J_j/J)^2), \quad (44)$$

where $s = 1, \dots, 2s_1$ and $c \approx 1.19967864$ is the solution to $\tanh c = 1/c$. The coefficients $a_{1,s} = s + \mathcal{O}(J_j/J)^2$ and $a_{2,s} = \mathcal{O}(J_j/J)^2$. The easiest way to see this is to first rotate the crystal so the quantization axis is along \mathbf{B} , as discussed in Appendix B. An expression for $a_{1,s}$ to second order in the J_j/J is given in Appendix D. We note that $b_s^* = \gamma B_{s,s_1}^{\text{lc}}(\theta, \phi)$ depends upon s, s_1 , and the direction of \mathbf{B} when anisotropic interactions are present.

The $C_V(B)$ double peaks are double Schottky anomalies at the reduced induction values $b_s^* \pm \frac{2c}{\beta} + \mathcal{O}(J_j/J)^2$. Hence, to (J_j/J) , the heights and midpoint slopes of the $2s_1$ low- T $M(B)$ steps are uniform and the same as for the isotropic case, but the step positions and hence their plateaus are not. Correspondingly, the heights and positions of the $2s_1$ $C_V(B)$ double peaks are uniform and the same as for the isotropic case, but positions of the zeroes are not. Hence, the non-universal level-crossing inductions $B_{s,s_1}^{\text{lc}}(\theta, \phi)$ fully determine the low- T thermodynamics of weakly anisotropic AFM dimers.

In the next three sections, we consider the special cases of $s_1 = 1/2, 1$ and $5/2$. Then, in Section VII and Appendix D, we present out general expression for $B_{s,s_1}^{\text{lc}}(\theta, \phi)$ accurate to second order in each of the J_j . We remark that a double peak in the low- T $C_V(B)$ curve has been seen experimentally in a much more complicated Fe_6 ring compound, and was attributed to level crossing.[8]

IV. ANALYTIC RESULTS FOR SPIN 1/2

Plots of C_V/k_B and M/γ versus $\gamma B/|J|$ for the isotropic spin 1/2 dimer were given previously.[14] For $s_1 = 1/2$ with an arbitrary \mathbf{B} and J_j for $j = a, b, d, e$, the rank 4 Hamiltonian matrix is block diagonal, since $s = 0, 1$ is a good quantum number. The eigenvalues are given by

$$\epsilon_1 = -\frac{J_a}{2}, \quad (45)$$

$$\epsilon_n = -\frac{J_a}{2} - J + \lambda_n, \quad n = 2, 3, 4, \quad (46)$$

where

$$0 = \lambda_n^3 + 2\lambda_n^2 J_b - \lambda_n [J_d^2 - J_b^2 + b^2] - b^2 \sin^2 \theta [J_b - J_d \cos(2\phi)]. \quad (47)$$

For the special cases $\mathbf{B} \parallel \hat{\mathbf{i}}$ for $i = x, y, z$, the λ_n^i satisfy

$$\lambda_n^z = 0, -J_b \pm F_z, \quad (48)$$

$$\lambda_n^{x,y} = -2J_{y,x}, -J_{x,y} \pm F_{x,y}, \quad (49)$$

where

$$F_i = \sqrt{b^2 + J_i^2}, \quad (50)$$

$$J_{x,y,z} = (J_b \pm J_d)/2, \quad J_d, \quad (51)$$

respectively, and where J_x (J_y) corresponds to the upper (lower) sign.

The magnetization for $\mathbf{B} \parallel \hat{\mathbf{i}}$ is given by

$$M_i = \frac{\gamma b \sinh(\beta F_i)}{F_i \mathcal{D}_i}, \quad (52)$$

$$\mathcal{D}_i = \cosh(\beta F_i) + \Delta_i/2, \quad (53)$$

$$\Delta_x = \exp(-\beta J_x) [\exp(-\beta J) + \exp(2\beta J_y)], \quad (54)$$

$$\Delta_y = \exp(-\beta J_y) [\exp(-\beta J) + \exp(2\beta J_x)], \quad (55)$$

$$\Delta_z = \exp(-\beta J_b) [\exp(-\beta J) + 1], \quad (56)$$

respectively. When the interactions are written in terms of the less physical J_f, J_b, J_d , and J_c , then $J_b \rightarrow J_b + J_f$ and $J_d \rightarrow J_d + J_c/2$, so that for $s_1 = 1/2$, J_f and J_c merely renormalize J_b and J_d . Neither of the single-ion spin anisotropy terms \mathcal{H}_a and \mathcal{H}_e affect the thermodynamics for $s_1 = 1/2$. We note that $M_y(J_d) = M_x(-J_d)$ for each B , as expected from $\mathcal{H}_d = -J_d(S_x^2 - S_y^2)$.

From Eqs. (45), (46), (48), and (49), the single level crossing induction ($s = 1$) for an $s_1 = 1/2$ dimer with $\mathbf{B} \parallel \hat{\mathbf{i}}$ occurs at

$$\gamma B_{1,1/2}^{\text{lc}} = \begin{cases} \sqrt{J^2 + J(J_b \pm J_d)}, & \mathbf{B} \parallel \hat{\mathbf{x}}, \hat{\mathbf{y}} \\ \sqrt{(J + J_b)^2 - J_d^2}, & \mathbf{B} \parallel \hat{\mathbf{z}} \end{cases}, \quad (57)$$

provided that $J + J_{x,y} < 0$ and $J + J_b < 0$, respectively.

To distinguish the different effects of the global anisotropy interactions J_b and J_d that affect the magnetization of $s_1 = 1/2$ dimers, in Figs. 2 and 3, we have respectively plotted the low- T M/γ versus $\gamma B/|J|$ with $J_b = 0.1J, J_d = 0$ and $J_d = 0.1J, J_b = 0$ for $\mathbf{B} \parallel \hat{\mathbf{z}}$ (solid) and $\mathbf{B} \parallel \hat{\mathbf{x}}$ (dashed), along with the isotropic case $J_b = J_d = 0$ (dotted). From Fig. 2, $J_b < 0$ and $J_d = 0$ causes a greater shift to higher B values at the magnetization step with $\mathbf{B} \parallel \hat{\mathbf{z}}$ than for $\mathbf{B} \parallel \hat{\mathbf{x}}$, consistent with Eq. (57). In addition, J_d finite with $J_b = 0$ has a very different effect upon the anisotropy of the magnetization step, as shown in Fig. 3. Although for $\mathbf{B} \parallel \hat{\mathbf{z}}$, B at the step is slightly reduced from its isotropic interaction value, for $\mathbf{B} \parallel \hat{\mathbf{x}}$, the magnetization step occurs at a larger B . These

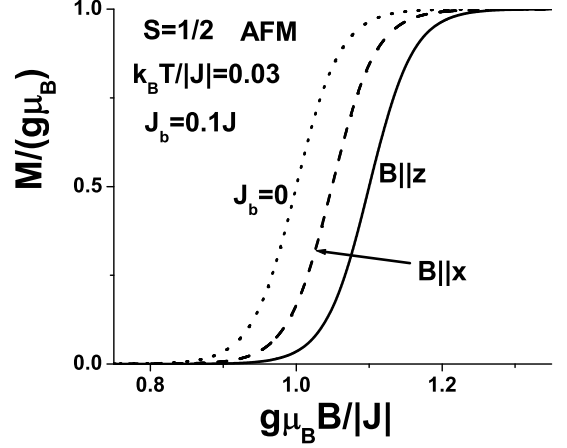


FIG. 2: Plots of M/γ versus $\gamma B/|J|$ at $k_B T/|J| = 0.03$ for the AFM spin 1/2 dimer with $J_b = 0.1J$, $J_d = 0$, with $\mathbf{B} \parallel \hat{\mathbf{z}}$ (solid), $\mathbf{B} \parallel \hat{\mathbf{x}}$ (dashed), along with the isotropic case $J_b = J_d = 0$ (dotted).

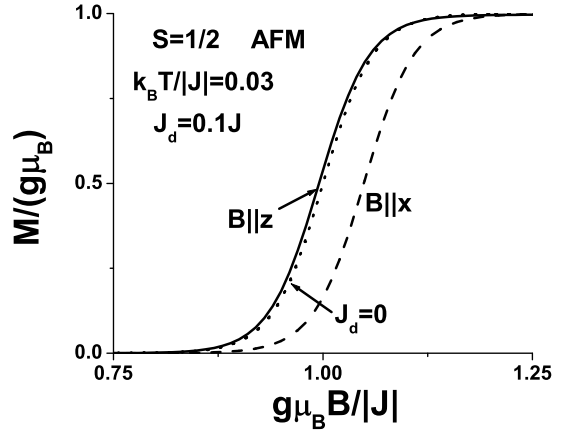


FIG. 3: Plots of M/γ versus $\gamma B/|J|$ at $k_B T/|J| = 0.03$ for the AFM spin 1/2 dimer with $J_d = 0.1J$, $J_b = 0$, with $\mathbf{B} \parallel \hat{\mathbf{z}}$ (solid), $\mathbf{B} \parallel \hat{\mathbf{x}}$ (dashed), along with the isotropic case $J_b = J_d = 0$ (dotted).

results are consistent with Eq. (57). The midpoint slopes are universal, in accordance with Eq. (44).

The specific heat of an $s_1 = 1/2$ dimer with $\mathbf{B} \parallel \hat{\mathbf{i}}$ is

$$C_{Vi} = \frac{k_B \beta^2 \mathcal{N}_i}{\mathcal{D}_i^2}, \quad (58)$$

where the \mathcal{D}_i are given by Eq. (53), and the \mathcal{N}_i are given in Appendix A. Plots at low T of C_V/k_B versus $\gamma B/|J|$ for $s_1 = 1/2$ dimers with the corresponding global anisotropies $J_b = 0.1J$ and $J_d = 0.1J$ are shown in Figs. 4 and 5, respectively. We note the universal curve shapes, but non-universal level-crossing positions, in quantitative



FIG. 4: Plot of C_V/k_B versus $\gamma B/|J|$ for the AFM spin 1/2 dimer with $J_b = 0.1J$, $J_d = 0$ at $k_B T/|J| = 0.03$ with the same curve notation as in Fig. 2.

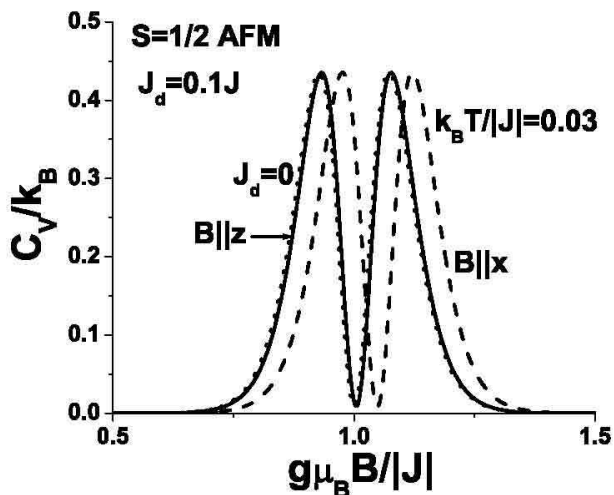


FIG. 5: Plot of C_V/k_B versus $\gamma B/|J|$ for the AFM spin 1/2 dimer with $J_d = 0.1J$, $J_b = 0$ at $k_B T/|J| = 0.03$ with the same curve notation as in Fig. 3.

agreement with Eqs. (40)-(42). In Fig. 4, the positions of the maxima and the central minimum in C_V track that of the magnetization step in Fig. 2 with the same parameters. With $J_d = 0.1J$, the behaviors in C_V and M for $\mathbf{B}||\hat{x}$ are also very similar. However, there is a slight difference in the behaviors for $\mathbf{B}||\hat{z}$. Note that M (Fig. 3) shows a slight reduction for $\mathbf{B}||\hat{z}$ in the induction required for the step, whereas C_V (Fig. 5) shows a slight increase in the positions of the peaks. This detail only appears when $J_d \neq 0$, for which the effective temperature is slightly higher than for $J_d = 0$.

V. ANALYTIC AND NUMERICAL RESULTS FOR SPIN 1

For dimers with $s_1 = 1$, the allowed s values are $s = 0, 1, 2$. The three $s = 1$ states are decoupled from the six remaining $s = 0, 2$ states. They satisfy a cubic equation given in Appendix A. For $\mathbf{B}||\hat{i}$ with $i = x, y, z$, this cubic equation simplifies to a linear and a quadratic equation, as for the $s = 1$ eigenstates of $s_1 = 1/2$ dimers.

The remaining six eigenstates corresponding nominally to $s = 0, 2$ are in general all mixed. The matrix leading to the hexatic equation from which the six eigenvalues can be obtained is given in Appendix A. That is sufficient to evaluate the eigenvalues for $s_1 = 1$ using symbolic manipulation software. When combined with the three $s = 1$ eigenvalues, one can then use Eqs. (34) and (35) to obtain the resulting exact magnetization and specific heat at an arbitrary \mathbf{B} . The combined nine eigenvalues depend upon all four anisotropy parameters J_j for $j = a, b, d, e$.

To the extent that the eigenvalues can be obtained from the solutions to either linear or quadratic equations, the expressions for the $B_{s,1}^{lc}$ are simple, and are given in Appendix A. In the global anisotropy case $J_a = J_e = 0$, the first level crossing induction $B_{1,1}^{lc}$ with $\mathbf{B}||\hat{i}$ is identical to $B_{1,1/2}^{lc}$, the level crossing with $s_1 = 1/2$ given by Eq. (57). For comparison, we expand the first and second level crossing inductions to first order in each of the J_j for $j = a, b, d, e$ for $\mathbf{B}||\hat{i}$ where $i = x, y, z$,

$$\gamma B_{1,1,z}^{lc(1)} = -J + \frac{J_a}{3} - J_b, \quad (59)$$

$$\gamma B_{1,1,x,y}^{lc(1)} = -J - \frac{J_a}{6} - \frac{J_b}{2} \mp \frac{1}{2}(J_d - J_e), \quad (60)$$

$$\gamma B_{2,1,z}^{lc(1)} = -2J - J_a - 3J_b, \quad (61)$$

$$\gamma B_{2,1,x,y}^{lc(1)} = -2J + \frac{J_a}{2} - \frac{J_b}{2} \mp \frac{5J_d}{2} \mp \frac{3J_e}{2}, \quad (62)$$

where the upper (lower) sign is for $\mathbf{B}||\hat{x}$ ($\mathbf{B}||\hat{y}$), respectively.

From these simple first-order results, it is possible to understand the qualitatively different behavior obtained with local, single-ion, anisotropy from that obtained with global anisotropy. In the isotropic case $J_j = 0 \forall j$, the first and second level crossings occur at $-J$ and $-2J$, respectively. For each induction direction, the signs of the J_b and J_d contributions to $B_{2,1}^{lc(1)} + 2J$ and $B_{1,1}^{lc(1)} + J$ are the same, whereas the signs of the J_a and J_e contributions to $B_{2,1}^{lc(1)} + 2J$ and $B_{1,1}^{lc(1)} + J$ are the *opposite*.

In Figs. 6-10, we plot M/γ versus $\gamma B/|J|$ for five low- T cases of AFM $s_1 = 1$ dimers, taking $k_B T/|J| = 0.03$. These curves all exhibit the universal features predicted by Eqs. (43) and (44). The corresponding C_V/k_B versus $\gamma B/|J|$ curves, which also obey Eqs. (40)-(42), are presented elsewhere.[25] In these figures, only one of the five anisotropy interactions J_j is non-vanishing, and we take

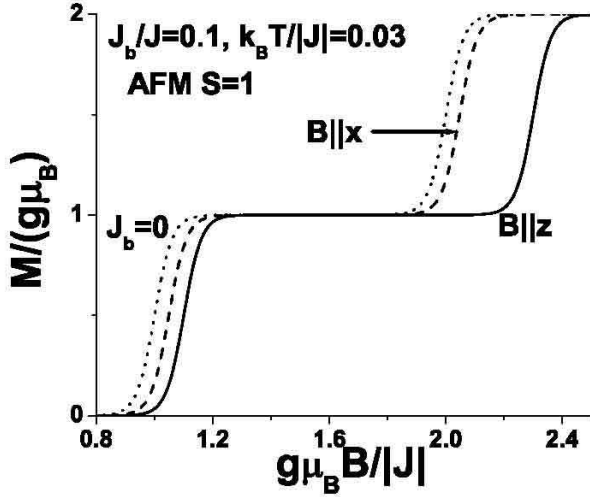


FIG. 6: Plot at $k_B T/|J| = 0.03$ and $J_b/J = 0.1$ of M/γ versus $\gamma B/|J|$ for the AFM spin 1 dimer, with the same curve notation as in Fig. 2.

$J_j/J = 0.1$, for $j = b, d, a, e$, and c , respectively. Unlike the case of $s_1 = 1/2$ dimers, for which J_c merely renormalizes J_d , for $s_1 = 1$ each of these interactions leads to distinct anisotropy effects in the low- T thermodynamics arising from the $B_{s,1}^{lc}(\theta, \phi)$.

We first show the results for the global anisotropy interactions. In Fig. 6, we plot $M(B)$ for $J_b = 0.1J$ (and all other $J_j = 0$) at $k_B T/|J| = 0.03$ for the AFM $s_1 = 1$ dimer. $B_{s,1}^{lc}(\theta, 0)$ is largest and increases monotonically with level-crossing number s for $\theta = 0$, but is independent of s for $\theta = \pi/2$, nearly quantitatively consistent with Eqs. (59)-(62). In Fig. 7, the corresponding results for $J_d = 0.1J$ (and the other $J_j = 0$) are shown. Again, $B_{s,1}^{lc}(\theta, 0)$ is largest and increases monotonically for $\theta = \pi/2$, and is nearly independent of s for $\theta = 0$, as for $s = 1/2$, nearly quantitatively consistent with Eqs. (59)-(62). Note that $B_{s,1}^{lc}(0, 0)$ is nearly indistinguishable from the isotropic case.

Next, in Figs. 8 and 9, we show the corresponding curves for $M(B)$ at low T for the local anisotropies $J_a = 0.1J$ and $J_e = 0.1J$, respectively, with the other $J_j = 0$. In contrast to the global anisotropies, $B_{s,1}^{lc}(\theta, 0) + sJ$ changes sign for both $\theta = 0, \pi/2$, nearly quantitatively consistent with Eqs. (59)-(62). We note that $B_{s,1}^{lc}(0, 0)$ is nearly indistinguishable from the isotropic case for $J_e \neq 0$ shown in Fig. 9.

Finally, in Fig. 10, we show the corresponding $M(B)$ curves for $J_c = 0.1J$. With this combination, $B_{s,1}^{lc}(\theta, 0)$ is independent of s for both $\theta = 0, \pi/2$, but is larger for $\theta = \pi/2$, nearly quantitatively consistent with Eqs. (59)-(62) with $J_d, J_e \rightarrow \pm J_c/2$, respectively.

In short, the case $s_1 = 1$ is sufficient to exhibit the very different behaviors obtained from the single-ion, local spin anisotropy interactions from those obtained from

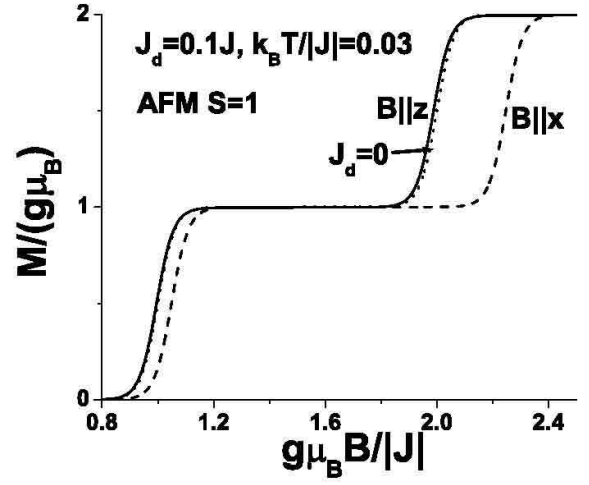


FIG. 7: Plot at $k_B T/|J| = 0.03$ and $J_d/J = 0.1$ of M/γ versus $\gamma B/|J|$ for the AFM spin 1 dimer, with the same curve notation as in Fig. 3.

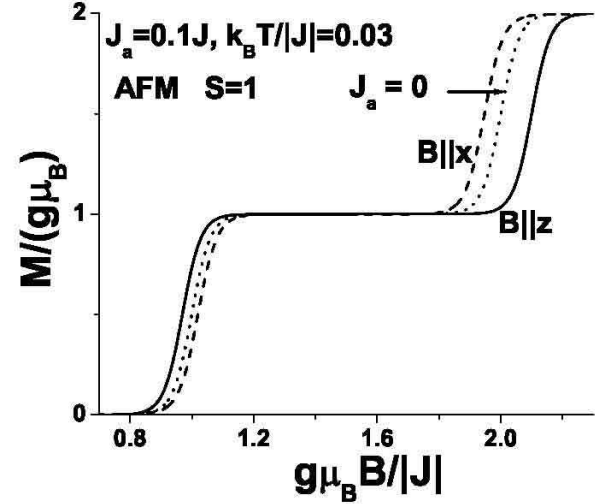


FIG. 8: Plot at $k_B T/|J| = 0.03$ and $J_a/J = 0.1$ of M/γ versus $\gamma B/|J|$ for the AFM spin 1 dimer. The curve notation is the same as in Fig. 2, except that the isotropic case (dotted) curve is for $J_a = 0$.

the global spin anisotropy interactions. As s_1 increases beyond 1, the situation becomes not only more complicated, but also more interesting, as shown in the following.

VI. EXACT NUMERICAL RESULTS FOR SPIN 5/2

For $s_1 = 5/2$, one of the cases of greatest experimental interest, when \mathcal{H}_a and \mathcal{H}_e are present, none of the allowed s, m values is a true quantum number. That is, \mathcal{H}_a and \mathcal{H}_e cause all of the states with nominally odd or even s to

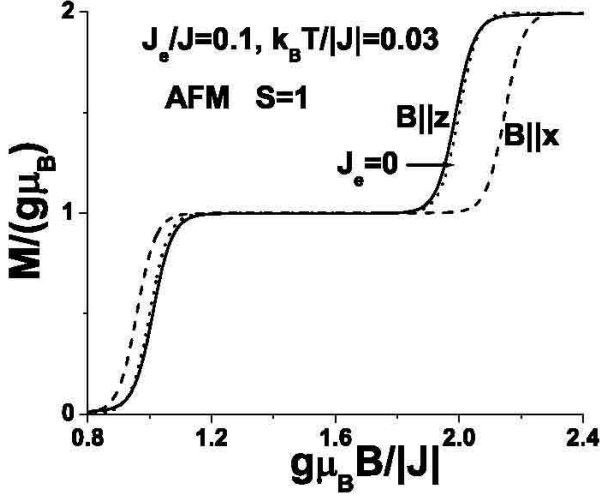


FIG. 9: Plot at $k_B T/|J| = 0.03$ and $J_e/J = 0.1$ of M/γ versus $\gamma B/|J|$ for the AFM spin 1 dimer. The curve notation is the same as in Fig. 2, except that the isotropic case (dotted) curve is for $J_e = 0$.

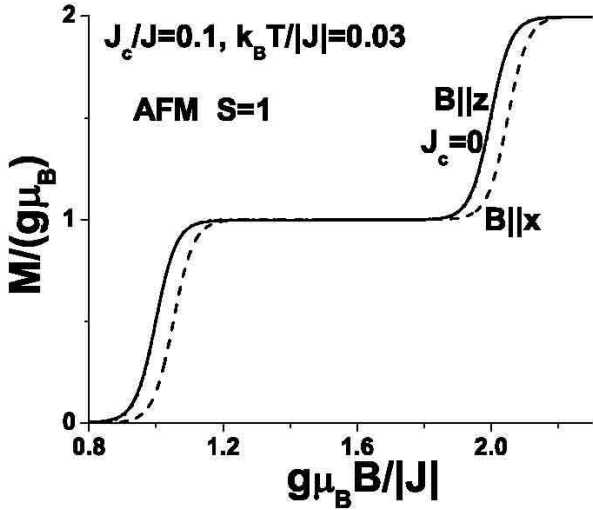


FIG. 10: Plot at $k_B T/|J| = 0.03$ and $J_c/J = 0.1$ of M/γ versus $\gamma B/|J|$ for the AFM spin 1 dimer. The curve notation is the same as in Fig. 2, except that the isotropic case (dotted) curve is for $J_c = 0$.

mix with one another. For $\mathbf{B}||\hat{i}$ for $i = x, y, z$, this simplifies in the crystal representation, as for $s_1 = 1$, since only states with odd or even m values in the appropriately chosen representation can mix. By using symbolic manipulation software, it is possible to solve for the exact eigenvalues of the $s_1 = 5/2$ dimer. However, because the analytic expressions for the eigenvalues are much more complicated than those for $s_1 = 1$ presented in Appendix A, we shall not attempt to present them, but will instead focus upon their numerical evaluation for specific cases.

To first order in the J_j , the first three level crossings

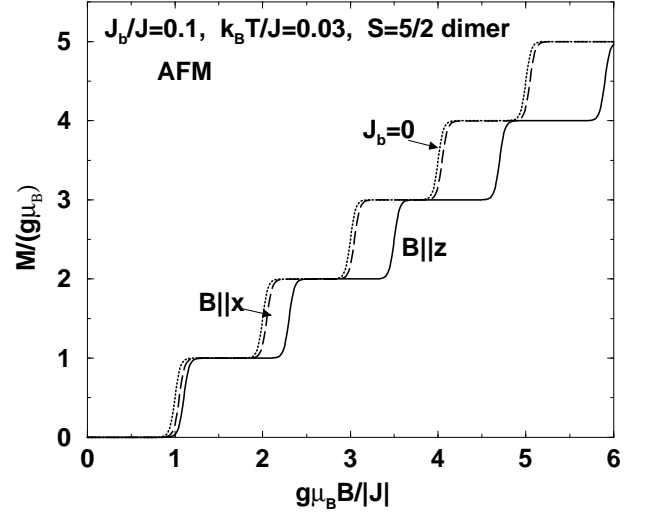


FIG. 11: Plot at $k_B T/|J| = 0.03$ of M/γ versus $\gamma B/|J|$ for the AFM spin 5/2 dimer with $J_b/J = 0.1$. The curve notation is the same as in Fig. 2.

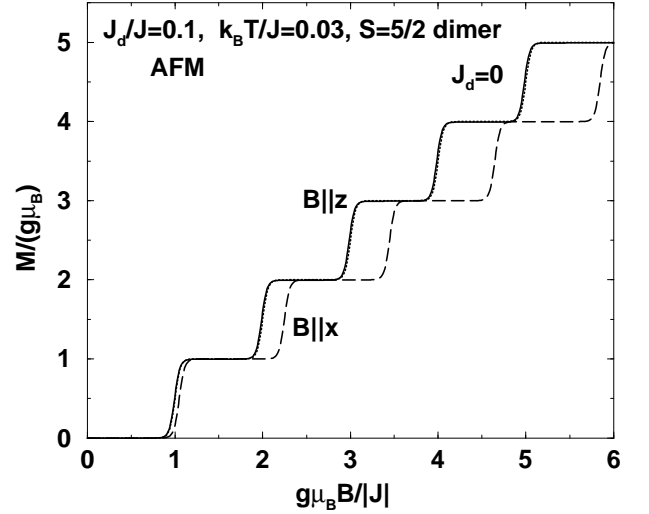


FIG. 12: Plot of M/γ versus $\gamma B/|J|$ for the AFM spin 5/2 dimer at $k_B T/|J| = 0.03$ with $J_d/J = 0.1$. The curve notation is the same as in Fig. 3.

for $\mathbf{B}||\hat{i}$ with $i = x, y, z$ are

$$\gamma B_{1,5/2,z}^{\text{lc}(1)} = -J + \frac{32J_a}{15} - J_b, \quad (63)$$

$$\gamma B_{1,5/2,x,y}^{\text{lc}(1)} = -J - \frac{16J_a}{15} - \frac{J_b}{2} \mp \frac{J_d}{2} \pm \frac{16J_e}{5}, \quad (64)$$

$$\gamma B_{2,5/2,z}^{\text{lc}(1)} = -2J - \frac{8J_a}{35} - 3J_b, \quad (65)$$

$$\gamma B_{2,5/2,x,y}^{\text{lc}(1)} = -2J + \frac{4J_a}{35} - \frac{J_b}{2} \mp \frac{5J_d}{2} \mp \frac{12J_e}{35}, \quad (66)$$

$$\gamma B_{3,5/2,z}^{\text{lc}(1)} = -3J - \frac{106J_a}{63} - 5J_b, \quad (67)$$

$$\gamma B_{3,5/2,x,y}^{\text{lc}(1)} = -3J + \frac{53J_a}{63} - \frac{J_b}{2} \mp \frac{9J_d}{2} \mp \frac{53J_e}{21}. \quad (68)$$

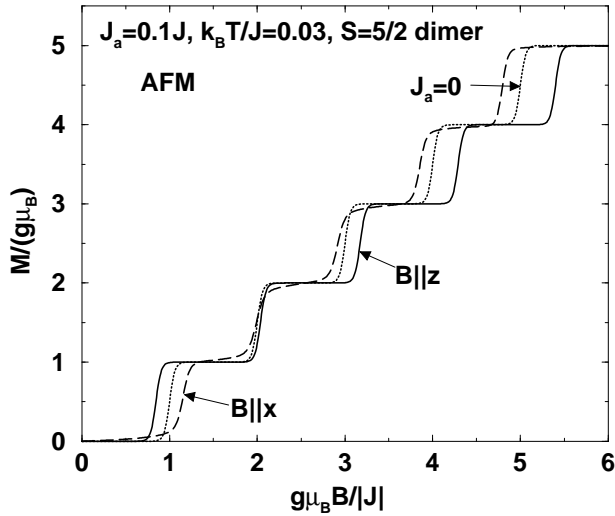


FIG. 13: Plot at $k_B T/|J| = 0.03$ and $J_a/J = 0.1$ of M/γ versus $\gamma B/|J|$ for the AFM spin 5/2 dimer. The curve notation is the same as in Fig. 8.

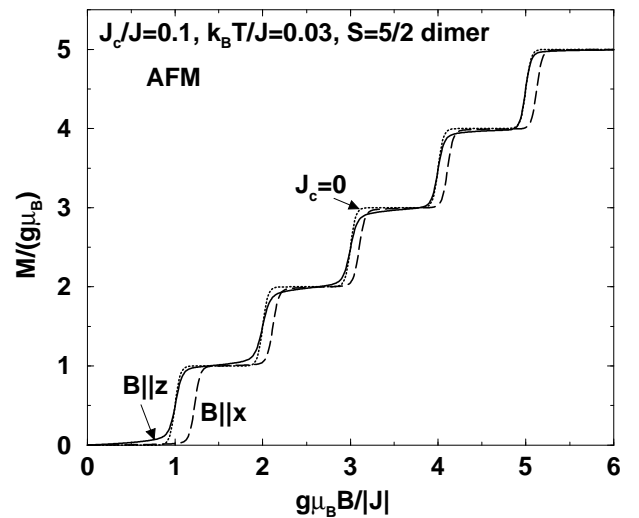


FIG. 14: Plot at $k_B T/|J| = 0.03$ and $J_c/J = 0.1$ of M/γ versus $\gamma B/|J|$ for the AFM spin 5/2 dimer. The curve notation is the same as in Fig. 10.

In Figs. 11-14, we plot M/γ and $C_V(B)$ versus $\gamma B/|J|$ for four low- T cases of AFM $s_1 = 5/2$ dimers, $J_b = 0.1J$, $J_d = 0.1J$, $J_a = 0.1J$, and $J_c = 0.1J$, respectively, and the other $J_j = 0$, taking $k_B T/|J| = 0.03$. Each of these curves exhibit the universal step behavior predicted in Eqs. (43) and (44). Corresponding C_V/k_B versus $\gamma B/|J|$ curves also exhibit the universal double peak behaviors predicted in Eqs. (40)-(42), and are shown elsewhere.[25] In Fig. 15, examples of $M(\theta)$ at fixed B and $\phi = 0$ are shown. Figures 13-15 are sufficient to distinguish the more interesting local spin anisotropy effects in AFM dimers with higher s_1 values from the non-existent or less interesting ones present with $s_1 = 1/2, 1$, respectively. In Figs. 11-14, the solid and dashed curves represent the $B||\hat{z}$ and $B||\hat{x}$ cases, and the dotted curve represents the isotropic case, $J_j = 0 \forall j$, as in Figs. 2-10.

We first examine the global spin anisotropy effects of \mathcal{H}_b and \mathcal{H}_d in Figs. 11 and 12. These figures exhibit the same behavior shown for $s_1 = 1/2, 1$ in the corresponding Figs. 2, 6 and 3, 7. Note that $B_{s,5/2}^{lc}(\theta, 0)$ is largest for $\theta = \pi/2$ with $J_b = 0.1J$ and for $\theta = 0$ with $J_d = 0.1J$, and increases monotonically with s , as for $s_1 = 1$ in both cases, nearly quantitatively consistent with Eqs. (63)-(68). By contrast, $B_{s,5/2}^{lc}(\theta, 0)$ for $\theta = \pi/2$ with $J_b = 0.1J$ and for $\theta = 0$ for $J_d = 0.1J$ are nearly indistinguishable from the isotropic case, also nearly quantitatively consistent with Eqs. (63)-(68).

In contrast, the local field anisotropy interactions show very different and much more interesting behaviors. In Fig. 13, we present our results for the effects of the single-ion axial anisotropy interaction \mathcal{H}_a , Eq. (5). As in Fig. 8 for $s_1 = 1$, $B_{s,5/2}^{lc}(\theta, 0) + sJ$ changes sign with increasing s . $B_{1,5/2}^{lc}(0, 0) + J < 0$, whereas for

$s \geq 2$, $B_{s,5/2}^{lc}(0, 0) + sJ > 0$ and increases monotonically with s . For $\theta = \pi/2$, nearly the opposite situation occurs. $B_{s,5/2}^{lc}(\pi/2, 0) + sJ$ is positive for $s = 1$ and decreases monotonically with increasing s . In both cases, $|B_{s,5/2}^{lc}(\theta, 0) + sJ|$ is a minimum for $s = 2$. These local axial anisotropy effects, consistent with Eqs. (63)-(68), are very different than the global anisotropy ones pictured in Figs. 11 and 12. They are also much richer and interesting than the corresponding case for $s_1 = 1$ pictured in Fig. 8.

In Fig. 14, we present our M/γ versus $\gamma B/|J|$ results for the case of the local azimuthally anisotropic exchange interaction, \mathcal{H}_c , Eq. (8), evaluated for AFM dimers at $k_B T/|J| = 0.03$ with $J_c = 0.1J$ and the remaining $J_j = 0$. $B_{s,5/2}^{lc(1)}$ for this case is obtained from Eqs. (63)-(68) by setting $J_d, J_e = \pm J_c/2$, respectively, and $J_a = J_b = 0$. $B_{s,5/2}^{lc}(0, 0)$ is nearly indistinguishable from the isotropic case, as in Fig. 10 for $s_1 = 1$, except for some minor curve shape effects far from the step midpoints. $B_{s,5/2}^{lc}(\pi/2, 0) + sJ$ is always positive, as for $s_1 = 1$ shown in Fig. 10, but has a minimum at $s = 3$. This is also in stark contrast to the monotonic global anisotropy behavior for $s_1 = 5/2$ seen in Figs. 11 and 12. Both of these behaviors are nearly quantitatively consistent with Eqs. (63)-(68) as modified to include J_c .

Although not pictured explicitly, the behavior for $J_e = 0.1J$ with the other $J_j = 0$ is rather like that of the $J_a = 0.1J$ curves pictured in Fig. 13 with $\hat{z} \leftrightarrow \hat{x}$, differing in ways similar to those differences between the $J_a = 0.1J$ and $J_e = 0.1J$ curves pictured for $s_1 = 1$ in Figs. 8 and 9. As indicated in Eqs. (63)-(68), the $B_{s,5/2}^{lc}(0, 0)$ are nearly independent of J_e . However, the $B_{s,5/2}^{lc}(\pi/2, 0) + sJ$ with $J_e = 0.1J$ are nearly three times as large as for $J_a = 0.1J$

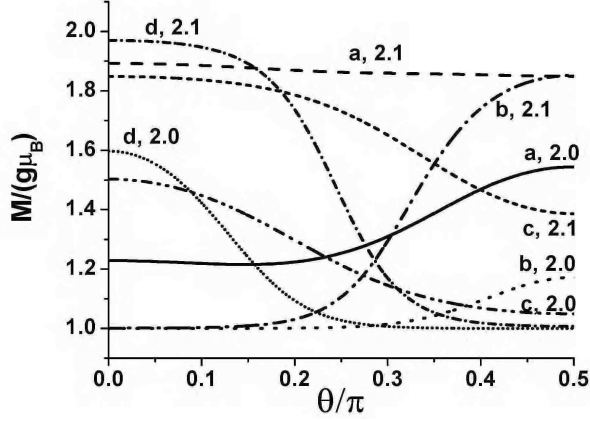


FIG. 15: Plot of M/γ at $\phi = 0$ versus θ/π near the second step at $\gamma B/|J| = 2.0, 2.1$ and $k_B T/|J| = 0.03$ for each $J_j/J = 0.1$ with $i = a, b, c, d$. Curves are labelled with $j, \gamma B/|J|$ values.

case, so that the minimum $|B_{s,5/2}^{\text{lc}}(\pi/2, 0) + sJ|$ is also a minimum for $s = 2$. More details are given in Section VII and Appendix D.

In addition, the angular dependencies of M are different for each of the four J_j we presented for $s_1 = 5/2$. In Fig. 15, we present the results for $M(B, \theta, \phi = 0)/\gamma$ versus θ/π near the second level crossing at $\gamma B/|J| = 2.0, 2.1$ and $k_B T/|J| = 0.03$ for each of the four $s_1 = 5/2$ AFM magnetization cases pictured in Figs. 11-14. Note that $M(B, \pi - \theta, 0) = M(B, \theta, 0)$. The J_a and J_b curves, while rather similar at $\gamma B/|J| = 2.0$, are very different at $\gamma B/|J| = 2.1$. Hence, $\mathbf{M}(\mathbf{B})$ depends strongly upon the particular type of spin anisotropy.

VII. ANALYTIC RESULTS FOR WEAKLY ANISOTROPIC DIMERS OF ARBITRARY SPIN

A. Induction representation eigenstates first order in the anisotropies

Since the diagonalization of the Hamiltonian matrix is difficult for an arbitrary magnetic field direction combined with an arbitrary combination of spin anisotropy interactions, and must be done separately for each value of s_1 , it is useful to consider a perturbation in the relative strengths J_j/J of the anisotropy interactions. We nominally assume $|J_j/J| \ll 1$ for $j = a, b, d, e$. However, to compare with low- T magnetization and specific heat experiments at various applied field directions and magnitudes, one cannot take the magnitude of the magnetic induction to be small. In order to incorporate the magnetic induction of an arbitrary strength and direction accurately, we therefore rotate the crystal axes $(\hat{x}, \hat{y}, \hat{z})$ to $(\hat{x}', \hat{y}', \hat{z}')$, so that $\mathbf{B} = B\hat{z}'$. The rotation matrix and a brief discussion of its ramifications are given in Appendix

B.

In these rotated coordinates, the Zeeman interaction $-bS_{z'}$, where $b = \gamma B$, is diagonal. We therefore denote this representation as the induction representation. The Hamiltonian \mathcal{H}' in this representation is given in Appendix B. In the induction representation, we choose the quantum states to be $|\varphi_s^m\rangle$. In the absence of the four anisotropy interactions J_j , $\mathcal{H}' = \mathcal{H}'_0$ is diagonal,

$$\mathcal{H}'_0 |\varphi_s^m\rangle = E_s^{m,(0)} |\varphi_s^m\rangle, \quad (69)$$

where

$$E_s^{m,(0)} = -Js(s+1)/2 - mb. \quad (70)$$

The operations of the remaining terms in \mathcal{H}' on the eigenstates $|\varphi_s^m\rangle$ are given in Appendix C. The first order correction to the energy in the induction representation, $E_{s,s_1}^{m,(1)} = \langle \varphi_s^m | \mathcal{H}' | \varphi_s^m \rangle$, is found to be

$$\begin{aligned} E_{s,s_1}^{m,(1)} = & -\frac{J_b}{2}[2s(s+1) - 1] - \frac{J_a}{2}[s(s+1) - 1] \\ & + \frac{\tilde{J}_{b,a}^{s,s_1}}{2}[m^2 + s(s+1) - 1] \\ & + \frac{1}{2}[s(s+1) - 3m^2] \\ & \times \left(\tilde{J}_{b,a}^{s,s_1} \cos^2 \theta + \tilde{J}_{d,e}^{s,s_1} \sin^2 \theta \cos(2\phi) \right), \quad (71) \end{aligned}$$

where

$$\tilde{J}_{b,a}^{s,s_1} = J_b + \alpha_{s,s_1} J_a, \quad (72)$$

$$\tilde{J}_{d,e}^{s,s_1} = J_d + \alpha_{s,s_1} J_e, \quad (73)$$

and α_{s,s_1} is given by Eq. (29).

Since the θ, ϕ dependence of $E_s^{m,(1)}$ arises from the term proportional to $\tilde{J}_{b,a}^{s,s_1} \cos^2 \theta + \tilde{J}_{d,e}^{s,s_1} \sin^2 \theta \cos(2\phi)$, it is tempting to think that the thermodynamics with $\tilde{J}_{d,e}^{s,s_1} = 0$ and $\mathbf{B} \parallel \hat{z}$ are equivalent to those with $\tilde{J}_{b,a}^{s,s_1} = 0$ and $\mathbf{B} \parallel \hat{x}$. However, as shown explicitly in the following, the θ, ϕ -independent parts of Eq. (71) strongly break this apparent equivalence, causing the $B_{s,s_1}^{\text{lc}}(\theta, \phi)$ for those two cases to differ. This implies that J_b and J_d are inequivalent, as are J_a and J_e , even to first order in the anisotropy strengths.

B. First order thermodynamics

In the Hartree approximation, the anisotropy interactions are included to first order only. In this approximation, s and m are still good quantum numbers, so the partition function

$$Z^{(1)} = \sum_{s=0}^{2s_1} \sum_{m=-s}^s e^{-\beta E_{s,s_1}^m}, \quad (74)$$

where $E_{s,s_1}^m = E_s^{m,(0)} + E_{s,s_1}^{m,(1)}$. Although it is difficult to perform the summation over the m values analytically, it is nevertheless elementary to evaluate Z numerically for an arbitrary B, θ, ϕ , and T from the eigenstate energies. The magnetization in the Hartree approximation is

$$M^{(1)}(B, \theta, \phi) = \frac{\gamma}{Z^{(1)}} \sum_{s=0}^{2s_1} \sum_{m=-s}^s m e^{-\beta E_{s,s_1}^m}. \quad (75)$$

Similarly, the specific heat in the Hartree approximation is

$$C_V^{(1)}(B, \theta, \phi) \approx \frac{k_B \beta^2}{(Z^{(1)})^2} \left[Z \sum_{s=0}^{2s_1} \sum_{m=-s}^s (E_{s,s_1}^m)^2 e^{-\beta E_{s,s_1}^m} - \left(\sum_{s=0}^{2s_1} \sum_{m=-s}^s E_{s,s_1}^m e^{-\beta E_{s,s_1}^m} \right)^2 \right]. \quad (76)$$

As a test of the accuracy of this Hartree calculation, we have compared the Hartree and exact $M(B)$ obtained for the $s_1 = 5/2$ dimer with $J_d = 0.1J$ and $\mathbf{B} \parallel \hat{z}$ at various T values in Fig. 16. The corresponding comparison between the Hartree and exact $C_V(B)$ is shown in Fig. 17. We see that the curves evaluated using the Hartree and the exact expressions for M and C_V with $s_1 = 5/2$ are indistinguishable at $k_B T/|J| = 0.03$. The C_V curves are noticeably different at $k_B T/|J| = 0.1$ for $\gamma B/|J| < 0.4$, and at $k_B T/|J| = 0.3$ they are noticeably different for $\gamma B/|J| < 2.6$. Corresponding noticeable differences in the M curves at the same B values appear at T values roughly three times as high as in the C_V curves.

At very low T , $k_B T/|J| \ll 1$, the most important states in this perturbative scheme are the minima for each s value, E_{s,s_1}^s , which determine the level crossings in the Hartree approximation. As $T \rightarrow 0$, we can ignore all of the $m \neq s$ states in Eqs. (74)-(76). This two-level approximation is the basis for the universal behavior given by Eqs. (40)-(44), which fits all of the exact curves we presented reasonably well.

C. First order response functions

1. Inelastic neutron scattering cross-section

Two response functions relevant for the study of SMM's are the inelastic neutron scattering cross-section $S(\mathbf{B}, \mathbf{q}, \omega)$ and the electron paramagnetic resonance (EPR) susceptibility $\chi(\mathbf{B}, \omega)$ in strong magnetic inductions \mathbf{B} . The low- T inelastic neutron cross-section $S(\mathbf{B}, \mathbf{q}, \omega)$ can be evaluated from

$$S(\mathbf{B}, \mathbf{q}, \omega) = \sum_{\alpha, \beta=1}^3 (\delta_{\alpha, \beta} - \hat{q}_\alpha \hat{q}_\beta) \int \frac{dt}{2\pi} e^{i\omega t} \times \text{Tr} \left(e^{-\beta \mathcal{H}} S_\alpha(\mathbf{q}, t) S_\beta(\mathbf{q}, 0) \right), \quad (77)$$

$$S_\alpha(\mathbf{q}, 0) = S_{1,\alpha} e^{i\mathbf{q} \cdot \mathbf{d}} + S_{2,\alpha} e^{-i\mathbf{q} \cdot \mathbf{d}}, \quad (78)$$

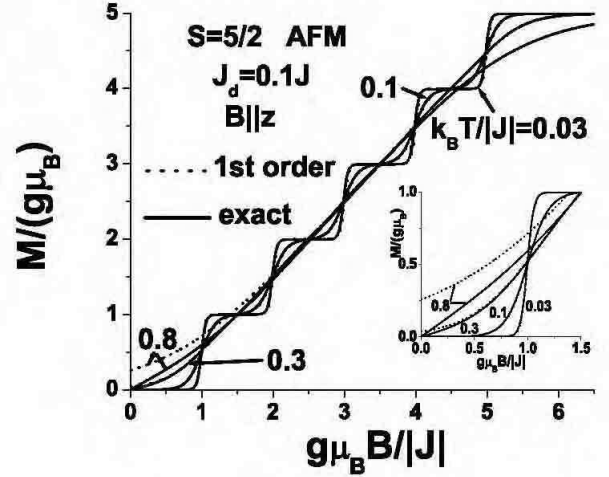


FIG. 16: Comparison of M/γ versus $\gamma B/|J|$ obtained using the Hartree asymptotic form (dotted) with the exact calculation (solid), for the $s_1 = 5/2$ AFM dimer with $J_d = 0.1J$, $J_a = J_b = J_c = 0$, at $k_B T/|J| = 0.03, 0.1, 0.3, 0.8$, as indicated. Inset: expanded view of the region $0 \leq \gamma B/|J| \leq 1.5$.

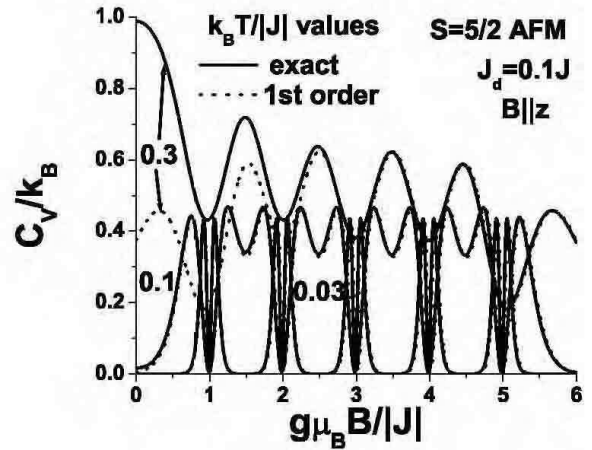


FIG. 17: Comparison of C_V/k_B versus $\gamma B/|J|$ obtained using the Hartree asymptotic form (dotted) with the exact calculation (solid), for the $s_1 = 5/2$ AFM dimer with $J_d = 0.1J$, $J_a = J_b = J_c = 0$, at $k_B T/|J| = 0.03, 0.1, 0.3$, as indicated.

where $2\mathbf{d}$ is the vector between the spins of a dimer and \hat{q}_α is the α th component of \mathbf{q}/q . It is customary to write the operators in the crystal representation, for which $\mathbf{d} = d\hat{z}$. [14, 26] With inelastic neutron scattering, one can probe the dimer with a strong magnetic field at various directions with respect to both the dimer axis and the scattering plane. To the extent that the eigenstates $\{|\phi_n\rangle\}$ and their energies ϵ_n can be evaluated exactly,

$$S(\mathbf{B}, \mathbf{q}, \omega) = \sum_{\alpha, \beta=1}^3 (\delta_{\alpha, \beta} - \hat{q}_\alpha \hat{q}_\beta) \sum_{n, n'=1}^{n_{s_1}} e^{-\beta \epsilon_n}$$

$$\begin{aligned} & \times \delta(\omega + \epsilon_n - \epsilon_{n'}) \\ & \times \langle \phi_n | \tilde{S}_\alpha(\mathbf{q}, 0) | \phi_{n'} \rangle \langle \phi_{n'} | \tilde{S}_\beta^\dagger(\mathbf{q}, 0) | \phi_n \rangle, \end{aligned} \quad (79)$$

$$\tilde{S}_\alpha(\mathbf{q}, 0) = US_\alpha(\mathbf{q}, 0)U^\dagger, \quad (80)$$

where U is the unitary operator that diagonalized \mathcal{H} . When exact expressions for $S(\mathbf{B}, \mathbf{q}, \omega)$ are tedious to obtain, it is straightforward to obtain it in the Hartree approximation, $S^{(1)}(\mathbf{B}, \mathbf{q}, \omega)$. But to do so, it is easiest to define the axes in the induction representation, for which $\{|\phi_n\rangle\} = \{|\tilde{\varphi}_s^m\rangle\}$ and the $\hat{e}_\alpha = \hat{\mathbf{x}}', \hat{\mathbf{y}}', \hat{\mathbf{z}}'$ for $\alpha = 1, 2, 3$, respectively. In the Hartree approximation obtained by setting the $|\tilde{\varphi}_s^m\rangle = |\varphi_s^m\rangle$, the bare wave functions, $S^{(1)}(\mathbf{B}, \mathbf{q}, \omega)$ for an arbitrary B, θ, ϕ is then

$$\begin{aligned} S_1^{(1)} &= \sum_{s=0}^{2s_1} \sum_{m=-s}^s e^{-\beta E_{s,s_1}^m} \\ & \times \left(\cos^2(\mathbf{q} \cdot \mathbf{d}) \sin^2 \theta_{b,q} \mathcal{F}_{1,s_1}^{m,s(0)}(\omega, \theta, \phi) \right. \\ & + \sin^2(\mathbf{q} \cdot \mathbf{d}) \sin^2 \theta_{b,q} \mathcal{F}_{2,s_1}^{m,s(0)}(\omega, \theta, \phi) \\ & + \cos^2(\mathbf{q} \cdot \mathbf{d}) \frac{2 - \sin^2 \theta_{b,q}}{4} \mathcal{F}_{3,s_1}^{m,s(0)}(\omega, \theta, \phi) \\ & \left. + \sin^2(\mathbf{q} \cdot \mathbf{d}) \frac{2 - \sin^2 \theta_{b,q}}{4} \mathcal{F}_{4,s_1}^{m,s(0)}(\omega, \theta, \phi) \right), \end{aligned} \quad (81)$$

where $\mathbf{q} \cdot \mathbf{d} = qd \cos \theta_q$ is invariant under the rotation, $2\mathbf{d}$ is the vector separating the dimer spins, $\theta_{b,q}$ is the angle between \mathbf{q} and \mathbf{B} , and

$$\mathcal{F}_{1,s_1}^{m,s(0)} = m^2 \delta(\omega), \quad (82)$$

$$\begin{aligned} \mathcal{F}_{2,s_1}^{m,s(0)} &= \sum_{\sigma'=\pm 1} \delta(\omega + E_{s,s_1}^m - E_{s+\sigma',s_1}^m) \\ & \times \left(D_{s+(\sigma'+1)/2,s_1}^m \right)^2, \end{aligned} \quad (83)$$

$$\mathcal{F}_{3,s_1}^{m,s(0)} = \sum_{\sigma=\pm 1} \delta(\omega + E_{s,s_1}^m - E_{s,\sigma}^{m+\sigma}) (A_s^{\sigma m})^2, \quad (84)$$

$$\begin{aligned} \mathcal{F}_{4,s_1}^{m,s(0)} &= \sum_{\sigma,\sigma'=\pm 1} \delta(\omega + E_{s,s_1}^m - E_{s+\sigma',s_1}^{m+\sigma}) \\ & \times \left(C_{s+(\sigma'+1)/2,s_1}^{-(\sigma'+1)/2-\sigma'm} \right)^2, \end{aligned} \quad (85)$$

where the coefficients are given respectively by Eqs. (21), (1), and (20), and we have suppressed the ω, θ, ϕ arguments of the $\mathcal{F}_{n,s_1}^{m,s(i)}$ functions for simplicity of presentation. In Eq. (81), the only dependencies upon the anisotropy energies is in the first-order eigenstate energies $E_{s,s_1}^m = E_s^{m,(0)} + E_{s,s_1}^{m,(1)}$ given by Eqs. (70) and (71), respectively.

As described in detail in Appendix C, corrections to the wave functions first order in the anisotropy interactions lead to the ‘‘extended Hartree’’ approximation, $S^{(1e)}(\mathbf{B}, \mathbf{q}, \omega)$, which exhibits additional transitions with

strengths first and second order in the anisotropy energies. $S^{(1e)}(\mathbf{B}, \mathbf{q}, \omega)$ contains terms arising from the traceless diagonal and off-diagonal parts of the α, β component matrix, and from the contributions of the diagonal part of the component matrix containing corrections to its trace. These latter terms are proportional to the same four functions of \mathbf{q} as in Eq. (81), and can be separated experimentally from the other terms by choosing the scattering plane such that $\mathbf{q} \perp \mathbf{B}$ (or $\sin \theta_{b,q} = 1$) for all (θ, ϕ) and by averaging over all azimuthal angles $\phi_{b,q}$. Then, the transitions from (s, m) to (s', m') , where $s' = s \pm 2, 3$ and $m' = m, m \pm 1, m \pm 2, m \pm 3$ with leading amplitudes second order in the anisotropy interactions upon depend upon the the local anisotropy interactions J_a and J_e through the three functions $f_n(\theta, \phi)$ with $n = 3, 6, 7$ given in Appendix D. Hence, if these transitions can be identified, a study of the (θ, ϕ) dependencies of their strengths can provide direct measurements of those parameters. Then, studying the weak transitions $(s, m) \rightarrow (s', m')$ with $s' = s, m \pm 1, \pm 2, \pm 3$ and $s' = s \pm 1, m' = m \pm 2$ can provide further measurements of the global anisotropy interactions J_d and J_d .

2. Electron paramagnetic resonance susceptibility

In an EPR experiment, one applies a strong magnetic field, plus a weak oscillatory transverse field, leading to the overall induction $\mathbf{B} = B\hat{\mathbf{z}}' + B_\perp[\hat{\mathbf{x}}' \cos(\omega t) - \sigma\hat{\mathbf{y}}' \sin(\omega t)]$, where we assume the oscillatory induction precesses clockwise (counterclockwise) for $\sigma = \pm 1$. [26] For a weak transverse induction B_\perp , one measures the resulting linear response $\chi_{-\sigma,\sigma}(\mathbf{B}, \omega)$ given by

$$\chi_{-\sigma,\sigma} = \frac{i\gamma^2}{Z} \int_0^\infty \frac{dt}{2\pi} e^{i(\omega+i\eta)t} \text{Tr} \left(e^{-\beta\mathcal{H}} [S_{-\sigma}(t), S_\sigma(0)] \right), \quad (86)$$

$$S_\sigma(t) = e^{i\mathcal{H}t} S_\sigma(0) e^{-i\mathcal{H}t}, \quad (87)$$

where $\eta = 0+$, the global spin raising and lowering operators S_\pm are defined in the induction representation, as described in Appendix B and Z is the partition function, and $[a, b] = ab - ba$ is the commutator. In principle, an exact expression for $\chi_{-\sigma,\sigma}(\mathbf{B}, \omega)$ can be obtained by starting in the induction representation with the basis $\{|\varphi_s^m\rangle\}$, diagonalizing \mathcal{H} with the unitary operator V , $V\mathcal{H}V^\dagger = \tilde{\mathcal{H}}'$, and the new basis $\{|\tilde{\phi}_n\rangle\}$ is obtained from $|\tilde{\phi}_n\rangle = V|\varphi_s^m\rangle$, leading to $\tilde{\mathcal{H}}'|\tilde{\phi}_n\rangle = \tilde{\epsilon}_n|\tilde{\phi}_n\rangle$. One then has

$$\begin{aligned} \chi_{-\sigma,\sigma}(\mathbf{B}, \omega) &= \frac{\gamma^2}{\pi Z} \sum_{n,n'=1}^{n_{s_1}} e^{-\beta\tilde{\epsilon}_n} \\ & \times \langle \tilde{\phi}_n | \tilde{S}_{-\sigma}(0) | \tilde{\phi}_{n'} \rangle \langle \tilde{\phi}_{n'} | \tilde{S}_\sigma(0) | \tilde{\phi}_n \rangle \\ & \times \left(\frac{1}{\omega + \tilde{\epsilon}_n - \tilde{\epsilon}_{n'} + i\eta} \right. \\ & \left. - \frac{1}{\omega - \tilde{\epsilon}_n + \tilde{\epsilon}_{n'} + i\eta} \right), \end{aligned} \quad (88)$$

where $\tilde{S}_\sigma(0) = VS_\sigma(0)V^\dagger$. It is then elementary to obtain $\chi''_{-\sigma,\sigma}(\omega)$ in the Hartree approximation valid to first order in the anisotropy parameters, which is well-behaved for all induction values. The imaginary part of $\chi_{-\sigma,\sigma}$ is then

$$\begin{aligned} \chi_{-\sigma,\sigma}^{(1)''}(\mathbf{B}, \omega) &= \frac{\gamma^2}{Z^{(1)}} \sum_{s=0}^{2s_1} \sum_{m=-s}^s \exp[-\beta E_{s,s_1}^m] \\ &\quad [s(s+1) - m^2 - \sigma m] \\ &\quad \times \left(\delta(E_{s,s_1}^m - E_{s,s_1}^{m+\sigma} + \omega) \right. \\ &\quad \left. - \delta(E_{s,s_1}^{m+\sigma} - E_{s,s_1}^m + \omega) \right), \quad (89) \end{aligned}$$

where $E_{s,s_1}^m = E_s^{m,(0)} + E_{s,s_1}^{m,(1)}$ is given by Eqs. (70) and (71) and $Z^{(1)}$ is given by Eq. (74). The arguments of the δ -function give rise to the resonant frequencies first order in the anisotropy energies, or to the first order resonant magnetic inductions,

$$\gamma B_{\text{res}}^{(1)} = \pm\omega + \frac{(2m + \sigma)}{2} g_{s,s_1}(\theta, \phi), \quad (90)$$

$$\begin{aligned} g_{s,s_1}(\theta, \phi) &= \tilde{J}_{b,a}^{s,s_1} (1 - 3 \cos^2 \theta) \\ &\quad - 3 \tilde{J}_{d,e}^{s,s_1} \sin^2 \theta \cos(2\phi), \quad (91) \end{aligned}$$

where $\tilde{J}_{b,a}^{s,s_1}$ and $\tilde{J}_{d,e}^{s,s_1}$ are given by Eqs. (72) and (73), respectively, and we have ignored the processes that give rise to finite transition widths.[27] By varying the direction and magnitude of \mathbf{B} , it is possible to obtain sufficient information to fit all of the parameters in the model. At low T the $m = s$ states dominate, so that only $\sigma = -1$ is allowed. By increasing \mathbf{B} past the s th level crossing, one can probe the effective s th state of the AFM dimer using EPR.

In Appendix C, we extend these results to include the corrections to the wave functions first order in the anisotropy interactions. With these corrections, additional EPR transitions are present, which can provide additional information useful in experimental identification of the anisotropy interactions. It is shown that there are 10 additional resonant magnetic induction strengths of the forms

$$\gamma B_{\text{res}}^{(1)} = \pm a_n \omega + b_n g_{s,s_1}(\theta, \phi) + c_n h_{s,s_1}(\theta, \phi), \quad (92)$$

$$\begin{aligned} h_{s,s_1}(\theta, \phi) &= -(J + 2J_b + J_a) \\ &\quad + \tilde{J}_{b,a}^{s,s_1} (1 + \cos^2 \theta) \\ &\quad + \tilde{J}_{d,e}^{s,s_1} \sin^2 \theta \cos(2\phi), \quad (93) \end{aligned}$$

where the a_n , b_n , and c_n are listed in Appendix C. We note that these additional resonant inductions are first order in the anisotropy interactions, but have amplitudes that are second order in the anisotropy interactions, so that in most cases, they may be difficult to detect, but their detection in certain materials would provide a clear

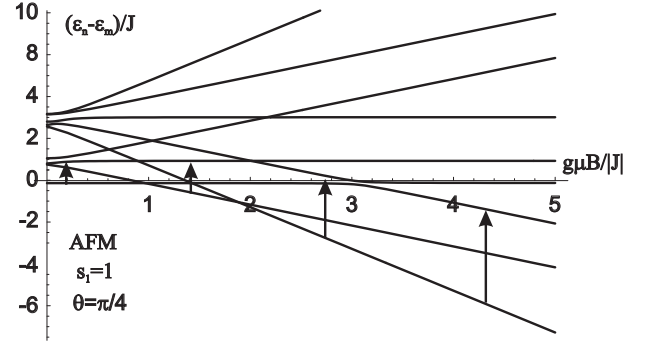


FIG. 18: Plot of the exact eigenvalues $\epsilon_n/|J|$ versus $\gamma B/|J|$ for $s_1 = 1$ AFM dimers with $J_a/J = 0.1$ and $\theta = \pi/4$. The arrows represent the strongest EPR transitions at their corresponding field strengths.

signal of the presence of significantly strong anisotropy interactions. In addition, resonant inductions with $c_n \neq 0$ are generally very large.

To illustrate one example of an effect of local spin anisotropy upon the EPR transitions, we consider the simple case of an $s_1 = 1$ AFM dimer with the only non-vanishing anisotropy energy $J_a/J = 0.1$ and $\theta = \pi/4$. The energy levels for this system are pictured in Fig. 18. In Fig. 19, the EPR transition energies versus $\gamma B/|J|$ for the $s_1 = 1$ AFM dimer with $J_a/J = 0.1$ and $\theta = \pi/4$ are shown. The widths of the lines are proportional to the strengths of the EPR matrix elements. Note that the ground state at $B = 0$ is approximately $|\psi_0^0\rangle$, but its energy is slightly negative due to an admixture of this state with the nominal $|\psi_2^m\rangle$ states with even m , as shown in Appendix A. The EPR matrix elements are very small at these B values, as the transitions only exist due to the admixture of the wave functions. At higher B strengths, the ground state goes through two level crossings, with the first level crossing being to the lowest energy $s = 1$ state, which is nominally $|\psi_1^1\rangle$, with some mixture of the other $|\psi_1^m\rangle$ states. The leading transition is to the nominal $|\psi_1^0\rangle$ state. Then, the second level crossing causes the ground state to be the nominal $|\psi_2^2\rangle$ state, which is of course modified by the mixing with the nominal $|\psi_0^0\rangle$ and the other nominal $|\psi_2^m\rangle$ for $m = 0, -2$. Note that near to $\gamma B/|J| = 3$, there is a level repulsion. The leading EPR transition is to the nominal $|\psi_2^1\rangle$ state, and because of the strong matrix elements, the splitting of the energies due to the level repulsion should be observable in EPR experiments.

D. Level crossings first order in the anisotropy energies

We can find an expression for the s^{th} AFM level crossing at the induction $B_{s,s_1}^{\text{lc}(1)}$ to first order in the anisotropy interactions for a general s_1 spin dimer by equating

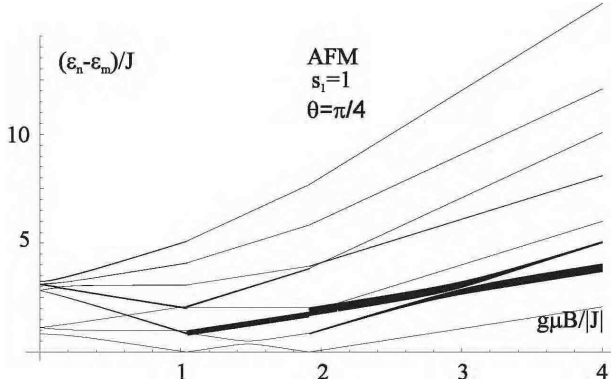


FIG. 19: Plot of the EPR transition energies $(\epsilon_n - \epsilon_m)/|J|$ versus $\gamma B/|J|$ from the ground state for the $s_1 = 1$ AFM dimer with $J_a/J = 0.1$ and $\theta = \pi/4$. The widths of the lines are proportional to the strengths of the matrix elements for the transitions.

$E_s^{s,(0)} + E_{s,s_1}^{s,(1)}$ to $E_{s-1}^{s-1,(0)} + E_{s-1,s_1}^{s-1,(1)}$, yielding

$$\begin{aligned} \gamma B_{s,s_1}^{\text{lc}(1)} = & -Js - J_b/2 - c_{s,s_1} J_a \\ & - \frac{(4s-3)}{2} [J_b \cos^2 \theta + J_d \sin^2 \theta \cos(2\phi)] \\ & + 3c_{s,s_1} [J_a \cos^2 \theta + J_e \sin^2 \theta \cos(2\phi)], \quad (94) \end{aligned}$$

$$c_{s,s_1} = \frac{[3 + 3s - 5s^2 - 4s^3 + 4s_1(s_1 + 1)]}{2(2s+1)(2s+3)}. \quad (95)$$

This expression is consistent with those obtained for $s_1 = 1/2, 1, 5/2$ given by Eqs. (57), (59)-(62), and (63)-(68). in Figs. 11-14. We note that $\gamma B_{s,s_1}^{\text{lc}(1)}$ contains the θ, ϕ -independent terms, $-Js - J_b/2 - c_{s,s_1} J_a$, which distinguish J_b from J_d and J_a from J_e .

In particular, we note that the single-ion anisotropy interactions behave very differently with increasing step number than do the global anisotropy interactions, especially for large s_1 . For the three cases we studied in detail, for $s_1 = 1/2$, $c_{1,1/2} = 0$, so that the local anisotropy terms are irrelevant, for $s_1 = 1$, $c_{1,1} = \frac{1}{6}$ and $c_{2,1} = -\frac{1}{2}$ have different signs, and for $s_1 = 5/2$ as in Fe_2 dimers, the first three $c_{s,5/2}$ coefficients are $\frac{16}{15}$, $-\frac{4}{35}$, and $-\frac{53}{63}$, respectively, the second being an order of magnitude smaller than the other two, and opposite in sign from the first. For $s_1 = 9/2$ dimers such as $[\text{Mn}_4]_2$, the first four $c_{s,9/2}$ are $\frac{16}{5}$, $\frac{4}{5}$, $-\frac{1}{3}$, and $-\frac{37}{33}$, which changes sign between $s = 2$ and $s = 3$, where its magnitude is a minimum.

This is in sharp contrast to the global anisotropy interactions, for which the analogous coefficient $(4s-3)/2$ increases monotonically with s , independent of s_1 . These differences should be possible to verify experimentally in careful low- T experiments at high magnetic fields applied at various directions on single crystals of those $s_1 = 5/2$ Fe_2 and $s_1 = 9/2$ $[\text{Mn}_4]_2$ dimers for which $|J|$ is sufficiently small.

E. Level crossings to second order in the anisotropy energies

To aid in the analysis of experimental data, we have extended this perturbative calculation to second order in each of the four principle J_j . Since we expect the $|J_j/J| \leq 0.1$ in most circumstances, this extension ought to be sufficient to accurately analyze most experimentally important samples. Since the c_{s,s_1} magnitudes can become larger than unity for $s_1 = 5/2$ and especially for $s_1 = 9/2$, we expect second order corrections to be significant in those cases. To second order in the anisotropy interactions, the eigenstate energies $E_{s,s_1}^{m,(2)}$ are given in Appendix C. We note that the $E_{s,s_1}^{m,(2)}$ contain divergences at $\gamma B/|J| = 0, 2s-1, 2s+3, s-1/2$, and $s+3/2$, so that near to those values, one would need to modify the perturbation expansion to take proper account of the degeneracies. Hence, the expressions for $E_{s,s_1}^{m,(2)}$ cannot be used in the asymptotic expressions for the thermodynamics, Eqs. (74)-(76). However, as the s th AFM level crossing occurs approximately at $\gamma B/|J| = s$, which is far from any divergences, we can safely use this second order expansion to obtain an expression for the level crossings second order in the anisotropy interaction energies. We find

$$\gamma B_{s,s_1}^{\text{lc}(2)} = \gamma B_{s,s_1}^{\text{lc}(1)} + \left(E_{s,s_1}^{s,(2)} - E_{s-1,s_1}^{s-1,(2)} \right) \Big|_{B=-Js/\gamma}, \quad (96)$$

where $\gamma B_{s,s_1}^{\text{lc}(1)}$ is given by Eq. (94).

The full expression for the second term in Eq. (96) is given in Appendix D. From this expression, it is easy to see that for $s_1 = 1/2$, $E_{1,1/2}^{\text{lc}(2)} = \frac{1}{2} f_1^{(2)}(\theta, \phi) + \frac{1}{8} f_4^{(2)}(\theta, \phi)$, where $f_1^{(2)}$ and $f_4^{(2)}$ are given in Appendix C. For $\mathbf{B} \parallel \hat{z}$, $E_{1,1/2}^{\text{lc}(2)} = -\frac{1}{2} J_d^2/|J|$, and with $\mathbf{B} \parallel \hat{x}, \hat{y}$, $E_{1,1/2}^{\text{lc}(2)} = -\frac{1}{8} (J_b \pm J_d)^2/|J|$, in agreement with the expansion to second order in the J_j of our exact formulas in Eq. (57). However, the second order functions have more complicated θ, ϕ dependencies than do the first order $B_{s,s_1}^{\text{lc}(1)}$ in Eq. (94). We have also explicitly checked each formula in Appendix D for $s_1 = 1$ and $s = 1, 2$. Thus, Eq. (96) is a highly accurate expression for the full θ, ϕ dependencies of all $s = 1, \dots, 2s_1 + 1$ level crossings of a single crystal dimer of single ion spin s_1 .

By superposing this non-universal level-crossing formula, Eq. (96), combined with the universal behavior presented in Eqs. (40)-(44), it is easy to use our results in accurate fits to experimental data at low temperatures and high magnetic induction strengths.

VIII. AFM DIMERS WITH STRONG ANISOTROPY INTERACTIONS

Finally, we consider some cases of strong anisotropy interactions, in which one or more of the J_j is comparable to J in magnitude. The cases of interest are those for which the anisotropy interactions can remove the level crossing effects in AFM dimers that give rise to the $2s_1+1$ $M(B)$ steps and $C_V(B)$ double peaks. These cases generally occur for strong FM anisotropy interactions, but there are some examples in which they can occur with strong AFM anisotropy interactions. We first consider the case of $s_1 = 1/2$ dimers, for which the situation can be analyzed analytically, at least for $\mathbf{B} \parallel \hat{z}$. Then, we consider the $s_1 = 5/2$ case numerically.

A. Analytic and numerical results for $s_1 = 1/2$ dimers

For the $s_1 = 1/2$ dimer, the energies for $\mathbf{B} \parallel \hat{i}$ are given by Eqs. (45)-(51). We are interested in examining the cases in which the anisotropy is strong enough to cause the level crossing to disappear. Strong anisotropy with J_b and J_d having the same sign as J do not differ significantly from the weak coupling cases, as they do not remove the level crossing, and do not affect significantly the heights of the magnetization step and the number and shapes of the $C_V(B)$ double peaks, but just shift their positions, as for weak anisotropy. There are then three AFM ($J < 0$) cases of interest. These are: (1) $J_b = J_d = |J|/2$, (2) $J_b = |J|$, and (3) $J_d = |J|$. The $M(B)$ and $C_V(B)$ curves for these cases with $\mathbf{B} \parallel \hat{z}$ at the very low- T value $k_B T/|J| = 0.01$ are shown as the solid, dotted, and dashed curves in Fig. 20 and 21, respectively.

For case (1), $J_b = J_d = |J|/2$, the same four eigenvalues are obtained for $\mathbf{B} \parallel \hat{z}$ and $\mathbf{B} \parallel \hat{x}$. Assuming $J < 0$, these are ranked from highest to lowest as

$$\epsilon_4 = -J/2 + \sqrt{b^2 + J^2/4}, \quad (97)$$

$$\epsilon_3 = -J, \quad (98)$$

$$\epsilon_2 = 0, \quad (99)$$

$$\epsilon_1 = -J/2 - \sqrt{b^2 + J^2/4}. \quad (100)$$

Note that $\epsilon_1 = \epsilon_2$ only at $b = 0$ (where $\epsilon_3 = \epsilon_4$), ϵ_1 decreases with increasing b , and ϵ_4 increases with increasing b , so the levels get further apart with increasing b . In this case, $M(B)$ shown as the dotted curve in Fig. 20 is broad, even at the very low T value plotted. In addition, $C_V(B)$, shown as the dotted curve in Fig. 19, exhibits a single Schottky-like anomaly, but with a different shape than that of the standard Schottky case, which arises from a splitting of the two lowest energies linear in b at $b = 0$. In this case, the peak value of C_V/k_B is 0.439229, the same as the uniform double peak value, but the peak position is as $b = \sqrt{2c|J|/\beta}$, where $c = 1.19967864$.

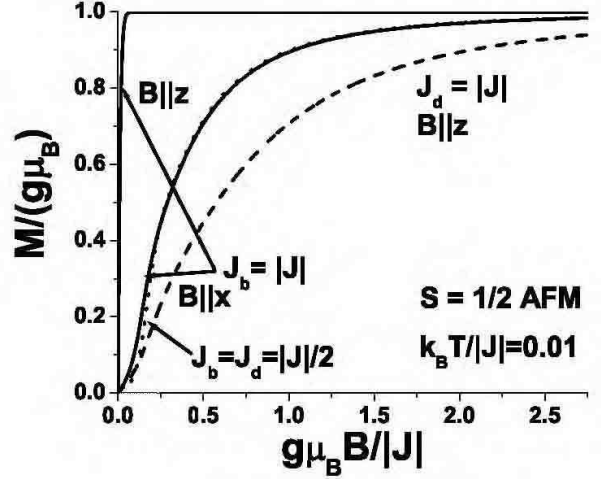


FIG. 20: Plots of M/γ versus $\gamma B/|J|$ at $k_B T/|J| = 0.01$ with $J_b = |J|$ (solid) for both $\mathbf{B} \parallel \hat{x}, \hat{z}$, $J_b = J_d = |J|/2$ (dotted), and $J_d = |J|$ with $\mathbf{B} \parallel \hat{z}$ (dashed) for the $s_1 = 1/2$ AFM dimer.

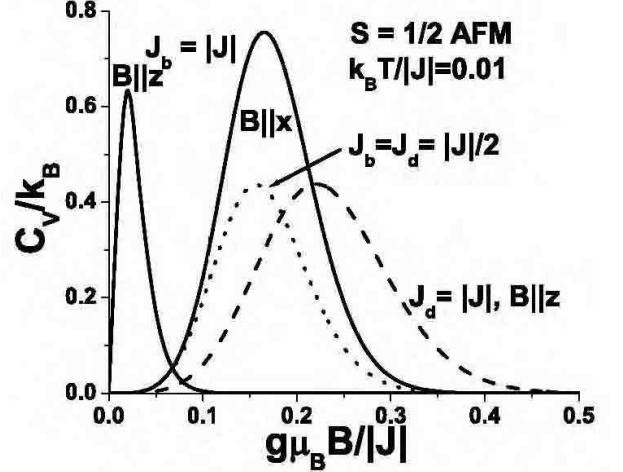


FIG. 21: Plots of C_V/k_B versus $\gamma B/|J|$ at $k_B T/|J| = 0.01$ with $J_b = |J|$ (solid) for both $\mathbf{B} \parallel \hat{x}, \hat{z}$, $J_b = J_d = |J|/2$ (dotted), and $J_d = |J|$ with $\mathbf{B} \parallel \hat{z}$ (dashed) for the $s_1 = 1/2$ AFM dimer.

Next, we examine case (2), $J_b = |J|$, $J_d = 0$. In this case the energies are different for the two field directions. For $\mathbf{B} \parallel \hat{z}$ that

$$\epsilon_4 = -J, \quad (101)$$

$$\epsilon_3 = b, \quad (102)$$

$$\epsilon_2 = 0, \quad (103)$$

$$\epsilon_1 = -b. \quad (104)$$

At $b = 0$, these energies comprise a triply degenerate (or spin 1) ground state at 0 and an excited $+|J|$ state. With increasing b , ϵ_1 decreases linearly, and ϵ_4 increases linearly, crossing ϵ_4 at $b = |J|$, which does not affect the

low- T thermodynamics. In this case, $M(B)$ is a sharp step at $B = 0$, shown as a solid curve in Fig. 20, and $C_V(B)$ is a conventional spin 1 Schottky anomaly at low b , as shown by the left solid curve in Fig. 21. From Eqs. (102)-(104), C_V/k_b has a maximum value at 0.637203 at $b = 1.8806775/\beta$. Note that the larger maximum value than in the other $C_V(B)$ cases arises from the higher degeneracy as $b \rightarrow 0$.

For $\mathbf{b}||\hat{\mathbf{x}}$, the energies for case (2) are

$$\epsilon_4 = -J/2 + \sqrt{b^2 + J^2/4}, \quad (105)$$

$$\epsilon_3 = 0, \quad (106)$$

$$\epsilon_2 = 0, \quad (107)$$

$$\epsilon_1 = -J/2 - \sqrt{b^2 + J^2/4}. \quad (108)$$

At $b = 0$, the ground state is again triply degenerate with energy 0, and the excited state has energy $|J|$. With increasing b , ϵ_1 separates from ϵ_2 and ϵ_3 , curving below them, and ϵ_4 increases quadratically. For this induction direction there is no level crossing, but there is some \mathbf{b} anisotropy at finite T , because of the quadratic versus linear b dependencies. C_V/k_B has the maximum value 0.761802 at $b = \sqrt{2c_1|J|}/\beta$, where $c_1 = 2.654658$, which is noticeably different from the case with $\mathbf{B}||\hat{\mathbf{z}}$. The $M(B)$ and $C_V(B)$ curves are the right solid curves in Figs. 20 and 21, respectively.

Now we consider case (3), $J_d = -J$, $J_b = 0$. Again, there are slight differences for $\mathbf{B}||\hat{\mathbf{z}}$ and $\mathbf{B}||\hat{\mathbf{x}}$. For $\mathbf{B}||\hat{\mathbf{z}}$, the eigenstate energies are

$$\epsilon_4 = -J + \sqrt{b^2 + J^2}, \quad (109)$$

$$\epsilon_3 = -J, \quad (110)$$

$$\epsilon_2 = 0, \quad (111)$$

$$\epsilon_1 = -J - \sqrt{b^2 + J^2}. \quad (112)$$

At $b = 0$, the ground state is doubly degenerate at energy 0. The other two states have energies $|J|$ and $2|J|$, respectively. As b increases, ϵ_1 decreases below ϵ_2 , and ϵ_4 increases monotonically. Hence, there is no level crossing, but at low T , two levels are relevant, in a fashion slightly different from a standard Schottky specific heat anomaly. The low- T $M(B)$ and $C_V(B)$ curves for this induction direction are shown as the dashed curves in Figs. 20 and 21, respectively. We note that they are rather similar from those of case (1), but have the broadest $M(B)$ increase and $C_V(B)$ peak of the three cases considered. C_V/k_B has the peak value 0.439229 which is the same as the uniform double-peak value, but its position is at $b = 2\sqrt{c|J|}/\beta$, where $c = 0.19967864$.

For $\mathbf{B}||\hat{\mathbf{x}}$, we have

$$\epsilon_4 = -2J, \quad (113)$$

$$\epsilon_3 = -J/2 + \sqrt{b^2 + J^2/4}, \quad (114)$$

$$\epsilon_2 = 0, \quad (115)$$

$$\epsilon_1 = -J/2 - \sqrt{b^2 + J^2/4}. \quad (116)$$

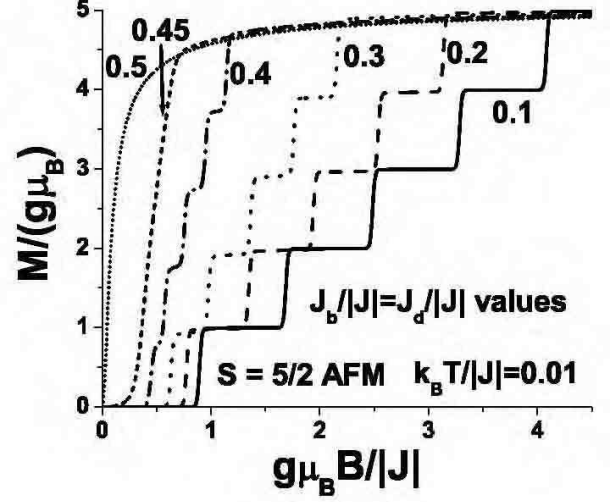


FIG. 22: Plots of M/γ versus $\gamma B/|J|$ at $k_B T/|J| = 0.01$ with $J_b = J_d = c|J|$ for the AFM $s_1 = 5/2$ dimer. The cases $c = 0.1$ (solid), $c = 0.2$ (dashed), $c = 0.3$ (dotted), $c = 0.4$ (dot-dashed), $c = 0.45$ (short dashed), and $c = 0.5$ (short dotted) are shown.

At $b = 0$, the eigenstates are the same as for the field in the z direction, with a doubly degenerate ground state at 0, and excited states at $|J|$ and $2|J|$. However, the field dependence is a bit different than for the z direction. Again the ground state decreases with increasing b , but the energy scale of the curvature is $|J|/2$ instead of $|J|$. In addition, ϵ_3 can cross ϵ_4 at $b = \sqrt{2}|J|$. This level crossing is irrelevant to the low- T behavior, however, but modifies the $M(B)$ curve somewhat at finite T .

B. AFM $s_1 = 5/2$ dimers with strong anisotropy interactions

We now consider some cases of strong anisotropy interactions in the $s_1 = 5/2$ dimer. In Fig. 22, we present low- T plots of $M(B)$ with $J_b = J_d = c|J|$, where $c = 0.1, 0.2, 0.3, 0.4, 0.45$ and 0.5 , as indicated. For the weak coupling case $c = 0.1$, the steps have uniform height. With increasing c , the curves shift monotonically to lower b values. Slight deviations in the uniformity of the step height are detectable in the first two steps for $c = 0.2$, but the nonuniformity in the step height is progressively more pronounced for $c = 0.3$ and 0.4 , respectively. However, for $c = 0.45$, the individual steps have completely disappeared, and are replaced by what appears to be a single, broad step centered at $b/J \approx 0.5$. At $c = 0.5$, $M(B)$ rises to its maximum value with a very steep slope at $b = 0$, not showing any evidence for any level crossings.

Next, we investigated the effects of large J_a . In Fig. 23 we plotted M/γ versus $\gamma B/|J|$ for $J_a = c|J|$, with $c = 0.1$

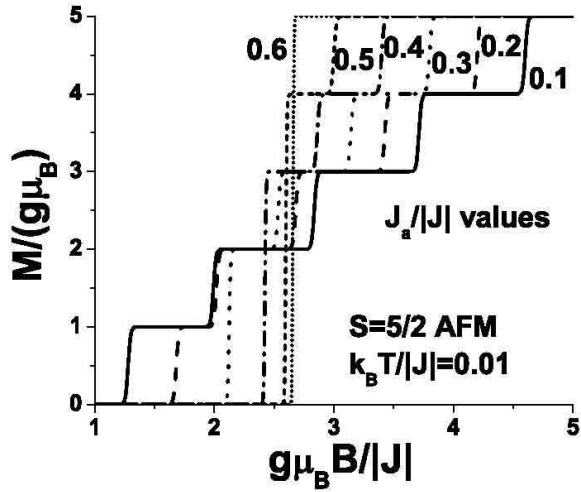


FIG. 23: Plots of M/γ versus $\gamma B/|J|$ at $k_B T/|J| = 0.01$ with $J_a = c|J|$ for the AFM $s_1 = 5/2$ dimer. The cases $c = 0.1$ (solid), $c = 0.2$ (dashed), $c = 0.3$ (dotted), $c = 0.4$ (dot-dashed), $c = 0.5$ (short dashed), and $c = 0.6$ (short dotted) are shown.

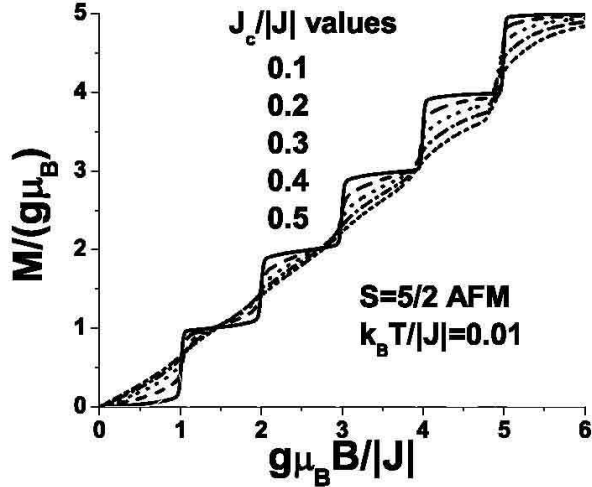


FIG. 24: Plots of M/γ versus $\gamma B/|J|$ at $k_B T/|J| = 0.01$ with $J_c = c|J|$ for the AFM $s_1 = 5/2$ dimer. The cases $c = 0.1$ (solid), $c = 0.2$ (dashed), $c = 0.3$ (dotted), $c = 0.4$ (dot-dashed), and $c = 0.5$ (short dotted) are shown.

(solid), 0.2 (dashed), 0.3 (dotted), 0.4 (dot-dashed), 0.5 (short dashed), and 0.6 (short dotted). We see the effects of strong J_a are very different from those of strong J_b and J_d shown in Fig. 22. Instead of the step positions decreasing monotonically with increasing $J_b = J_d$, as J_a increases, the highest three step positions decrease with increasing J_a , but the lowest two step positions increase with increasing J_a .

We now consider the case of large J_c . In Fig. 24, we plotted M/γ versus $b/|J|$ at $k_B T/|J| = 0.01$ for the $s_1 = 5/2$ AFM dimer with $J_c = c|J|$, where $c =$

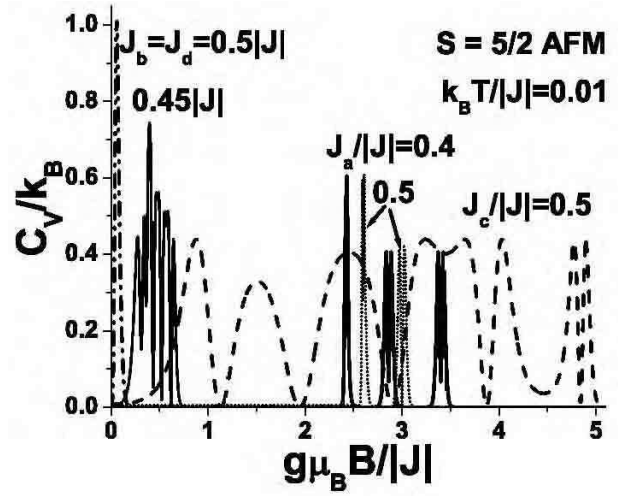


FIG. 25: Plots of C_V/k_B versus $\gamma B/|J|$ at $k_B T/|J| = 0.01$ for the AFM $s_1 = 5/2$ dimer. The cases $J_b = J_d = c|J|$ for $c = 0.45$ (solid) and $c = 0.5$ (dot-dashed), $J_a = c|J|$ for $c = 0.4$ (solid) and 0.5 (short-dashed) and $J_c = 0.5|J|$ (thick dashed) are shown.

0.1, 0.2, 0.3, 0.4, and 0.5. These results are shown respectively as the solid, dashed, dotted, dot-dashed, and short dotted curves. Unlike the strong global anisotropy case pictured in Fig. 22 and the strong local axial anisotropy case pictured in Fig. 23, these curves do not shift significantly to lower b values with increasing $J_c/|J|$, but the step shapes are greatly altered. With $c = 0.4$, the first two steps are hard to discern, but rounded remnants of the three last steps are evident. At $c = 0.5$, the third step is hard to detect, and the remnants of the last two steps are reduced in magnitude. We remark that the curve with $c = -0.3$ is indistinguishable from the dotted curve for $c = 0.3$, so that in this case, strong $J_c/|J|$ of either sign can grossly alter the $M(B)$ step behavior.

In Fig. 25, we show C_V/k_B versus $b/|J|$ low- T curves for some of the AFM $s_1 = 5/2$ cases pictured in Fig. 22-24. The solid and dotted curves on the left-hand side of the figure correspond to $J_b = J_d = c|J|$ with $c = 0.45$ and 0.5 , respectively, the solid and dot-dashed curves in the central portion of the figure correspond to $J_a/|J| = 0.4$ and 0.5 , respectively, and the dashed curve running throughout the domain pictured corresponds to $J_c = 0.5|J|$. We note that for the global anisotropy case shown, strong anisotropy pushes the $C_V(B)$ peaks to lower b , and squeezes them together, so that they tend to overlap. At the limiting case $J_b = J_d = 0.5|J|$, the individual level crossings have been eliminated, and all ten of the peaks are combined into a single Schottky anomaly. For the local axial anisotropy interaction, strong FM anisotropic interaction squeeze the $C_V(B)$ together in the middle of the domain, with the limiting case of a single peak at $J_a/|J| = 0.6$. For the strong azimuthal anisotropic exchange interaction case, however,

strong FM anisotropy shifts the double peak positions only slightly, and broadens the double peaks, so that only the highest set is clearly discernable, even at the very low T value plotted. In each case, the deviation of the peak height from the two-level prediction, Eq. (41), is substantial, indicating more than two levels are important at low T , as for the three-level system with $s_1 = 1/2$ and $J_b = |J|$. Thus, the different types of strong spin anisotropy lead to clearly different low- T $C_V(B)$ behaviors for $s_1 > 1/2$ dimers.

IX. SUMMARY AND CONCLUSIONS

In summary, we solved for the low-temperature magnetization and specific heat of equal spin s_1 antiferromagnetic dimer single molecule magnets, including the most general set of anisotropic spin exchange interactions quadratic in the spin operators. The magnetization and specific heat exhibit steps and zeroes, respectively, at the non-universal level-crossing induction values $B_{s,s_1}^{\text{lc}}(\theta, \phi)$, but the magnetization steps and their midpoint slopes, plus the two peaks surrounding the specific heat zeroes all exhibit universal behavior at sufficiently low temperatures to first order in the anisotropy interaction strengths. Strong anisotropy interactions generally lead to highly non-universal behavior in antiferromagnetic dimers. Local (or single-ion) anisotropy interactions lead to low-temperature magnetization step plateaus that have a much richer variation with the magnetic induction \mathbf{B} than do those obtained from global anisotropy interactions, provided that $s_1 > 1/2$. For the most general quadratic anisotropic spin interactions at an arbitrary \mathbf{B} , we derived simple, asymptotic analytic expressions for the low-temperature magnetization, specific heat, inelastic neutron scattering cross-section, and electron paramagnetic response susceptibility, which are accurate for weak anisotropy. We also derived an accurate expression for the level-crossing induction $B_{s,s_1}^{\text{lc}}(\theta, \phi)$, enabling fast and accurate fits to experimental data.

There were two low- T $M(B)$ studies of Fe_2 dimers.[16, 17] For μ -oxalatotetrakis(acetylacetonato) Fe_2 , all five peaks in dM/dH were measured in pulsed magnetic fields H . These evenly spaced peaks indicated little, if any, spin anisotropy effects.[16] On the other hand, studies of the first 2-3 dM/dH peaks in powdered samples of $[\text{Fe}(\text{salen})\text{Cl}]_2$, where salen is N, N' -ethylenebis(salicylideneiminato), were much more interesting.[17] These data showed a broad first peak at $B = 17 - 20\text{T}$ that was only partially resolvable into two separate peaks, followed by a sharp second peak at $B = 36\text{T}$, consistent with local axial anisotropy of strength $|J_a/J| \approx 0.1$, as obtained from the derivatives of the curves shown in Fig. 13. From Eqs. (63)-(68), one could also have $|(J_a \pm 3J_e)/J| \approx 0.1$. These amounts might perhaps be combined with a smaller $|J_c/J|$, ob-

tained from the derivatives of the curves pictured in Fig. 14.

Without a detailed single crystal study with magnetic fields along different crystal directions, it is impossible to determine the relative amounts of J_a and J_e that would best fit the data. However, the existing data on $[\text{Fe}(\text{salen})\text{Cl}]_2$ appear to be inconsistent with a predominant global anisotropy interaction of either type, as obtained from the derivatives of the curves shown in Figs. 11 and 12. Only single crystal studies could determine if a small amount of such global anisotropy interactions were present in addition to one or more presumably larger local spin anisotropy interactions. In comparing the two materials cited above, it appears that the interaction of a Cl^- ion neighboring each Fe^{3+} ion leads to strong local (or single-ion) anisotropy effects. In order to verify this hypothesis and to elucidate the details of the interactions, further experiments using single crystals in different field orientations on this and related Fe_2 dimers with 1-3 similarly bonded Cl^- ions are urged.[19, 20] We also urge single crystal data on some of the $s_1 = 9/2$ $[\text{Mn}_4]_2$ dimers, [14, 21, 22], as well as on $s_1 = 1/2$ dimers lacking in predicted local spin anisotropy effects. [11, 12, 13, 14] To aid in the fits, we derived simple, useful formulas for the magnetization and specific heat at low temperature and sufficiently large magnetic induction. More important, we derived accurate analytic formulas for the electron paramagnetic resonance susceptibility $\chi(|bmB, \omega)$ and the inelastic neutron scattering $S(\mathbf{B}, \mathbf{q}, \omega)$, which allow for a precise determination of the various microscopic anisotropy energies.

With local anisotropy interactions, the total spin s is not a good quantum number, potentially modifying our understanding of quantum tunneling processes in single molecule magnets. It might also be possible to fit a variety of experimental results using a smaller, consistent set of model parameters.[6] We emphasize that the study of dimer single molecule magnets, for which the most general anisotropic quadratic exchange interactions can be solved exactly, may be our best hope for attaining a more fundamental understanding of the underlying physics of more general single molecule magnets.

ACKNOWLEDGMENTS

We thank the Max-Planck-Institut für Physik komplexer Systeme, Dresden, Germany, the University of North Dakota, Grand Forks, ND, USA, and Talat S. Rahman for their kind hospitality and support. This work was supported by the Netherlands Foundation for the Fundamental Research of Matter and by the NSF under contract NER-0304665.

APPENDIX A

Single-ion operators for arbitrary s_1, s_2

For completeness, we present the results of the single-ion operators for general dimers consisting of magnetic ions with spins s_1 and s_2 . We find

$$S_{i,z}|\psi_s^m\rangle = \frac{m}{2}\left(1 - (-1)^i \xi_{s,s_1,s_2}\right)|\psi_s^m\rangle - \frac{1}{2}(-1)^i\left(D_{s,s_1,s_2}^m|\psi_{s-1}^m\rangle + D_{s+1,s_1,s_2}^m|\psi_{s+1}^m\rangle\right), \quad (117)$$

$$S_{i,\sigma}|\psi_s^m\rangle = \frac{A_s^{\sigma m}}{2}\left(1 - (-1)^i \xi_{s,s_1,s_2}\right)|\psi_s^{m+\sigma}\rangle - \frac{\sigma}{2}(-1)^i\left(C_{s,s_1,s_2}^{\sigma m}|\psi_{s-1}^{m+\sigma}\rangle - C_{s+1,s_1,s_2}^{-1-\sigma m}|\psi_{s+1}^{m+\sigma}\rangle\right), \quad (118)$$

$$C_{s,s_1,s_2}^m = \eta_{s,s_1,s_2}\sqrt{(s-m)(s-m-1)}, \quad (119)$$

$$D_{s,s_1,s_2}^m = \eta_{s,s_1,s_2}\sqrt{s^2 - m^2}, \quad (120)$$

$$\eta_{s,s_1,s_2} = \sqrt{\frac{[(s_1 + s_2 + 1)^2 - s^2][s^2 - (s_1 - s_2)^2]}{(4s^2 - 1)s^2}}, \quad (121)$$

$$\xi_{s,s_1,s_2} = \frac{s_1(s_1 + 1) - s_2(s_2 + 1)}{s(s + 1)}. \quad (122)$$

Note that for $s_1 = s_2$, $\xi_{s,s_1,s_1} = 0$ and η_{s,s_1,s_1} reduces to Eq. (22) for η_{s,s_1} . Also, note that these relations preserve the global spin properties of $S_z = S_{1,z} + S_{2,z}$ and $S_\sigma = S_{1,\sigma} + S_{2,\sigma}$, $S_z|\psi_s^m\rangle = m|\psi_s^m\rangle$ and $S_\sigma|\psi_s^m\rangle = A_s^{\sigma m}|\psi_s^{m+\sigma}\rangle$, as for equal spin dimers. In addition, the spins on asymmetric dimers with $s_1 \neq s_2$ would be expected to also have different local anisotropy interactions, so that \mathcal{H}_a and \mathcal{H}_e would become

$$\mathcal{H}'_a = -\sum_{i=1}^2 J_{a,i} S_{i,z}^2, \quad (123)$$

$$\mathcal{H}'_e = -\sum_{i=1}^2 J_{e,i} (S_{i,x}^2 - S_{i,y}^2). \quad (124)$$

Specific heat details for $s_1 = 1/2$

We first present the numerators of the exact expressions for the specific heat with $s_1 = 1/2$ and $\mathbf{B}||\hat{\mathbf{i}}$ for $i = x, y, z$. We have

$$\begin{aligned} \mathcal{N}_{x,y} &= F_{x,y}^2 + \frac{1}{4}(J + 2J_{y,x})^2 e^{\beta[2(J_{y,x} - J_{x,y}) - J]} \\ &\quad + F_{x,y} \sinh(\beta F_{x,y}) e^{-\beta J_{x,y}} \\ &\quad \times [(J + J_{x,y}) e^{-\beta J} + (J_{x,y} - 2J_{y,x}) e^{2\beta J_{y,x}}] \end{aligned}$$

$$\begin{aligned} &+ \frac{1}{2} e^{-\beta J_{x,y}} \cosh(\beta F_{x,y}) \\ &\times \left([(J + J_{x,y})^2 + F_{x,y}^2] e^{-\beta J} \right. \\ &\quad \left. + [(2J_{y,x} - J_{x,y})^2 + F_{x,y}^2] e^{2\beta J_{y,x}} \right), \quad (125) \end{aligned}$$

$$\begin{aligned} \mathcal{N}_z &= F_z^2 \cosh(2\beta F_z) + \frac{J^2}{4} e^{-\beta(J+2J_b)} \\ &\quad + \frac{1}{2} \cosh(\beta F_z) \left(\Delta_z (J_b^2 + F_z^2) \right. \\ &\quad \left. + e^{-\beta(J+J_b)} J(J+2J_b) \right) \\ &\quad + F_z \sinh(\beta F_z) \left(J_b \Delta_z + J e^{-\beta(J+J_b)} \right). \quad (126) \end{aligned}$$

Eigenvalues for $s_1 = 1$ in the crystal representation

In the remainder of this appendix, we provide some details of our exact results for $s_1 = 1$. The cubic equation for the three $s = 1$ eigenvalues is given by

$$\begin{aligned} \epsilon_n &= -J - J_b - J_a + \lambda_n, \quad \text{for } n = 2, 3, 4, \quad (127) \\ 0 &= -\lambda_n^3 - (J_a - J_b)\lambda_n^2 + \lambda_n[b^2 + (J_d - J_e)^2] \\ &\quad + (J_a - J_b)[b^2 \cos^2 \theta + (J_d - J_e)^2] \\ &\quad - (J_d - J_e)(b^2 \sin^2 \theta \cos(2\phi)). \quad (128) \end{aligned}$$

For $\mathbf{B}||\hat{\mathbf{z}}$, the cubic equation is easily solved to yield

$$\lambda_n = J_b - J_a, \pm \sqrt{b^2 + (J_d - J_e)^2}. \quad (129)$$

For $\mathbf{B}||\hat{\mathbf{x}}, \hat{\mathbf{y}}$, we have

$$\lambda_n = \pm(J_e - J_d), -J_{y,x} \pm \sqrt{b^2 + \bar{J}_{x,y}^2}, \quad (130)$$

$$\bar{J}_{x,y} = \frac{1}{2}[J_a - J_b \mp (J_d - J_e)], \quad (131)$$

where \bar{J}_x (\bar{J}_y) corresponds to the upper (lower) sign.

The six eigenvalues for the mixed $s = 0, 2$ states satisfy

$$\epsilon_n = -3J - \frac{4}{3}J_a - 2J_b + \lambda_n \quad (132)$$

We first define

$$a = -\frac{\sqrt{8}}{3}J_a, \quad (133)$$

$$b_\perp = -b \sin \theta e^{-i\phi}, \quad (134)$$

$$b_3 = \sqrt{\frac{3}{2}}b_\perp, \quad (135)$$

$$d = -\sqrt{6}(J_d + J_e/3), \quad (136)$$

$$d_3 = \sqrt{\frac{3}{2}}d, \quad (137)$$

$$e = -\frac{2}{\sqrt{3}}J_e, \quad (138)$$

$$\tilde{J} = J - \frac{2}{9}J_a, \quad (139)$$

and

$$Q_n^p = n(J_b + J_a/3) + pb \cos \theta. \quad (140)$$

Then the λ_n are the eigenvalues of the Hermitian matrix $\overset{\leftrightarrow}{M}$ given by

$$\overset{\leftrightarrow}{M} = \begin{pmatrix} Q_{-2}^{-2} & b_{\perp} & d & 0 & 0 & e \\ b_{\perp}^* & Q_1^{-1} & b_3 & d_3 & 0 & 0 \\ d & b_3^* & Q_2^0 & b_3 & d & a \\ 0 & d_3 & b_3^* & Q_1^1 & b_{\perp} & 0 \\ 0 & 0 & d & b_{\perp}^* & Q_{-2}^2 & e \\ e & 0 & a & 0 & e & Q_2^0 + 3\tilde{J} \end{pmatrix}. \quad (141)$$

The resulting sixth order polynomial for the λ_n is given elsewhere.[25] We note that for $\mathbf{B}||\hat{\mathbf{i}}$, $\overset{\leftrightarrow}{M}$ is block diagonal, breaking up into matrices of ranks two and four. These cases are discussed in detail elsewhere.[25] Here we only present the simplest data for which the eigenvalues are determined either by linear or by quadratic equations.

Simple special cases

When only one of the $J_j \neq 0$, the eigenvalues for $\mathbf{B}||\hat{\mathbf{z}}$ simplify considerably. For $J_b \neq 0$, we have

$$\lambda_n^z = 3J + 2J_b, 2J_b, J_b \pm b, -2J_b \pm 2b. \quad (142)$$

For $J_d \neq 0$, we find

$$\lambda_n^z = 0, 3J, \pm\sqrt{b^2 + 9J_d^2}, \pm 2\sqrt{b^2 + 3J_d^2}. \quad (143)$$

For $J_a \neq 0$, the eigenvalues can also be found analytically,

$$\lambda_n^z = -\frac{2J_a}{3} \pm 2b, \frac{J_a}{3} \pm b, \frac{J_a}{3} + \frac{3J}{2} \pm \sqrt{\frac{9}{4}J^2 + J_a^2 - JJ_a}. \quad (144)$$

We note that the ground state energy in this case is

$$E_1 = -\frac{3}{2}J - J_a - \sqrt{\frac{9}{4}J^2 + J_a^2 - JJ_a}, \quad (145)$$

which explicitly involves mixing of the $s = m = 0$ and the $s = 2, m = 0$ states.

At the first level crossing with $\mathbf{B}||\hat{\mathbf{z}}$, we have for $J_a \neq 0$ and the other $J_j = 0$,

$$\gamma_{B_{1,1}}^{\text{lc},z} = \frac{1}{2} \left(J + [9J^2 + 4J_a^2 - 4JJ_a]^{1/2} \right). \quad (146)$$

We note that the first level crossing for $J_b, J_d \neq 0$ for $\mathbf{B}||\hat{\mathbf{i}}$ is equivalent to that of $s_1 = 1/2$, given by Eq. (57). At the second level crossing, simple formulas are only obtained for $\mathbf{B}||\hat{\mathbf{z}}$ with one $J_j \neq 0$. For $\mathbf{B}||\hat{\mathbf{z}}$ and $J_a \neq 0$, $J_b \neq 0$ and $J_d \neq 0$, respectively, we have

$$\gamma_{B_{2,1}}^{\text{lc},z} = \begin{cases} \begin{matrix} -2J - J_a, \\ -2J - 3J_b, \end{matrix} & (147) \\ \frac{1}{3} \left(20J^2 - 30J_d^2 + 8[4J^4 - 6J^2J_d^2]^{1/2} \right)^{1/2}. \end{cases}$$

APPENDIX B

Rotation to the induction representation

The rotation from the crystal representation to the induction representation is obtained from

$$\begin{pmatrix} \hat{x} \\ \hat{y} \\ \hat{z} \end{pmatrix} = \begin{pmatrix} \cos \theta \cos \phi & -\sin \phi & \sin \theta \cos \phi \\ \cos \theta \sin \phi & \cos \phi & \sin \theta \sin \phi \\ -\sin \theta & 0 & \cos \theta \end{pmatrix} \begin{pmatrix} \hat{x}' \\ \hat{y}' \\ \hat{z}' \end{pmatrix}, \quad (148)$$

leading to $\mathbf{B} = B\hat{\mathbf{z}}'$. [28] This operation is equivalent to a rotation by $-\pi/2$ about the z axis, a rotation by θ about the transformed x axis, and then a rotation by $\pi/2 - \phi$ about the transformed z axis. [29] In effect, in using the above rotation matrix, we made the arbitrary choice that the rotated z axis lies in the $x'z'$ plane. After the above rotation, it is still possible to rotate the crystal by an arbitrary angle χ about the z' axis, keeping $\mathbf{B}||\hat{\mathbf{z}}'$. Hence, there are in effect an infinite number of equivalent rotations leading to $\mathbf{B} = B\hat{\mathbf{z}}'$. The resulting Hamiltonian matrix will then have off-diagonal elements that depend upon χ . However, all such rotations necessarily lead to the identical, χ -independent, set of eigenvalues of the resulting diagonalized Hamiltonian matrix. We have explicitly checked that the above rotation gives the exact cubic expression, Eq. (47), for the $s_1 = 1/2$ eigenvalues, and also leads to the correct eigenstate energies second order in each of the J_j for $s_1 = 1$. We also showed explicitly that χ does not enter the eigenstate energies second order in J_b for arbitrary s, s_1, m .

Global Hamiltonian

The global axial and azimuthal anisotropy interactions in the rotated frame are

$$\begin{aligned} \mathcal{H}'_b &= -J_b \left(S_{z'}^2 \cos^2 \theta + S_{x'}^2 \sin^2 \theta \right. \\ &\quad \left. - \sin(2\theta) \{S_{x'}, S_{z'}\} / 2 \right), \\ \mathcal{H}'_d &= -J_d \left[\cos(2\phi) \left(S_{x'}^2 \cos^2 \theta + S_{z'}^2 \sin^2 \theta - S_y^2 \right. \right. \\ &\quad \left. \left. + \sin(2\theta) \{S_{x'}, S_{z'}\} / 2 \right) \right. \\ &\quad \left. - \sin(2\phi) \left(\cos \theta \{S_{x'}, S_{y'}\} + \sin \theta \{S_{y'}, S_{z'}\} \right) \right], \end{aligned} \quad (149)$$

where $\{A, B\} = AB + BA$ is the anticommutator.

Global Hamiltonian matrix elements

The operations of the rotated global anisotropy interactions upon these states may be written as

$$\begin{aligned} \mathcal{H}'_b |\varphi_s^m\rangle &= -\frac{J_b}{4} \left[(4m^2 + 2[s(s+1) - 3m^2] \sin^2 \theta) |\varphi_s^m\rangle \right. \\ &\quad - \sin(2\theta) \sum_{\sigma=\pm 1} (2m + \sigma) A_s^{\sigma m} |\varphi_s^{m+\sigma}\rangle \\ &\quad \left. + \sin^2 \theta \sum_{\sigma=\pm 1} F_s^{\sigma m} |\varphi_s^{m+2\sigma}\rangle \right], \end{aligned} \quad (151)$$

and

$$\begin{aligned} \mathcal{H}'_d |\varphi_s^m\rangle &= -\frac{J_d}{4} \left(2 \sin^2 \theta \cos(2\phi) [3m^2 - s(s+1)] |\varphi_s^m\rangle \right. \\ &\quad + 2 \sin \theta \sum_{\sigma=\pm 1} (2m + \sigma) A_s^{\sigma m} \\ &\quad \times [\cos \theta \cos(2\phi) + i\sigma \sin(2\phi)] |\varphi_s^{m+\sigma}\rangle \\ &\quad + \sum_{\sigma=\pm 1} F_s^{\sigma m} [(1 + \cos^2 \theta) \cos(2\phi) \\ &\quad \left. + 2i\sigma \cos \theta \sin(2\phi)] |\varphi_s^{m+2\sigma}\rangle \right), \end{aligned} \quad (152)$$

where F_s^x is defined by Eq. (17). We note that in this representation, both \mathcal{H}_b and \mathcal{H}_d preserve the global spin quantum number s , but allow $\Delta m = \pm 1, \pm 2$ transitions.

Local Hamiltonian

With regard to the local spin anisotropy terms in the rotated coordinate system, we write

$$\mathcal{H}'_a = -J_a \left(\mathcal{O}_1 \cos^2 \theta + \mathcal{O}_2 \sin^2 \theta - \frac{\sin(2\theta)}{2} \mathcal{O}_3 \right) \quad (153)$$

and

$$\begin{aligned} \mathcal{H}'_e &= -J_e \left[\cos(2\phi) \left(\mathcal{O}_1 \sin^2 \theta + \mathcal{O}_2 \cos^2 \theta \right. \right. \\ &\quad \left. \left. + \frac{1}{2} \sin(2\theta) \mathcal{O}_3 - \mathcal{O}_4 \right) \right. \\ &\quad \left. - \sin(2\phi) \left(\mathcal{O}_5 \cos \theta + \mathcal{O}_6 \sin \theta \right) \right], \end{aligned} \quad (154)$$

where

$$\mathcal{O}_1 = \sum_{i=1}^2 S_{iz'}^2, \quad (155)$$

$$\mathcal{O}_2 = \sum_{i=1}^2 S_{ix'}^2, \quad (156)$$

$$\mathcal{O}_3 = \sum_{i=1}^2 (S_{iz'} S_{ix'} + S_{ix'} S_{iz'}), \quad (157)$$

$$\mathcal{O}_4 = \sum_{i=1}^2 S_{iy'}^2, \quad (158)$$

$$\mathcal{O}_5 = \sum_{i=1}^2 (S_{ix'} S_{iy'} + S_{iy'} S_{ix'}), \quad (159)$$

and

$$\mathcal{O}_6 = \sum_{i=1}^2 (S_{iy'} S_{iz'} + S_{iz'} S_{iy'}). \quad (160)$$

Local Hamiltonian matrix element components

The operations of these interactions are given by

$$\begin{aligned} \mathcal{O}_1 |\varphi_s^m\rangle &= \frac{1}{2} \left(G_{s,s_1}^m |\varphi_s^m\rangle \right. \\ &\quad \left. + \sum_{\sigma'=\pm 1} H_{s,s_1}^{m,\sigma'} |\varphi_{s+2\sigma'}^m\rangle \right), \end{aligned} \quad (161)$$

$$\begin{aligned} \mathcal{O}_2 |\varphi_s^m\rangle &= \frac{1}{8} \left(M_{s,s_1}^m |\varphi_s^m\rangle - \sum_{\sigma'=\pm 1} N_{s,s_1}^{m,\sigma'} |\varphi_{s+2\sigma'}^m\rangle \right. \\ &\quad + \sum_{\sigma=\pm 1} L_{s,s_1}^{\sigma m} |\varphi_s^{m+2\sigma}\rangle \\ &\quad \left. + \sum_{\sigma,\sigma'=\pm 1} K_{s,s_1}^{\sigma m,\sigma'} |\varphi_{s+2\sigma'}^{m+2\sigma}\rangle \right), \end{aligned} \quad (162)$$

$$\begin{aligned} \mathcal{O}_3 |\varphi_s^m\rangle &= \frac{1}{4} \sum_{\sigma=\pm 1} \left(P_{s,s_1}^{m,\sigma} |\varphi_s^{m+\sigma}\rangle \right. \\ &\quad \left. - \sum_{\sigma'=\pm 1} \sigma \sigma' R_{s,s_1}^{m,\sigma,\sigma'} |\varphi_{s+2\sigma'}^{m+\sigma}\rangle \right), \end{aligned} \quad (163)$$

$$\begin{aligned} \mathcal{O}_4 |\varphi_s^m\rangle &= \frac{1}{8} \left(M_{s,s_1}^m |\varphi_s^m\rangle - \sum_{\sigma'=\pm 1} N_{s,s_1}^{m,\sigma'} |\varphi_{s+2\sigma'}^m\rangle \right. \\ &\quad - \sum_{\sigma=\pm 1} L_{s,s_1}^{\sigma m} |\varphi_s^{m+2\sigma}\rangle \\ &\quad \left. - \sum_{\sigma,\sigma'=\pm 1} K_{s,s_1}^{\sigma m,\sigma'} |\varphi_{s+2\sigma'}^{m+2\sigma}\rangle \right), \end{aligned} \quad (164)$$

$$\begin{aligned} \mathcal{O}_5 |\varphi_s^m\rangle &= \frac{1}{4i} \sum_{\sigma=\pm 1} \sigma \left(L_{s,s_1}^{\sigma m} |\varphi_s^{m+2\sigma}\rangle \right. \\ &\quad \left. + \sum_{\sigma'=\pm 1} K_{s,s_1}^{\sigma m,\sigma'} |\varphi_{s+2\sigma'}^{m+2\sigma}\rangle \right), \end{aligned} \quad (165)$$

$$\begin{aligned} \mathcal{O}_6 |\varphi_s^m\rangle &= \frac{1}{4i} \sum_{\sigma=\pm 1} \left(\sigma P_{s,s_1}^{m,\sigma} |\varphi_s^{m+\sigma}\rangle \right. \\ &\quad \left. - \sum_{\sigma'=\pm 1} \sigma' R_{s,s_1}^{m,\sigma,\sigma'} |\varphi_{s+2\sigma'}^{m+\sigma}\rangle \right), \end{aligned} \quad (166)$$

where

$$M_{s,s_1}^m = -4m^2 \alpha_{s,s_1} + 4[s(s+1) - 1](1 - \alpha_{s,s_1}), \quad (167)$$

$$N_{s,s_1}^{m,\sigma'} = \sum_{\sigma=\pm 1} C_{s+(\sigma'+1)/2,s_1}^{-\sigma\sigma'm-(\sigma'+1)/2} C_{s+(3\sigma'+1)/2,s_1}^{\sigma\sigma'm+(\sigma'-1)/2} \quad (168)$$

$$P_{s,s_1}^{m,\sigma} = 2A_s^{\sigma m} (2m + \sigma) \alpha_{s,s_1}, \quad (169)$$

and

$$\begin{aligned} R_{s,s_1}^{m,\sigma,\sigma'} &= C_{s+(\sigma'+1)/2,s_1}^{-m\sigma\sigma'-(\sigma'+1)/2} D_{s+(3\sigma'+1)/2,s_1}^{m+\sigma} \\ &\quad + C_{s+(3\sigma'+1)/2,s_1}^{-m\sigma\sigma'-(\sigma'+1)/2} D_{s+(\sigma'+1)/2,s_1}^m, \end{aligned} \quad (170)$$

where η_{s,s_1} , G_{s,s_1}^m , $H_{s,s_1}^{m,\sigma'}$, $K_{s,s_1}^{x,\sigma'}$, and L_{s,s_1}^x are given by Eqs. (22) and (25)-(28), respectively. We note that for $\sigma' = \pm 1$, $N_{s,s_1}^{m,\sigma'} = 2H_{s,s_1}^{m,\sigma'}$.

APPENDIX C

Inelastic neutron scattering cross-section

Here we outline the derivation and provide the important results for the low- T inelastic neutron scattering cross-section, $S(\mathbf{B}, \mathbf{q}, \omega)$. At low T , we set $E_{s,s_1}^m \approx E_s^{m,(0)} + E_{s,s_1}^{m,(1)}$ given by Eqs. (70) and (71). Since this energy was evaluated in the induction representation, it is easiest to evaluate $S(\mathbf{q}, \omega)$ by choosing the axes $\hat{\mathbf{e}}_\alpha = \hat{\mathbf{i}}'$, where $i = x, y, z$. The $\hat{\mathbf{i}}'$ can be obtained from the $\hat{\mathbf{i}}$ using the inverse of the rotation matrix in Eq. (148). Then, for $\hat{\mathbf{q}} = (\sin \theta_q \cos \phi_q, \sin \theta_q \sin \phi_q, \cos \theta_q)$ in the crystal representation, we have

$$\hat{\mathbf{q}} = (\sin \theta_{b,q} \cos \phi_{b,q}, \sin \theta_{b,q} \sin \phi_{b,q}, \cos \theta_{b,q}) \quad (171)$$

in the induction representation, where

$$\begin{aligned} \cos \theta_{b,q} &= \cos \theta \cos \theta_q + \sin \theta \sin \theta_q \cos(\phi - \phi_q), \\ \sin \theta_{b,q} \cos \phi_{b,q} &= \sin \theta_q \cos \theta \cos(\phi - \phi_q) - \sin \theta \cos \theta_q, \\ \sin \theta_{b,q} \sin \phi_{b,q} &= -\sin \theta_q \sin(\phi - \phi_q). \end{aligned} \quad (172)$$

Then, expanding the wave functions to first order in the anisotropy interactions,

$$\begin{aligned} |\tilde{\varphi}_s^m\rangle &= |\varphi_s^m\rangle + \sum_{\substack{s',m' \\ (s',m') \neq (s,m)}} |\varphi_{s'}^{m'}\rangle \left(\langle \varphi_{s'}^{m'} | N_{s,m}^{(1)} | \varphi_s^m \rangle + \dots \right), \\ &= |\varphi_s^m\rangle \\ &+ \frac{1}{\gamma B} \sum_{\sigma=\pm 1} \left(\sigma U_{s,s_1}^{m,\sigma} |\varphi_s^{m+\sigma}\rangle + \frac{\sigma}{2} \mathcal{V}_{s,s_1}^{m,\sigma} |\varphi_s^{m+2\sigma}\rangle \right) \\ &+ \sum_{\sigma'=\pm 1} \frac{\mathcal{W}_{s,s_1}^{m,\sigma'}}{J[\sigma'(2s+1)+2]} |\varphi_{s+2\sigma'}^m\rangle \\ &+ \sum_{\sigma,\sigma'=\pm 1} \left(\frac{\mathcal{X}_{s,s_1}^{m,\sigma,\sigma'}}{\sigma\gamma B + J[\sigma'(2s+1)+2]} |\varphi_{s+2\sigma'}^{m+\sigma}\rangle \right. \\ &\left. + \frac{\mathcal{Y}_{s,s_1}^{m,\sigma,\sigma'}}{2\sigma\gamma B + J[\sigma'(2s+1)+2]} |\varphi_{s+2\sigma'}^{m+2\sigma}\rangle \right) + \dots, \end{aligned} \quad (173)$$

where

$$\begin{aligned} U_{s,s_1}^{m,\sigma}(\theta, \phi) &= \frac{1}{4}(2m+\sigma)A_s^{\sigma m} \left[\sin(2\theta) \left(\tilde{J}_{b,a}^{s,s_1} \right. \right. \\ &\quad \left. \left. - \tilde{J}_{d,e}^{s,s_1} \cos(2\phi) \right) \right. \\ &\quad \left. - 2i\sigma \tilde{J}_{d,e}^{s,s_1} \sin \theta \sin(2\phi) \right], \end{aligned} \quad (175)$$

$$\begin{aligned} \mathcal{V}_{s,s_1}^{m,\sigma}(\theta, \phi) &= -\frac{1}{4}F_s^{\sigma m} \left[\tilde{J}_{b,a}^{s,s_1} \sin^2 \theta \right. \\ &\quad \left. + \tilde{J}_{d,e}^{s,s_1} (1 + \cos^2 \theta) \cos(2\phi) \right. \\ &\quad \left. + 2i\sigma \tilde{J}_{d,e}^{s,s_1} \cos \theta \sin(2\phi) \right], \end{aligned} \quad (176)$$

$$\begin{aligned} \mathcal{W}_{s,s_1}^{m,\sigma'}(\theta, \phi) &= -\frac{1}{2}H_{s,s_1}^{m,\sigma'} [J_a \cos^2 \theta + J_e \sin^2 \theta \cos(2\phi)] \\ &\quad + \frac{1}{8}N_{s,s_1}^{m,\sigma'} \sin^2 \theta [J_a - J_e \cos(2\phi)], \end{aligned} \quad (177)$$

$$\begin{aligned} \mathcal{X}_{s,s_1}^{m,\sigma,\sigma'}(\theta, \phi) &= -\frac{\sigma\sigma'}{8}R_{s,s_1}^{m,\sigma,\sigma'} \left(\sin(2\theta) [J_a - J_e \cos(2\phi)] \right. \\ &\quad \left. - 2i\sigma J_e \sin \theta \sin(2\phi) \right), \end{aligned} \quad (178)$$

and

$$\begin{aligned} \mathcal{Y}_{s,s_1}^{m,\sigma,\sigma'}(\theta, \phi) &= -\frac{1}{8}K_{s,s_1}^{\sigma m,\sigma'} \left[J_a \sin^2 \theta \right. \\ &\quad \left. + J_e \left((1 + \cos^2 \theta) \cos(2\phi) \right. \right. \\ &\quad \left. \left. + 2i\sigma \cos \theta \sin(2\phi) \right) \right], \end{aligned} \quad (179)$$

where $H_{s,s_1}^{m,\sigma'}$ and $K_{s,s_1}^{x,\sigma'}$ are given by Eqs. (26) and (27), respectively, $N_{s,s_1}^{m,\sigma'}$ and $R_{s,s_1}^{m,\sigma,\sigma'}$ are given by Eqs. (168) and (170), respectively, and $\tilde{J}_{b,a}^{s,s_1}$ and $\tilde{J}_{d,e}^{s,s_1}$ are given by Eqs. (72) and (73), respectively. We note that for $\sigma' = \pm 1$, $N_{s,s_1}^{m,\sigma'} = 2H_{s,s_1}^{m,\sigma'}$.

Now, we evaluate the matrix elements

$$M_{\bar{s},s,\alpha}^{\bar{m},m}(\mathbf{q}) = \langle \tilde{\varphi}_{\bar{s}}^{\bar{m}} | S_\alpha^\dagger(\mathbf{q}, 0) | \tilde{\varphi}_s^m \rangle, \quad (180)$$

including the leading corrections to the wave functions due to the anisotropy interactions. We then find to first order in the anisotropy interactions,

$$\begin{aligned} M_{\bar{s},s,z'}^{\bar{m},m}(\mathbf{q}) &= \cos(\mathbf{q} \cdot \mathbf{d}) \left(m \delta_{\bar{s},s} \delta_{\bar{m},m} + m \langle N_{\bar{s},\bar{m}}^{(1)} | \varphi_s^m \rangle \right. \\ &\quad \left. + \bar{m} \langle \varphi_{\bar{s}}^{\bar{m}} | N_{s,m}^{(1)} \rangle \right) - i \sin(\mathbf{q} \cdot \mathbf{d}) \sum_{\sigma'=\pm 1} \\ &\quad \times \left(D_{s+(\sigma'+1)/2,s_1}^m \delta_{\bar{s},s+\sigma'} \delta_{\bar{m},m} \right. \\ &\quad \left. + D_{s+(\sigma'+1)/2,s_1}^m \langle N_{\bar{s},\bar{m}}^{(1)} | \varphi_{s+\sigma'}^m \rangle \right. \\ &\quad \left. + D_{\bar{s}+(\sigma'+1)/2,s_1}^{\bar{m}} \langle \varphi_{\bar{s}+\sigma'}^{\bar{m}} | N_{s,m}^{(1)} \rangle \right), \end{aligned} \quad (181)$$

$$\begin{aligned} M_{\bar{s},s,x'}^{\bar{m},m}(\mathbf{q}) &= \frac{1}{2} \sum_{\sigma=\pm 1} \left[\cos(\mathbf{q} \cdot \mathbf{d}) \left(A_s^{\sigma m} \delta_{\bar{s},s} \delta_{\bar{m},m+\sigma} \right. \right. \\ &\quad \left. \left. + A_s^{\sigma m} \langle N_{\bar{s},\bar{m}}^{(1)} | \varphi_s^{m+\sigma} \rangle + A_{\bar{s}}^{-1+\sigma\bar{m}} \langle \varphi_{\bar{s}}^{\bar{m}-\sigma} | N_{s,m}^{(1)} \rangle \right) \right. \\ &\quad \left. - i\sigma \sin(\mathbf{q} \cdot \mathbf{d}) \sum_{\sigma'=\pm 1} (-\sigma') \right. \\ &\quad \times \left(C_{s+(\sigma'+1)/2,s_1}^{-\sigma\sigma' m - (\sigma'+1)/2} \delta_{\bar{s},s+\sigma'} \delta_{\bar{m},m+\sigma} \right. \\ &\quad \left. + C_{s+(\sigma'+1)/2,s_1}^{-\sigma\sigma' m - (\sigma'+1)/2} \langle N_{\bar{s},\bar{m}}^{(1)} | \varphi_{s+\sigma'}^{m+\sigma} \rangle \right. \\ &\quad \left. - C_{\bar{s}+(\sigma'+1)/2,s_1}^{\sigma\sigma'\bar{m} - (\sigma'+1)/2} \langle \varphi_{\bar{s}+\sigma'}^{\bar{m}-\sigma} | N_{s,m}^{(1)} \rangle \right) \left. \right], \end{aligned} \quad (182)$$

and $M_{\bar{s},s,y'}^{\bar{m},m}(\mathbf{q})$ is obtained from $M_{\bar{s},s,x'}^{\bar{m},m}(\mathbf{q})$ by multiplying the entire quantity inside the summation over σ by $-i\sigma$.

Now, it is convenient to break up the contributions from $|M_{\bar{s},s,x'}^{\bar{m},m}(\mathbf{q})|^2$ and $|M_{\bar{s},s,y'}^{\bar{m},m}(\mathbf{q})|^2$ into their symmetric and antisymmetric parts, with

$$|M_{\bar{s},s,\text{sym}}^{\bar{m},m}(\mathbf{q})|^2 = \frac{1}{2} \left(|M_{\bar{s},s,x'}^{\bar{m},m}(\mathbf{q})|^2 + |M_{\bar{s},s,y'}^{\bar{m},m}(\mathbf{q})|^2 \right), \quad (183)$$

etc. Then, the combined contributions from $|M_{\bar{s},s,z'}^{\bar{m},m}(\mathbf{q})|^2$ and $|M_{\bar{s},s,\text{sym}}^{\bar{m},m}(\mathbf{q})|^2$ arising from the first order perturbations of the wave functions in addition to the Hartree approximation are

$$\begin{aligned} S_1^{(1e)}(\mathbf{B}, \mathbf{q}, \omega) &= \sum_{s=0}^{2s_1} \sum_{m=-s}^s e^{-\beta E_{s,s_1}^m} \\ &\times \left(\cos^2(\mathbf{q} \cdot \mathbf{d}) \sin^2 \theta_{b,q} \mathcal{F}_{1,s_1}^{m,s}(\omega, \theta, \phi) \right. \\ &+ \sin^2(\mathbf{q} \cdot \mathbf{d}) \sin^2 \theta_{b,q} \mathcal{F}_{2,s_1}^{m,s}(\omega, \theta, \phi) \\ &+ \cos^2(\mathbf{q} \cdot \mathbf{d}) \frac{2 - \sin^2 \theta_{b,q}}{4} \mathcal{F}_{3,s_1}^{m,s}(\omega, \theta, \phi) \\ &\left. + \sin^2(\mathbf{q} \cdot \mathbf{d}) \frac{2 - \sin^2 \theta_{b,q}}{4} \mathcal{F}_{4,s_1}^{m,s}(\omega, \theta, \phi) \right), \end{aligned} \quad (184)$$

where

$$\mathcal{F}_{n,s_1}^{m,s}(\omega, \theta, \phi) = \sum_{i=0}^2 \mathcal{F}_{n,s_1}^{m,s(i)}(\omega, \theta, \phi) \quad (185)$$

are the contributions to the \mathcal{F}_n through second order in the anisotropy interactions, respectively. The terms to zeroth order in the anisotropy interactions are given by Eqs. (82)-(85) in the text. The non-vanishing first order terms are

$$\begin{aligned} \mathcal{F}_{2,s_1}^{m,s(1)} &= f_1^{(1)}(\theta, \phi) \sum_{\sigma'=\pm 1} \delta(\omega + E_{s,s_1}^m - E_{s+\sigma',s_1}^m) \\ &\times D_{s+(\sigma'+1)/2,s_1}^m Q_2^{\sigma'}, \end{aligned} \quad (186)$$

$$\begin{aligned} \mathcal{F}_{4,s_1}^{m,s(1)} &= -f_1^{(1)}(\theta, \phi) \sum_{\sigma,\sigma'=\pm 1} \delta(\omega + E_{s,s_1}^m - E_{s+\sigma',s_1}^{m+\sigma}) \\ &\times C_{s+(\sigma'+1)/2,s_1}^{-(\sigma'+1)/2-\sigma\sigma'm} Q_4^{\sigma,\sigma'}, \end{aligned} \quad (187)$$

$$Q_2^{\sigma'} = \sum_{\bar{\sigma}=\pm 1} \frac{\bar{\sigma} D_{s+(\sigma'+1+2\bar{\sigma}\sigma')/2,s_1}^m H_{s+\sigma'(1-\bar{\sigma})/2,s_1}^{m,\bar{\sigma}\sigma'}}{2[\sigma'(2s+1)+1+\bar{\sigma}]}, \quad (188)$$

$$Q_4^{\sigma,\sigma'} = \sum_{\bar{\sigma}=\pm 1} \frac{\bar{\sigma} C_{s+(\sigma'+1+2\bar{\sigma}\sigma')/2,s_1}^{\sigma\sigma'm+(\sigma'-1)/2} H_{s+\sigma'(1-\bar{\sigma})/2,s_1}^{m+\sigma(1-\bar{\sigma})/2,\bar{\sigma}\sigma'}}{2[\sigma'(2s+1)+1+\bar{\sigma}]}, \quad (189)$$

$$f_1^{(1)}(\theta, \phi) = \frac{1}{J} \left(J_a - 3[J_a \cos^2 \theta + J_e \sin^2 \theta \cos(2\phi)] \right), \quad (190)$$

where we suppress the ω, θ, ϕ arguments of the $\mathcal{F}_{n,s_1}^{m,s(i)}$ functions for simplicity of presentation. The contributions $\mathcal{F}_{n,s_1}^{m,s(2)}(\omega, \theta, \phi)$ second order in the anisotropy interactions may be written as

$$\begin{aligned} \mathcal{F}_{1,s_1}^{m,s(2)} &= \sum_{\sigma,\sigma'=\pm 1} \sum_{p=0}^2 \sum_{p'=0}^1 \delta(\omega + E_{s,s_1}^m - E_{s+2p'\sigma',s_1}^{m+p\sigma}) \\ &\times \mathcal{A}_1^{p,p'}(\theta, \phi), \end{aligned} \quad (191)$$

$$\begin{aligned} \mathcal{F}_{2,s_1}^{m,s(2)} &= \sum_{\sigma,\sigma'=\pm 1} \sum_{p=0}^2 \sum_{p'=0}^1 \delta(\omega + E_{s,s_1}^m - E_{s+(2p'+1)\sigma',s_1}^{m+p\sigma}) \\ &\times \mathcal{A}_2^{p,p'}(\theta, \phi), \end{aligned} \quad (192)$$

$$\begin{aligned} \mathcal{F}_{3,s_1}^{m,s(2)} &= \sum_{\sigma,\sigma'=\pm 1} \sum_{p=0}^3 \sum_{p'=0}^1 \delta(\omega + E_{s,s_1}^m - E_{s+2p'\sigma',s_1}^{m+p\sigma}) \\ &\times \mathcal{A}_3^{p,p'}(\theta, \phi), \end{aligned} \quad (193)$$

$$\begin{aligned} \mathcal{F}_{4,s_1}^{m,s(2)} &= \sum_{\sigma,\sigma'=\pm 1} \sum_{p=0}^3 \sum_{p'=0}^1 \delta(\omega + E_{s,s_1}^m - E_{s+(2p'+1)\sigma',s_1}^{m+p\sigma}) \\ &\times \mathcal{A}_4^{p,p'}(\theta, \phi). \end{aligned} \quad (194)$$

We note that we have suppressed the $\sigma, \sigma', m, s, s_1$ dependencies of the $\mathcal{A}_n^{p,p'}(\theta, \phi)$ for brevity. These functions are given by

$$\mathcal{A}_1^{0,0} = \mathcal{A}_1^{0,1} = 0, \quad (195)$$

$$\begin{aligned} \mathcal{A}_1^{1,0} &= [f_1^{(2)}(\theta, \phi) + 2\alpha_{s,s_1} f_2^{(2)}(\theta, \phi) \\ &+ \alpha_{s,s_1}^2 f_3^{(2)}(\theta, \phi)] (G_{1,1}^\sigma)^2, \end{aligned} \quad (196)$$

$$\begin{aligned} \mathcal{A}_1^{2,0} &= [f_4^{(2)}(\theta, \phi) + 2\alpha_{s,s_1} f_5^{(2)}(\theta, \phi) \\ &+ \alpha_{s,s_1}^2 f_6^{(2)}(\theta, \phi)] (G_{1,2}^\sigma)^2, \end{aligned} \quad (197)$$

$$\mathcal{A}_1^{1,1} = f_3^{(2)}(\theta, \phi) (G_{1,4}^{\sigma,\sigma'})^2, \quad (198)$$

$$\mathcal{A}_1^{1,2} = f_6^{(2)}(\theta, \phi) (G_{1,5}^{\sigma,\sigma'})^2, \quad (199)$$

$$\mathcal{A}_2^{0,(1\pm 1)/2} = f_7^{(2)(\theta,\phi)} (G_{2,3}^{\pm\sigma',\sigma'})^2, \quad (200)$$

$$\begin{aligned} \mathcal{A}_2^{1,0} &= (G_{2,1}^{\sigma,\sigma'})^2 [f_1^{(2)}(\theta, \phi) + 2\alpha_{s,s_1} f_2^{(2)}(\theta, \phi) \\ &+ \alpha_{s,s_1}^2 f_3^{(2)}(\theta, \phi)] + (G_{2,4}^{\sigma,\sigma',-\sigma'})^2 f_3^{(2)}(\theta, \phi) \\ &+ 2G_{2,1}^{\sigma,\sigma'} G_{2,4}^{\sigma,\sigma',-\sigma'} [f_2^{(2)}(\theta, \phi) + \alpha_{s,s_1} f_3^{(2)}(\theta, \phi)], \end{aligned} \quad (201)$$

$$\begin{aligned} \mathcal{A}_2^{2,0} &= (G_{2,2}^{\sigma,\sigma'})^2 [f_4^{(2)}(\theta, \phi) + 2\alpha_{s,s_1} f_5^{(2)}(\theta, \phi) \\ &+ \alpha_{s,s_1}^2 f_6^{(2)}(\theta, \phi)] + (G_{2,5}^{\sigma,\sigma',-\sigma'})^2 f_6^{(2)}(\theta, \phi) \\ &+ 2G_{2,2}^{\sigma,\sigma'} G_{2,5}^{\sigma,\sigma',-\sigma'} [f_5^{(2)}(\theta, \phi) + \alpha_{s,s_1} f_6^{(2)}(\theta, \phi)], \end{aligned} \quad (202)$$

$$\mathcal{A}_2^{1,1} = f_3^{(2)}(\theta, \phi) (G_{2,4}^{\sigma,\sigma',\sigma'})^2, \quad (203)$$

$$\mathcal{A}_2^{2,1} = f_6^{(2)}(\theta, \phi) (G_{2,5}^{\sigma,\sigma',\sigma'})^2, \quad (204)$$

$$\mathcal{A}_3^{1\pm 1,0} = [f_1^{(2)}(\theta, \phi) + 2\alpha_{s,s_1} f_2^{(2)}(\theta, \phi)]$$

$$+\alpha_{s,s_1}^2 f_3^{(2)}(\theta, \phi) \left(G_{3,1}^{\sigma, \pm\sigma} \right)^2, \quad (205)$$

$$\begin{aligned} \mathcal{A}_3^{2\pm 1,0} &= [f_4^{(2)}(\theta, \phi) + 2\alpha_{s,s_1} f_5^{(2)}(\theta, \phi) \\ &+ \alpha_{s,s_1}^2 f_6^{(2)}(\theta, \phi) \left(G_{3,2}^{\sigma, \pm\sigma} \right)^2, \end{aligned} \quad (206)$$

$$\mathcal{A}_3^{1\pm 1,1} = f_3^{(2)}(\theta, \phi) \left(G_{3,4}^{\sigma, \sigma', \pm\sigma} \right)^2, \quad (207)$$

$$\begin{aligned} \mathcal{A}_3^{1,1} &= \left(G_{3,3}^{\sigma, \sigma'} \right)^2 f_7^{(2)}(\theta, \phi) + \left(G_{3,5}^{\sigma, \sigma', -\sigma} \right)^2 f_6^{(2)}(\theta, \phi) \\ &+ 2G_{3,3}^{\sigma, \sigma'} G_{3,5}^{\sigma, \sigma', -\sigma} f_9^{(2)}(\theta, \phi), \end{aligned} \quad (208)$$

$$\mathcal{A}_3^{3,1} = f_6^{(2)}(\theta, \phi) \left(G_{3,5}^{\sigma, \sigma', \sigma} \right)^2, \quad (209)$$

$$\begin{aligned} \mathcal{A}_4^{1\pm 1,0} &= \left(G_{4,1}^{\sigma, \sigma', \pm\sigma} \right)^2 [f_1^{(2)}(\theta, \phi) \\ &+ 2\alpha_{s,s_1} f_2^{(2)}(\theta, \phi) + \alpha_{s,s_1}^2 f_3^{(2)}(\theta, \phi)] \\ &+ \left(G_{4,4}^{\sigma, \sigma', \pm\sigma, -\sigma'} \right)^2 f_3^{(2)}(\theta, \phi) \\ &+ 2G_{4,1}^{\sigma, \sigma', \pm\sigma} G_{4,4}^{\sigma, \sigma', \pm\sigma, -\sigma'} \\ &\times [f_2^{(2)}(\theta, \phi) + \alpha_{s,s_1} f_3^{(2)}(\theta, \phi)], \end{aligned} \quad (210)$$

$$\begin{aligned} \mathcal{A}_4^{1,0} &= \left(G_{4,2}^{\sigma, \sigma', -\sigma} \right)^2 [f_4^{(2)}(\theta, \phi) \\ &+ 2\alpha_{s,s_1} f_5^{(2)}(\theta, \phi) + \alpha_{s,s_1}^2 f_6^{(2)}(\theta, \phi)] \\ &+ \left(G_{4,5}^{\sigma, \sigma', -\sigma, -\sigma'} \right)^2 f_6^{(2)}(\theta, \phi) \\ &+ 2G_{4,2}^{\sigma, \sigma', -\sigma} G_{4,5}^{\sigma, \sigma', -\sigma, -\sigma'} \\ &\times [f_5^{(2)}(\theta, \phi) + \alpha_{s,s_1} f_6^{(2)}(\theta, \phi)] \\ &+ \left(G_{4,3}^{\sigma, \sigma', -\sigma'} \right)^2 f_7^{(2)}(\theta, \phi) + 2G_{4,3}^{\sigma, \sigma', -\sigma'} \\ &\times \left(G_{4,2}^{\sigma, \sigma', -\sigma} [f_8^{(2)}(\theta, \phi) + \alpha_{s,s_1} f_9^{(2)}(\theta, \phi)] \right. \\ &\left. + G_{4,5}^{\sigma, \sigma', -\sigma, -\sigma'} f_9^{(2)}(\theta, \phi) \right), \end{aligned} \quad (211)$$

$$\begin{aligned} \mathcal{A}_4^{3,0} &= \left(G_{4,2}^{\sigma, \sigma', \sigma} \right)^2 [f_4^{(2)}(\theta, \phi) \\ &+ 2\alpha_{s,s_1} f_5^{(2)}(\theta, \phi) + \alpha_{s,s_1}^2 f_6^{(2)}(\theta, \phi)] \\ &+ \left(G_{4,5}^{\sigma, \sigma', \sigma, -\sigma'} \right)^2 f_6^{(2)}(\theta, \phi) + 2G_{4,2}^{\sigma, \sigma', \sigma} G_{4,5}^{\sigma, \sigma', \sigma, -\sigma'} \\ &\times [f_5^{(2)}(\theta, \phi) + \alpha_{s,s_1} f_6^{(2)}(\theta, \phi)], \end{aligned} \quad (212)$$

$$\mathcal{A}_4^{1\pm 1,1} = f_3^{(2)}(\theta, \phi) \left(G_{4,4}^{\sigma, \sigma', \pm\sigma, \sigma'} \right)^2, \quad (213)$$

$$\begin{aligned} \mathcal{A}_4^{1,1} &= \left(G_{4,5}^{\sigma, \sigma', -\sigma, \sigma'} \right)^2 f_6^{(2)}(\theta, \phi) \\ &+ \left(G_{4,3}^{\sigma, \sigma', \sigma'} \right)^2 f_7^{(2)}(\theta, \phi) \\ &+ 2G_{4,3}^{\sigma, \sigma', \sigma'} G_{4,5}^{\sigma, \sigma', -\sigma, \sigma'} f_9^{(2)}(\theta, \phi), \end{aligned} \quad (214)$$

$$\mathcal{A}_4^{3,1} = f_6^{(2)}(\theta, \phi) \left(G_{4,5}^{\sigma, \sigma', \sigma, \sigma'} \right)^2, \quad (215)$$

where the second order angular functions are given by

$$\begin{aligned} f_1^{(2)}(\theta, \phi) &= \frac{\sin^2 \theta}{J^2} \left([J_b - \cos(2\phi) J_d]^2 \cos^2 \theta \right. \\ &\left. + J_d^2 \sin^2(2\phi) \right), \end{aligned} \quad (216)$$

$$f_2^{(2)}(\theta, \phi) = \frac{\sin^2 \theta}{J^2} \left([J_b - J_d \cos(2\phi)] [J_a - J_e \cos(2\phi)] \right.$$

$$\left. \times \cos^2 \theta + J_d J_e \sin^2(2\phi) \right), \quad (217)$$

$$\begin{aligned} f_3^{(2)}(\theta, \phi) &= \frac{\sin^2 \theta}{J^2} \left([J_a - \cos(2\phi) J_e]^2 \cos^2 \theta \right. \\ &\left. + J_e^2 \sin^2(2\phi) \right), \end{aligned} \quad (218)$$

$$\begin{aligned} f_4^{(2)}(\theta, \phi) &= \frac{1}{J^2} \left(J_b \sin^2 \theta + J_d (1 + \cos^2 \theta) \cos(2\phi) \right)^2 \\ &+ 4 \frac{J_d^2}{J^2} \cos^2 \theta \sin^2(2\phi), \end{aligned} \quad (219)$$

$$\begin{aligned} f_5^{(2)}(\theta, \phi) &= \frac{1}{J^2} [J_b \sin^2 \theta + J_d (1 + \cos^2 \theta) \cos(2\phi)] \\ &\times [J_a \sin^2 \theta + J_e (1 + \cos^2 \theta) \cos(2\phi)] \\ &+ 4 \frac{J_d J_e}{J^2} \cos^2 \theta \sin^2(2\phi), \end{aligned} \quad (220)$$

$$\begin{aligned} f_6^{(2)}(\theta, \phi) &= \frac{1}{J^2} \left(J_a \sin^2 \theta + J_e (1 + \cos^2 \theta) \cos(2\phi) \right)^2 \\ &+ 4 \frac{J_e^2}{J^2} \cos^2 \theta \sin^2(2\phi), \end{aligned} \quad (221)$$

$$f_7^{(2)}(\theta, \phi) = \frac{1}{J^2} \left(J_a - 3[J_a \cos^2 \theta + J_e \sin^2 \theta \cos(2\phi)] \right)^2,$$

$$\begin{aligned} f_8^{(2)}(\theta, \phi) &= \frac{1}{J^2} \left(J_a - 3[J_a \cos^2 \theta + J_e \sin^2 \theta \cos(2\phi)] \right) \\ &\times \left(J_b \sin^2 \theta + J_d (1 + \cos^2 \theta) \cos(2\phi) \right), \end{aligned} \quad (222)$$

$$\begin{aligned} f_9^{(2)}(\theta, \phi) &= \frac{1}{J^2} \left(J_a - 3[J_a \cos^2 \theta + J_e \sin^2 \theta \cos(2\phi)] \right) \\ &\times \left(J_a \sin^2 \theta + J_e (1 + \cos^2 \theta) \cos(2\phi) \right), \end{aligned} \quad (223)$$

and the constants are given by

$$G_{1,1}^\sigma = \frac{J(2m + \sigma)}{2\gamma B} A_s^{\sigma m}, \quad (224)$$

$$G_{1,2}^\sigma = \frac{J F_s^{\sigma m}}{4\gamma B}, \quad (225)$$

$$G_{1,4}^{\sigma, \sigma'} = \frac{R_{s,s_1}^{m, \sigma, \sigma'}}{4 \left(\sigma \gamma B + J[\sigma'(2s + 1) + 2] \right)}, \quad (226)$$

$$G_{1,5}^{\sigma, \sigma'} = \frac{K_{s,s_1}^{\sigma m, \sigma'}}{4 \left(2\sigma \gamma B + J[\sigma'(2s + 1) + 2] \right)}, \quad (227)$$

$$\begin{aligned} G_{2,1}^{\sigma, \sigma'} &= \frac{J\sigma(2m + \sigma)}{2\gamma B} \sum_{\bar{\sigma}=\pm 1} \left(\bar{\sigma} A_{s-\sigma'(\bar{\sigma}-1)/2}^{\sigma m} \right. \\ &\left. \times D_{s+(1+\sigma')/2, s_1}^{m+\sigma(\bar{\sigma}+1)/2} \right), \end{aligned} \quad (228)$$

$$\begin{aligned} G_{2,2}^{\sigma, \sigma'} &= -\frac{J\sigma}{8\gamma B} \sum_{\bar{\sigma}=\pm 1} \bar{\sigma} D_{s+(1+\sigma')/2, s_1}^{m+\sigma(\bar{\sigma}+1)} \\ &\times F_{s-\sigma'(\bar{\sigma}-1)/2, s_1}^{\sigma m}, \end{aligned} \quad (229)$$

$$G_{2,3}^{\sigma, \sigma'} = \sum_{\bar{\sigma}=\pm 1} \left(\frac{\bar{\sigma} D_{s+\sigma'(\bar{\sigma}+1)/2, s_1}^m}{4[\sigma'(2s + 1) + 2 + \sigma\sigma'(1 - \bar{\sigma})]} \right)$$

$$\times H_{s+\sigma(1-\bar{\sigma})/2,s_1}^{m,\sigma'}), \quad (230)$$

$$G_{2,4}^{\sigma,\sigma',\sigma''} = -\frac{1}{4} \sum_{\bar{\sigma}=\pm 1} \left(\sigma\sigma'\bar{\sigma}D_{s+\sigma'(\bar{\sigma}+1)+(\sigma''+1)/2,s_1}^{m+\sigma(\bar{\sigma}+1)/2} \right. \\ \left. \times \frac{R_{s+\sigma''(1-\bar{\sigma})/2,s_1}^{m,\sigma,\sigma'}}{\sigma\gamma B/J + \sigma'(2s+1+\sigma''-\sigma''\bar{\sigma})+2} \right), \quad (231)$$

$$G_{2,5}^{\sigma,\sigma',\sigma''} = -\frac{1}{8} \sum_{\bar{\sigma}=\pm 1} \left(\bar{\sigma}K_{s+\sigma''(1-\bar{\sigma})/2,s_1}^{\sigma m,\sigma'} \right. \\ \left. \times \frac{D_{s+(\bar{\sigma}+1)\sigma'+(\sigma''+1)/2,s_1}^{m+\sigma(\bar{\sigma}+1)}}{2\sigma\gamma B/J + \sigma'(2s+1+\sigma''-\sigma''\bar{\sigma})+2} \right), \quad (232)$$

$$G_{3,1}^{\sigma,\sigma'} = \frac{\sigma'J}{2\gamma B} \left((2m+\sigma')A_s^{\sigma(m+\sigma')}A_s^{\sigma'm} \right. \\ \left. - (2m+2\sigma+\sigma')A_s^{\sigma'(m+\sigma)}A_s^{\sigma m} \right), \quad (233)$$

$$G_{3,2}^{\sigma,\sigma'} = -\frac{\sigma J}{8\gamma B} \left(A_s^{\sigma'(m+2\sigma)}F_s^{\sigma m} \right. \\ \left. - A_s^{\sigma'm}F_s^{\sigma(m+\sigma')} \right), \quad (234)$$

$$G_{3,3}^{\sigma,\sigma'} = \sum_{\bar{\sigma}=\pm 1} \frac{\bar{\sigma}A_{s+(\bar{\sigma}+1)\sigma'}^{\sigma m}H_{s,s_1}^{m-\sigma(\bar{\sigma}-1)/2,\sigma'}}{4[\sigma'(2s+1)+2]}, \quad (235)$$

$$G_{3,4}^{\sigma,\sigma',\sigma''} = -\sum_{\bar{\sigma}=\pm 1} \left(\frac{J\sigma\sigma'\bar{\sigma}A_{s+(\bar{\sigma}+1)\sigma'}^{\sigma''m+\sigma\sigma''(\bar{\sigma}+1)/2}}{4(\sigma\gamma B + J[\sigma'(2s+1)+2])} \right. \\ \left. \times R_{s,s_1}^{m-\sigma''(\bar{\sigma}-1)/2,\sigma,\sigma'} \right), \quad (236)$$

$$G_{3,5}^{\sigma,\sigma',\sigma''} = -\sum_{\bar{\sigma}=\pm 1} \left(\frac{J\bar{\sigma}A_{s+(\bar{\sigma}+1)\sigma'}^{\sigma''m+(1+\bar{\sigma})\sigma\sigma''}}{8(2\sigma\gamma B + J[\sigma'(2s+1)+2])} \right. \\ \left. \times K_{s,s_1}^{\sigma m+(1-\bar{\sigma})\sigma\sigma''/2,\sigma'} \right), \quad (237)$$

$$G_{4,1}^{\sigma,\sigma',\sigma''} = \frac{\sigma'\sigma''J}{2\gamma B} \sum_{\bar{\sigma}=\pm 1} \bar{\sigma}[2m+\sigma''+\sigma(1-\bar{\sigma})] \\ \times C_{s+(\sigma'+1)/2,s_1}^{-\sigma\sigma'm-\sigma\sigma''(\bar{\sigma}+1)/2-(\sigma'+1)/2} \\ \times A_{s+\sigma'(1-\bar{\sigma})/2}^{\sigma''m+\sigma\sigma''(1-\bar{\sigma})/2}, \quad (238)$$

$$G_{4,2}^{\sigma,\sigma',\sigma''} = -\frac{\sigma'\sigma''J}{8\gamma B} \sum_{\bar{\sigma}=\pm 1} \bar{\sigma}F_{s+\sigma'(1-\bar{\sigma})/2}^{\sigma m+\sigma\sigma''(1-\bar{\sigma})/2} \\ \times C_{s+(\sigma'+1)/2,s_1}^{-\sigma'\sigma''m-\sigma\sigma''(\bar{\sigma}+1)-(\sigma'+1)/2}, \quad (239)$$

$$G_{4,3}^{\sigma,\sigma',\sigma''} = \sum_{\bar{\sigma}=\pm 1} \left(\frac{\sigma''\bar{\sigma}H_{s+\sigma''(1-\bar{\sigma})/2,s_1}^{m+\sigma(1-\bar{\sigma})/2,\sigma'}}{4[\sigma'(2s+1)+2+\sigma'\sigma''(1-\bar{\sigma})]} \right. \\ \left. \times C_{s+(\sigma''+1)/2+\sigma'(\bar{\sigma}+1),s_1}^{-\sigma\sigma''m-(\sigma''+1)/2} \right), \quad (240)$$

$$G_{4,4}^{\sigma,\sigma',\sigma'',\sigma'''} = -\frac{1}{4} \sum_{\bar{\sigma}=\pm 1} \left(\sigma\sigma'\sigma'''\bar{\sigma}R_{s+\sigma''(1-\bar{\sigma})/2,s_1}^{m+\sigma''(1-\bar{\sigma})/2,\sigma,\sigma'} \right. \\ \left. \times \frac{C_{s+(\sigma'''+1)/2+\sigma'(\bar{\sigma}+1),s_1}^{-\sigma''\sigma''m-\sigma\sigma'''\sigma''(\bar{\sigma}+1)/2-(\sigma'''+1)/2}}{\sigma\gamma B/J + \sigma'(2s+1+\sigma''-\sigma'''\bar{\sigma})+2} \right), \quad (241)$$

$$G_{4,5}^{\sigma,\sigma',\sigma'',\sigma'''} = -\frac{1}{8} \sum_{\bar{\sigma}=\pm 1} \left(\sigma'''\bar{\sigma}JK_{s+\sigma''(1-\bar{\sigma})/2,s_1}^{\sigma m+\sigma\sigma''(1-\bar{\sigma})/2,\sigma'} \right. \\ \left. \times \frac{C_{s+(\sigma'''+1)/2+\sigma'(\bar{\sigma}+1),s_1}^{-\sigma''\sigma''m-(\sigma'''+1)/2-\sigma\sigma''\sigma''(\bar{\sigma}+1)}}{2\sigma\gamma B/J + \sigma'(2s+1+\sigma''-\sigma'''\bar{\sigma})+2} \right), \quad (242)$$

where we have used the identities $A_s^{-m-1} = A_s^m$, $F_s^{-m-2} = F_s^m$, $H_{s+2\sigma',s_1}^{m,-\sigma'} = H_{s,s_1}^{m,\sigma'}$, $R_{s+2\sigma',s_1}^{m+\sigma,-\sigma,-\sigma'} = R_{s,s_1}^{m,\sigma,\sigma'}$, and $K_{s+2\sigma',s_1}^{-2-\sigma m,-\sigma'} = K_{s,s_1}^{\sigma m,\sigma'}$.

For completeness, we write the contributions to $S(\mathbf{B}, \mathbf{q}, \omega)$ from the off-diagonal and antisymmetric diagonal matrix element terms that are first order in the anisotropy interactions. These could be measured by collecting data at specific $(\theta_{b,q}, \phi_{b,q})$ values. We have

$$S_2^{(1e)} = \sum_{s=0}^{2s_1} \sum_{m=-s}^s e^{-\beta E_{s,s_1}^m} \sin^2 \theta_{b,q} \cos(2\phi_{b,q}) \\ \times \left\{ \cos^2(\mathbf{q} \cdot \mathbf{d}) \sum_{\sigma=\pm 1} \delta(\omega + E_{s,s_1}^m - E_{s,s_1}^{m+\sigma}) \right. \\ \times G_{5,1}^{\sigma} \left(f_2^{(1)}(\theta, \phi) + \alpha_{s,s_1} f_3^{(1)}(\theta, \phi) \right) \\ \left. + \sin^2(\mathbf{q} \cdot \mathbf{d}) \sum_{\sigma,\sigma'=\pm 1} \delta(\omega + E_{s,s_1}^m - E_{s+\sigma',s_1}^{m+\sigma}) \right. \\ \times \left[G_{5,2}^{\sigma,\sigma'} \left(f_2^{(1)}(\theta, \phi) + \alpha_{s,s_1} f_3^{(1)}(\theta, \phi) \right) \right. \\ \left. \left. + G_{5,3}^{\sigma,\sigma'} f_3^{(1)}(\theta, \phi) \right] \right\}, \quad (243)$$

$$S_3^{(1e)} = \sum_{s=0}^{2s_1} \sum_{m=-s}^s e^{-\beta E_{s,s_1}^m} \sin(2\theta_{b,q}) \left\{ \cos^2(\mathbf{q} \cdot \mathbf{d}) \right. \\ \times \left(h_1(\theta, \phi, \phi_{b,q}) + \alpha_{s,s_1} h_2(\theta, \phi, \phi_{b,q}) \right) \\ \times \left[\delta(\omega) G_{6,1} \right. \\ \left. + \sum_{\sigma=\pm 1} \delta(\omega + E_{s,s_1}^m - E_{s,s_1}^{m+\sigma}) G_{6,2} \right] \\ \left. + \sin^2(\mathbf{q} \cdot \mathbf{d}) \left[\sum_{\sigma'=\pm 1} \delta(\omega + E_{s,s_1}^m - E_{s+\sigma',s_1}^m) \right. \right. \\ \times \left\{ \left(h_1^{(1)}(\theta, \phi, \phi_{b,q}) + \alpha_{s,s_1} h_2^{(1)}(\theta, \phi, \phi_{b,q}) \right) \right. \\ \left. \times G_{6,3}^{\sigma'} + h_2^{(1)}(\theta, \phi, \phi_{b,q}) G_{6,4}^{\sigma'} \right\} \\ \left. - \sum_{\sigma,\sigma'=\pm 1} \delta(\omega + E_{s,s_1}^m - E_{s+\sigma',s_1}^{m+\sigma}) \right\}$$

$$\begin{aligned} & \times \left\{ \left(h_1^{(1)}(\theta, \phi, \phi_{b,q}) + \alpha_{s,s_1} h_2^{(1)}(\theta, \phi, \phi_{b,q}) \right) \right. \\ & \left. \times G_{6,5}^{\sigma,\sigma'} + h_2^{(1)}(\theta, \phi, \phi_{b,q}) G_{6,6}^{\sigma,\sigma'} \right\}, \end{aligned} \quad (244)$$

and

$$\begin{aligned} S_4^{(1e)} &= \sum_{s=0}^{2s_1} \sum_{m=-s}^s e^{-\beta E_{s,s_1}^m} \sin^2 \theta_{b,q} \sin(2\phi_{b,q}) \\ & \times \left\{ \cos^2(\mathbf{q} \cdot \mathbf{d}) \sum_{\sigma=\pm 1} \delta(\omega + E_{s,s_1}^m - E_{s,s_1}^{m+\sigma}) \right. \\ & \times G_{7,1}^\sigma \left(f_4^{(1)}(\theta, \phi) + \alpha_{s,s_1} f_5^{(1)}(\theta, \phi) \right) \\ & + \sin^2(\mathbf{q} \cdot \mathbf{d}) \sum_{\sigma,\sigma'=\pm 1} \delta(\omega + E_{s,s_1}^m - E_{s+\sigma',s_1}^{m+\sigma}) \\ & \times \left[G_{7,2}^{\sigma,\sigma'} \left(f_4^{(1)}(\theta, \phi) + \alpha_{s,s_1} f_5^{(1)}(\theta, \phi) \right) \right. \\ & \left. \left. + G_{7,3}^{\sigma,\sigma'} f_5^{(1)}(\theta, \phi) \right] \right\}. \end{aligned} \quad (245)$$

The angular functions and coefficients are given by

$$f_2^{(1)}(\theta, \phi) = \frac{1}{J} \left(J_b \sin^2 \theta + J_d (1 + \cos^2 \theta) \cos(2\phi) \right), \quad (246)$$

$$f_3^{(1)}(\theta, \phi) = \frac{1}{J} \left(J_a \sin^2 \theta + J_e (1 + \cos^2 \theta) \cos(2\phi) \right), \quad (247)$$

$$f_4^{(1)}(\theta, \phi) = \frac{J_d}{J} \cos \theta \sin(2\phi), \quad (248)$$

$$f_5^{(1)}(\theta, \phi) = \frac{J_e}{J} \cos \theta \sin(2\phi), \quad (249)$$

$$h_1^{(1)}(\theta, \phi, \phi_{b,q}) = \frac{1}{J} \left(\cos \phi_{b,q} \sin(2\theta) [J_b - J_d \cos(2\phi)] + 2 \sin \phi_{b,q} J_d \sin \theta \sin(2\phi) \right), \quad (250)$$

$$h_2^{(1)}(\theta, \phi, \phi_{b,q}) = \frac{1}{J} \left(\cos \phi_{b,q} \sin(2\theta) [J_a - J_e \cos(2\phi)] + 2 \sin \phi_{b,q} J_e \sin \theta \sin(2\phi) \right), \quad (251)$$

$$G_{5,1}^\sigma = -\frac{J(2m+\sigma)(A_s^{\sigma m})^2}{8\gamma B}, \quad (252)$$

$$\begin{aligned} G_{5,2}^{\sigma,\sigma'} &= -\frac{\sigma J}{16\gamma B} C_{s+(\sigma'+1)/2,s_1}^{-\sigma\sigma' m - (1+\sigma')/2} \\ & \times \sum_{\bar{\sigma}=\pm 1} \bar{\sigma} C_{s+(\sigma'+1)/2,s_1}^{\sigma\sigma' m + (\sigma'+2\bar{\sigma}\sigma'-1)/2} \\ & \times F_{s+\sigma'(1-\bar{\sigma})/2}^{\bar{\sigma}\sigma m - (1-\bar{\sigma})/2}, \end{aligned} \quad (253)$$

$$G_{5,3}^{\sigma,\sigma'} = \frac{1}{16} C_{s+(\sigma'+1)/2,s_1}^{-\sigma\sigma' m - (1+\sigma')/2}$$

$$\begin{aligned} & \times \sum_{\bar{\sigma}=\pm 1} \left(\frac{\bar{\sigma} C_{s+(1+\sigma'+2\bar{\sigma}\sigma')/2,s_1}^{-\sigma\sigma' m - (1+\sigma'+2\bar{\sigma}\sigma')/2}}{2\sigma\gamma B/J + \sigma'(2s+1) + 1 + \bar{\sigma}} \right. \\ & \left. \times K_{s-\sigma'(\bar{\sigma}-1)/2,s_1}^{\bar{\sigma}\sigma m + (\bar{\sigma}-1)/2, \bar{\sigma}\sigma'} \right), \end{aligned} \quad (254)$$

$$G_{6,1} = \frac{Jm}{2\gamma B} [s(s+1) - 3m^2], \quad (255)$$

$$G_{6,2}^\sigma = \frac{J}{8\gamma B} (A_s^{\sigma m})^2 (2m + \sigma), \quad (256)$$

$$\begin{aligned} G_{6,3}^{\sigma'} &= -\frac{\sigma' J}{8\gamma B} D_{s+(\sigma'+1)/2,s_1}^m \\ & \times \sum_{\sigma,\bar{\sigma}=\pm 1} \left[(2m\bar{\sigma} + \sigma) A_{s+\sigma'(\bar{\sigma}+1)/2}^{\sigma\bar{\sigma}m} \right. \\ & \left. \times C_{s+(\sigma'+1)/2,s_1}^{-\sigma\sigma' m - (1+\bar{\sigma}\sigma')/2} \right], \end{aligned} \quad (257)$$

$$\begin{aligned} G_{6,4}^{\sigma'} &= \frac{J}{16} D_{s+(\sigma'+1)/2,s_1}^m \sum_{\sigma,\bar{\sigma}=\pm 1} \\ & \times \left(\frac{\bar{\sigma} C_{s+(1+\sigma'-2\bar{\sigma}\sigma')/2,s_1}^{\sigma\sigma' m - (1-\bar{\sigma}\sigma')/2}}{\sigma\gamma B + J[-\sigma'(2s+1) + \bar{\sigma} - 1]} \right. \\ & \left. \times R_{s+\sigma'(\bar{\sigma}+1)/2,s_1}^{m,\bar{\sigma}\sigma,-\bar{\sigma}\sigma'} \right), \end{aligned} \quad (258)$$

$$\begin{aligned} G_{6,5}^{\sigma,\sigma'} &= -\frac{\sigma' J}{8\gamma B} C_{s+(\sigma'+1)/2,s_1}^{-\sigma\sigma' m - (\sigma'+1)/2} (2m + \sigma) \\ & \times \sum_{\bar{\sigma}=\pm 1} \bar{\sigma} D_{s+(\sigma'+1)/2,s_1}^{m+\sigma(\bar{\sigma}+1)/2} A_{s-\sigma'(\bar{\sigma}-1)/2}^{\sigma m}, \end{aligned} \quad (259)$$

$$\begin{aligned} G_{6,6}^{\sigma,\sigma'} &= \frac{J}{16} C_{s+(\sigma'+1)/2,s_1}^{-\sigma\sigma' m - (\sigma'+1)/2} \sum_{\bar{\sigma}=\pm 1} \\ & \times \left(\frac{\bar{\sigma} R_{s-\sigma'(\bar{\sigma}-1)/2,s_1}^{m+\sigma(1-\bar{\sigma})/2, \bar{\sigma}\sigma, \bar{\sigma}\sigma'}}{\sigma\gamma B + J[\sigma'(2s+1) + 1 + \bar{\sigma}]} \right. \\ & \left. \times D_{s+(1+\sigma'+2\bar{\sigma}\sigma')/2,s_1}^{m+\sigma(\bar{\sigma}+1)/2} \right), \end{aligned} \quad (260)$$

$$G_{7,1}^\sigma = \frac{J}{4\gamma B} (2m + \sigma) (A_s^{\sigma m})^2, \quad (261)$$

$$\begin{aligned} G_{7,2}^{\sigma,\sigma'} &= -\frac{\sigma J}{8\gamma B} C_{s+(\sigma'+1)/2,s_1}^{-\sigma\sigma' m - (\sigma'+1)/2} \\ & \times \sum_{\bar{\sigma}=\pm 1} \left(\bar{\sigma} C_{s+(\sigma'+1)/2,s_1}^{\sigma\sigma' m - (1-\sigma'-2\bar{\sigma}\sigma')/2} \right. \\ & \left. \times F_{s+\sigma'(1-\bar{\sigma})/2}^{\bar{\sigma}\sigma m - (1-\bar{\sigma})/2} \right), \end{aligned} \quad (262)$$

$$\begin{aligned} G_{7,3}^{\sigma,\sigma'} &= \frac{1}{8} C_{s+(\sigma'+1)/2,s_1}^{-\sigma\sigma' m - (\sigma'+1)/2} \\ & \times \sum_{\bar{\sigma}=\pm 1} \left(\bar{\sigma} K_{s+\sigma'(1-\bar{\sigma})/2,s_1}^{\bar{\sigma}\sigma m - (1-\bar{\sigma})/2, \bar{\sigma}\sigma'} \right. \\ & \left. \times \frac{C_{s+(1+\sigma'+2\bar{\sigma}\sigma')/2,s_1}^{-\sigma\sigma' m - (1+\sigma'+2\bar{\sigma}\sigma')/2}}{2\sigma\gamma B/J + \sigma'(2s+1) + 1 + \bar{\sigma}} \right). \end{aligned} \quad (263)$$

Higher order corrections to the EPR response

Here we evaluate the EPR response $\chi''_{-\sigma,\sigma}(\mathbf{B},\omega)$ including the corrections to the induction representation wave functions first order in the anisotropy interactions. It can be shown that second order perturbations to the wave functions only contribute to the EPR response to third (and higher) order in the anisotropy interactions, and are hence neglected. From Eq. (88), we expand the exact wave functions $|\tilde{\phi}_n\rangle$ to first order in the anisotropy interactions. To this order, s and m are still good quantum numbers, so we rewrite $|\tilde{\phi}_n\rangle = |\tilde{\varphi}_s^m\rangle$. We then find

$$\begin{aligned} \chi''_{-\sigma,\sigma}(\mathbf{B},\omega) &\approx \frac{\gamma^2}{Z(1)} \sum_{s=0}^{2s_1} \sum_{m=-s}^s \sum_{s'=0}^{2s_1} \sum_{m'=-s'}^{s'} \exp[-\beta E_{s,s_1}^m] \\ &\times \left(\delta(E_{s,s_1}^m - E_{s',s_1}^{m'} + \omega) \right. \\ &\quad \left. - \delta(E_{s',s_1}^{m'} - E_{s,s_1}^m + \omega) \right) \\ &\times \left[\sum_{\bar{\sigma}=\pm 1} \delta_{s',s} \delta_{m',m+\bar{\sigma}} |Z_0^{\bar{\sigma}\sigma}|^2 \right. \\ &\quad + \delta_{s',s} \sum_{\sigma'=\pm\sigma} \delta_{m',m+\sigma+\sigma'} |Z_0^{\sigma+\sigma'}|^2 \\ &\quad + \delta_{m',m+\sigma} \sum_{\sigma''=\pm\sigma} \delta_{s',s+2\sigma''} |Z_{2\sigma''}^\sigma|^2 \\ &\quad \left. + \sum_{\sigma',\sigma''=\pm\sigma} \delta_{s',s+2\sigma''} \left(\delta_{m',m+\sigma+\sigma'} |Z_{2\sigma''}^{\sigma+\sigma'}|^2 \right. \right. \\ &\quad \left. \left. + \delta_{m',m+\sigma+2\sigma'} |Z_{2\sigma''}^{\sigma+2\sigma'}|^2 \right) \right], \quad (264) \end{aligned}$$

where the amplitudes $Z_{s'-s}^{m'-m}$ are given to first order in the anisotropy energies by

$$Z_0^{+\sigma} = A_s^{\sigma m} + \mathcal{O}(J_i/J)^2, \quad (265)$$

$$Z_0^{\sigma+\sigma'} = \frac{\sigma'}{\gamma B} \left(A_s^{\sigma(m+\sigma')} \mathcal{U}_{s,s_1}^{m,\sigma'} - A_s^{\sigma m} (\mathcal{U}_{s,s_1}^{m+\sigma+\sigma',-\sigma'})^* \right), \quad (266)$$

$$Z_0^{-\sigma} = \frac{-\sigma}{2\gamma B} \left(A_s^{-2+\sigma m} \mathcal{V}_{s,s_1}^{m,-\sigma} - A_s^{\sigma m} (\mathcal{V}_{s,s_1}^{m-\sigma,\sigma})^* \right), \quad (267)$$

$$Z_{2\sigma''}^\sigma = \frac{A_s^{\sigma m} \mathcal{W}_{s,s_1}^{m,\sigma''} - A_s^{\sigma m} (\mathcal{W}_{s+2\sigma'',s_1}^{m+\sigma,-\sigma''})^*}{J[\sigma''(2s+1)+2]}, \quad (268)$$

$$\begin{aligned} Z_{2\sigma''}^{\sigma+\sigma'} &= \frac{1}{\sigma'\gamma B + J[\sigma''(2s+1)+2]} \\ &\times \left(A_s^{\sigma(m+\sigma')} \mathcal{X}_{s,s_1}^{m,\sigma',\sigma''} \right. \\ &\quad \left. - A_s^{\sigma m} (\mathcal{X}_{s+2\sigma'',s_1}^{m+\sigma+\sigma',-\sigma',-\sigma''})^* \right), \quad (269) \end{aligned}$$

$$Z_{2\sigma''}^{\sigma+2\sigma'} = \frac{1}{2\sigma'\gamma B + J[\sigma''(2s+1)+2]}$$

$$\begin{aligned} &\times \left(A_{s+2\sigma''}^{\sigma(m+2\sigma')} \mathcal{Y}_{s,s_1}^{m,\sigma',\sigma''} \right. \\ &\quad \left. - A_s^{\sigma m} (\mathcal{Y}_{s+2\sigma'',s_1}^{m+\sigma+2\sigma',-\sigma',-\sigma''})^* \right), \quad (270) \end{aligned}$$

leading to

$$\begin{aligned} |Z_0^{\sigma+\sigma'}|^2 &= \frac{J^2}{(2\gamma B)^2} \left(A_s^{\sigma(m+\sigma')} (2m+\sigma') A_s^{\sigma' m} \right. \\ &\quad \left. - A_s^{\sigma m} (2m+2\sigma+\sigma') A_s^{\sigma'(m+\sigma)} \right)^2 \\ &\times \left(f_1^{(2)}(\theta,\phi) + 2\alpha_{s,s_1} f_2^{(2)}(\theta,\phi) \right. \\ &\quad \left. + \alpha_{s,s_1}^2 f_3^{(2)}(\theta,\phi) \right), \quad (271) \end{aligned}$$

$$\begin{aligned} |Z_0^{-\sigma}|^2 &= \frac{J^2(2m-\sigma)^2 (A_s^{\sigma m-1})^2}{(4\gamma B)^2} \left(f_4^{(2)}(\theta,\phi) \right. \\ &\quad \left. + 2\alpha_{s,s_1} f_5^{(2)}(\theta,\phi) + \alpha_{s,s_1}^2 f_6^{(2)}(\theta,\phi) \right), \quad (272) \end{aligned}$$

$$\begin{aligned} |Z_{2\sigma''}^\sigma|^2 &= \frac{f_7^{(2)}(\theta,\phi)}{16[\sigma''(2s+1)+2]^2} \\ &\times \left(\sum_{\bar{\sigma}=\pm 1} \bar{\sigma} A_{s+\sigma''(1+\bar{\sigma})}^{\sigma m} H_{s,s_1}^{m+\sigma(1-\bar{\sigma})/2,\sigma''} \right)^2, \quad (273) \end{aligned}$$

$$\begin{aligned} |Z_{2\sigma''}^{\sigma+\sigma'}|^2 &= \frac{J^2 f_3^{(2)}(\theta,\phi)}{16(\sigma'\gamma B + J[\sigma''(2s+1)+2])^2} \\ &\times \left(\sum_{\bar{\sigma}=\pm 1} \bar{\sigma} A_{s+\sigma''(1+\bar{\sigma})}^{\sigma m+\sigma\sigma'(1+\bar{\sigma})/2} R_{s,s_1}^{m+\sigma(1-\bar{\sigma})/2,\sigma',\sigma''} \right)^2, \quad (274) \end{aligned}$$

$$\begin{aligned} |Z_{2\sigma''}^{\sigma+2\sigma'}|^2 &= \frac{J^2 f_6^{(2)}(\theta,\phi)}{64(2\sigma'\gamma B + J[\sigma''(2s+1)+2])^2} \\ &\times \left(\sum_{\bar{\sigma}=\pm 1} \bar{\sigma} A_{s+\sigma''(1+\bar{\sigma})}^{\sigma m+\sigma\sigma'(1+\bar{\sigma})} K_{s,s_1}^{\sigma' m+\sigma\sigma'(1-\bar{\sigma})/2,\sigma''} \right)^2, \quad (275) \end{aligned}$$

where $E_{s,s_1}^m = E_{s,s_1}^{m,(0)} + E_{s,s_1}^{m,(1)}$ is given by Eqs. (70) and (71), A_s^m , F_{s,s_1}^x , $H_{s,s_1}^{m,\sigma'}$, $K_{s,s_1}^{x,\sigma'}$, α_{s,s_1} , and $R_{s,s_1}^{m,\sigma,\sigma'}$ are given by Eqs. (1), (17), (26), (27), (29), and (170), respectively, the $f_n^{(2)}(\theta,\phi)$ are given in Eqs. (216)-(222), and we have used the relations following Eq. (242). We note that since $\sigma = \pm 1$ for clockwise and counterclockwise oscillatory induction senses, setting $\sigma', \sigma'' = \pm 1$ is equivalent to setting them equal to $\pm\sigma$.

For the three cases with $m' = m$, there are no associated resonant magnetic inductions, and since the EPR frequency ω cannot be easily varied in an experiment, these terms are irrelevant. For the 10 remaining cases with $m' \neq m$, the resonant magnetic induction is then

found to have the form given by Eq. (92). The term with amplitude $Z_0^{2\sigma}$ has $a_1 = 1/2$, $b_1 = 2(m + \sigma)$, and $c_1 = 0$. The term with amplitude $Z_0^{-\sigma}$ has $a_2 = 1$, $b_2 = (2m - \sigma)/2$, and $c_2 = 0$. The two terms with amplitudes $Z_{2\sigma''}^\sigma$, where $\sigma'' = \pm\sigma$ have $a_3 = 1$, $b_3 = \sigma[2 + \sigma''(2s + 1)]$, and $c_3 = -(2m + \sigma)/2$. The two terms with amplitudes $Z_{2\sigma''}^{2\sigma}$, where $\sigma'' = \pm\sigma$, have $a_4 = 2$, $b_4 = 2\sigma[2 + \sigma''(2s + 1)]$, and $c_4 = 4(m + \sigma)$. The four terms with amplitudes $Z_{2\sigma''}^{\sigma+2\sigma'}$, where $\sigma', \sigma'' = \pm\sigma$, have $a_5 = 1/(1 + 2\sigma\sigma')$, $b_5 = [2 + \sigma''(2s + 1)]/(\sigma + 2\sigma')$, and $c_5 = m + \sigma' + \sigma/2$.

APPENDIX D

Second order induction representation Hamiltonian

In this appendix, we evaluate the corrections to the eigenstate energies second order in the four anisotropy interaction energies J_j for $j = a, b, d, e$. The operations of the rotated Hamiltonian \mathcal{H}' upon the eigenstates $|\varphi_s^m\rangle$ may be written as

$$\begin{aligned} \mathcal{H}'|\varphi_s^m\rangle &= (E_s^{m,(0)} + E_{s,s_1}^{m,(1)})|\varphi_s^m\rangle + \sum_{\sigma'=\pm 1} \mathcal{W}_{s,s_1}^{m,\sigma'}|\varphi_{s+2\sigma'}^m\rangle \\ &+ \sum_{\sigma=\pm 1} \left(\mathcal{U}_{s,s_1}^{m,\sigma}|\varphi_s^{m+\sigma}\rangle + \mathcal{V}_{s,s_1}^{m,\sigma}|\varphi_s^{m+2\sigma}\rangle \right) \\ &+ \sum_{\sigma,\sigma'=\pm 1} \left(\mathcal{X}_{s,s_1}^{m,\sigma,\sigma'}|\varphi_{s+2\sigma'}^{m+\sigma}\rangle \right. \\ &\quad \left. + \mathcal{Y}_{s,s_1}^{m,\sigma,\sigma'}|\varphi_{s+2\sigma'}^{m+2\sigma}\rangle \right), \end{aligned} \quad (276)$$

where $E_{s,s_1}^{m,(0)}$ and $E_{s,s_1}^{m,(1)}$ are given by Eqs. (70) and (71), respectively, and the \mathcal{U} to \mathcal{Y} functions are given by Eqs. (175) to (179), respectively.

Second order eigenstate energies

From Eq. (276), the second order eigenstate energies may be written as

$$\begin{aligned} E_{s,s_1}^{m,(2)} &= \frac{1}{\gamma B} \sum_{\sigma=\pm 1} \sigma \left(|\mathcal{U}_{s,s_1}^{m,\sigma}|^2 + \frac{1}{2} |\mathcal{V}_{s,s_1}^{m,\sigma}|^2 \right) \\ &+ \sum_{\sigma'=\pm 1} \frac{|\mathcal{W}_{s,s_1}^{m,\sigma'}|^2}{J[2 + (2s + 1)\sigma']} \\ &+ \sum_{\sigma,\sigma'=\pm 1} \left(\frac{|\mathcal{X}_{s,s_1}^{m,\sigma,\sigma'}|^2}{J[2 + (2s + 1)\sigma'] + \sigma\gamma B} \right. \\ &\quad \left. + \frac{|\mathcal{Y}_{s,s_1}^{m,\sigma,\sigma'}|^2}{J[2 + (2s + 1)\sigma'] + 2\sigma\gamma B} \right). \end{aligned} \quad (277)$$

For simplicity, we rewrite this as

$$\begin{aligned} E_{s,s_1}^{m,(2)} &= E_{s,s_1}^{m,(2)\mathcal{U}} + E_{s,s_1}^{m,(2)\mathcal{V}} + E_{s,s_1}^{m,(2)\mathcal{W}} \\ &\quad + E_{s,s_1}^{m,(2)\mathcal{X}} + E_{s,s_1}^{m,(2)\mathcal{Y}}, \end{aligned} \quad (278)$$

$$\begin{aligned} E_{s,s_1}^{m,(2)\mathcal{U}} &= \frac{m \sin^2 \theta}{2\gamma B} [4s(s + 1) - 8m^2 - 1] \\ &\quad \times \left(\cos^2 \theta [\tilde{J}_{b,a}^{s,s_1} - \cos(2\phi) \tilde{J}_{d,e}^{s,s_1}]^2 \right. \\ &\quad \left. + \sin^2(2\phi) (\tilde{J}_{d,e}^{s,s_1})^2 \right), \end{aligned} \quad (279)$$

$$\begin{aligned} E_{s,s_1}^{m,(2)\mathcal{V}} &= -\frac{m}{8\gamma B} [2s(s + 1) - 2m^2 - 1] \\ &\quad \times \left([\sin^2 \theta \tilde{J}_{b,a}^{s,s_1} + (1 + \cos^2 \theta) \cos(2\phi) \tilde{J}_{d,e}^{s,s_1}]^2 \right. \\ &\quad \left. + 4 \cos^2 \theta \sin^2(2\phi) (\tilde{J}_{d,e}^{s,s_1})^2 \right), \end{aligned} \quad (280)$$

$$\begin{aligned} E_{s,s_1}^{m,(2)\mathcal{W}} &= \frac{d_{s,s_1}^m}{16J} \left(J_a - 3[J_a \cos^2 \theta + J_e \sin^2 \theta \cos(2\phi)] \right)^2, \end{aligned} \quad (281)$$

$$\begin{aligned} E_{s,s_1}^{m,(2)\mathcal{X}} &= \frac{f_{s,s_1}^m(\gamma B/J) \sin^2 \theta}{2J} \\ &\quad \times \left([J_a - J_e \cos(2\phi)]^2 \cos^2 \theta \right. \\ &\quad \left. + \sin^2(2\phi) J_e^2 \right), \end{aligned} \quad (282)$$

$$\begin{aligned} E_{s,s_1}^{m,(2)\mathcal{Y}} &= \frac{g_{s,s_1}^m(\gamma B/J)}{64J} \left[\left(J_a \sin^2 \theta \right. \right. \\ &\quad \left. \left. + J_e (1 + \cos^2 \theta) \cos(2\phi) \right)^2 \right. \\ &\quad \left. + 4 \cos^2 \theta \sin^2(2\phi) J_e^2 \right], \end{aligned} \quad (283)$$

where

$$\begin{aligned} d_{s,s_1}^m &= -\frac{(s^2 - m^2)[(s - 1)^2 - m^2] \eta_{s,s_1}^2 \eta_{s-1,s_1}^2}{(2s - 1)} \\ &\quad + \eta_{s+2,s_1}^2 \eta_{s+1,s_1}^2 \\ &\quad \times \frac{[(s + 1)^2 - m^2][(s + 2)^2 - m^2]}{(2s + 3)}, \\ f_{s,s_1}^m(x) &= -\frac{\eta_{s,s_1}^2 \eta_{s-1,s_1}^2 (s^2 - m^2)}{(2s - 1)^2 - x^2} \\ &\quad \times \left((2s - 1)[(s - 1)(s - 2) + m^2] \right. \\ &\quad \left. - m(2s - 3)x \right) \\ &\quad + \frac{\eta_{s+2,s_1}^2 \eta_{s+1,s_1}^2 [(s + 1)^2 - m^2]}{(2s + 3)^2 - x^2} \\ &\quad \times \left((2s + 3)[(s + 2)(s + 3) + m^2] \right. \\ &\quad \left. - m(2s + 5)x \right), \end{aligned} \quad (284)$$

$$\begin{aligned} g_{s,s_1}^m(x) &= -\frac{2\eta_{s,s_1}^2 \eta_{s-1,s_1}^2}{(2s - 1)^2 - 4x^2} \left((2s - 1)m^4 \right. \\ &\quad \left. + m^2(6s^2 - 18s + 11) \right. \\ &\quad \left. + s(s - 1)(s - 2)(s - 3) \right) \end{aligned}$$

$$\begin{aligned}
& -4mx(2s-3)(s^2-3s+1+m^2) \Big) \quad (285) \\
& + \frac{2\eta_{s+2,s_1}^2 \eta_{s+1,s_1}^2}{(2s+3)^2 - 4x^2} \left((2s+3)[m^4 \right. \\
& + m^2(6s^2+30s+35) \\
& + (s+1)(s+2)(s+3)(s+4)] \\
& \left. -4mx(2s+5)(s^2+5s+5+m^2) \right). \quad (286)
\end{aligned}$$

There is a remarkable amount of symmetry in the angular dependence of the eigenstate energies. We note that $E_{s,s_1}^{m,(2)\mathcal{X}}(\theta, \phi)$ and $E_{s,s_1}^{m,(2)\mathcal{U}}(\theta, \phi)$ have the same forms, differing in the replacements of the interactions $\tilde{J}_{b,a}^{s,s_1}$ and $\tilde{J}_{d,e}^{s,s_1}$ with J_a and J_e , respectively, and with different overall constant functions. The same comparison can also be made with $E_{s,s_1}^{m,(2)\mathcal{Y}}(\theta, \phi)$ and $E_{s,s_1}^{m,(2)\mathcal{V}}(\theta, \phi)$. In addition, we note that there is a remarkable similarity in the θ, ϕ dependence of $E_{s,s_1}^{m,(2)\mathcal{W}}$ with that of the local spin anisotropy part of $B_{s,s_1}^{lc(1)}(\theta, \phi)$ given by Eq. (94).

The contributions to the s th level crossing second order in the anisotropy interactions are calculated as indicated in Eq. (96), and are found to be

$$\left(E_{s,s_1}^{s,(2)} - E_{s-1,s_1}^{s-1,(2)} \right) \Big|_{B=-J_s/\gamma} = J \sum_{n=1}^7 a_n(s, s_1) f_n^{(2)}(\theta, \phi), \quad (287)$$

where the $f_n^{(2)}$ are given by Eqs. (216)-(222), respectively.

Second order level crossing coefficients

The coefficients are given by

$$a_1(s, s_1) = \frac{(9 - 20s + 12s^2)}{2s}, \quad (288)$$

$$a_2(s, s_1) = \frac{[a_{2,0}(s) + 4s_1(s_1 + 1)a_{2,1}(s)]}{s(2s + 1)(2s + 3)}, \quad (289)$$

$$a_{2,0}(s) = 3(9 + s - 23s^2 + 4s^3 + 12s^4), \quad (290)$$

$$a_{2,1}(s) = 9 - 8s - 4s^2, \quad (290)$$

$$a_3(s, s_1) = a_3^{\mathcal{U}}(s, s_1) + a_3^{\mathcal{X}}(s, s_1), \quad (291)$$

$$\begin{aligned}
a_3^{\mathcal{U}}(s, s_1) &= \frac{[3 - 3s - 3s^2 + 4s_1(s_1 + 1)]^2}{2(2s + 3)^2} \\
&\quad - \frac{(s-1)[3 + 3s - 3s^2 + 4s_1(s_1 + 1)]^2}{2s(2s + 1)^2}, \quad (292)
\end{aligned}$$

$$\begin{aligned}
a_3^{\mathcal{X}}(s, s_1) &= \frac{[s(s+2) - 4s_1(s_1+1)]}{2(s+1)(s+3)(2s+1)^2(2s+3)^2} \\
&\quad \times \frac{a_{3,0}^{\mathcal{X}}(s) + 4s_1(s_1+1)a_{3,1}^{\mathcal{X}}(s)}{(2s+5)(3s+1)},
\end{aligned}$$

$$a_{3,0}^{\mathcal{X}}(s) = (s+1)(s+3)(51 + 114s$$

$$+ 209s^2 + 302s^3 + 164s^4 + 24s^5), \quad (293)$$

$$\begin{aligned}
a_{3,1}^{\mathcal{X}}(s) &= 129 + 318s + 395s^2 \\
&\quad + 442s^3 + 300s^4 + 72s^5,
\end{aligned}$$

$$a_4(s, s_1) = \frac{(4s-3)}{8s}, \quad (294)$$

$$a_5(s, s_1) = -\frac{3[a_{5,0}(s) + 4s_1(s_1 + 1)]}{4s(2s + 1)(2s + 3)}, \quad (295)$$

$$a_{5,0}(s) = 3 + 3s - 5s^2 - 4s^3, \quad (296)$$

$$a_6(s, s_1) = a_6^{\mathcal{Y}}(s, s_1) + a_6^{\mathcal{V}}(s, s_1), \quad (297)$$

$$\begin{aligned}
a_6^{\mathcal{Y}}(s, s_1) &= \frac{[3 - 3s - 3s^2 + 4s_1(s_1 + 1)]^2}{8(2s - 1)(2s + 3)^2} \\
&\quad - \frac{(s-1)[3 + 3s - 3s^2 + 4s_1(s_1 + 1)]^2}{8s(2s - 3)(2s + 1)^2}, \quad (298)
\end{aligned}$$

$$\begin{aligned}
a_6^{\mathcal{V}}(s, s_1) &= \frac{1}{4(2s-3)(2s-1)(2s+1)^2(2s+3)^2} \\
&\quad \times \frac{\sum_{n=0}^2 a_{6,n}^{\mathcal{V}}(s)[4s_1(s_1+1)]^n}{(2s+5)(4s+1)(4s+3)},
\end{aligned}$$

$$\begin{aligned}
a_{6,0}^{\mathcal{V}}(s) &= s \left(-216 + 837s + 5052s^2 + 3521s^3 \right. \\
&\quad \left. - 12414s^4 - 21876s^5 - 7464s^6 \right. \\
&\quad \left. + 6720s^7 + 5376s^8 + 1024s^9 \right), \quad (299)
\end{aligned}$$

$$\begin{aligned}
a_{6,1}^{\mathcal{V}}(s) &= 3 \left(81 + 102s + 10s^2 \right. \\
&\quad \left. + 196s^3 + 296s^4 + 80s^5 \right), \quad (300)
\end{aligned}$$

$$\begin{aligned}
a_{6,2}^{\mathcal{V}}(s) &= 189 + 258s - 100s^2 + 152s^3 \\
&\quad + 640s^4 + 256s^5, \quad (301)
\end{aligned}$$

$$\begin{aligned}
a_7(s, s_1) &= \frac{[s(s+2) - 4s_1(s_1+1)]}{4(2s+1)^3(2s+3)^3(2s+5)} \\
&\quad \times \left(4s_1(s_1+1)(-1 + 38s + 60s^2 + 24s^3) \right. \\
&\quad \left. + (s+1)(3 + 67s + 94s^2 + 44s^3 + 8s^4) \right). \quad (302)
\end{aligned}$$

By expanding the solutions in the crystal representation to second order in the J_j , we have explicitly checked these expressions for $s_1 = 1/2$, $s = 1$, and for $s_1 = 1$, $s = 1, 2$. We note that for $s_1 = 1/2$, only a_1 and a_4 are non-vanishing.

Two-level thermodynamic coefficients $a_{1,s}$

Here we present the expression for $a_{1,s}$ to $\mathcal{O}(J_j/J)^2$ appearing in Eqs. (39) and (41)-(44) in the text. We have

$$a_{1,s} = s + \sum_{n=1}^6 b_n(s, s_1) f_n^{(2)}(\theta, \phi) + \mathcal{O}(J_j/J)^3, \quad (303)$$

where the $f_n(\theta, \phi)$ are given by Eqs. (216)-(221), and

$$b_1(s, s_1) = \frac{(2s-1)^2}{2s} \Theta(s-1), \quad (304)$$

$$b_2(s, s_1) = \frac{(2s-1)^2}{s} \alpha_{s,s_1} \Theta(s-1), \quad (305)$$

$$b_3(s, s_1) = \frac{(2s-1)^2}{2s} \alpha_{s,s_1}^2 \Theta(s-1) + b_3^{\mathcal{X}}(s, s_1), \quad (306)$$

$$b_3^{\mathcal{X}}(s, s_1) = -\frac{s(27+44s+27s^2+6s^3)}{6(s+1)^2(s+3)^2(2s+3)^2(2s+5)} \\ \times \left([4s_1(s_1+1) - s(s+2)] \right. \\ \left. \times [4s_1(s_1+1) - (s+1)(s+3)] \right), \quad (307)$$

$$b_4(s, s_1) = \frac{(2s-1)}{8s} \Theta(s-1), \quad (308)$$

$$b_5(s, s_1) = \frac{(2s-1)}{4s} \alpha_{s,s_1} \Theta(s-1), \quad (309)$$

$$b_6(s, s_1) = \frac{(2s-1)}{8s} \alpha_{s,s_1}^2 \Theta(s-1) + b_6^{\mathcal{Y}}(s, s_1), \quad (310)$$

$$b_6^{\mathcal{Y}}(s, s_1) = \frac{s(s-1)}{8(4s^2-1)} [(s^2-1-4s_1(s_1+1))] \\ \times [s(s-2) - 4s_1(s_1+1)] \\ - \frac{sb_{6,1}(s)[(s(s+2) - 4s_1(s_1+1))]}{72(2s+1)(2s+3)^2(2s+5)(4s+3)^2} \\ \times [(s+1)(s+3) - 4s_1(s_1+1)], \quad (311)$$

$$b_{6,1}(s) = 369 + 1011s + 1420s^2 + 1076s^3 \\ + 416s^4 + 64s^5, \quad (312)$$

where $\Theta(x) = 1$ for $x \geq 0$, $\Theta(x) = 0$ for $x < 0$ is the Heaviside step function.

* Electronic address: efremov@theory.phy.tu-dresden.de

† Electronic address: klemm@phys.ksu.edu

- [1] R. Sessoli, D. Gatteschi, A. Caneschi, and M. A. Novak, *Nature (London)* **365**, 141 (1993).
- [2] J. R. Friedman, M. P. Sarachik, J. Tejada, and R. Ziolo, *Phys. Rev. Lett.* **76**, 3830 (1996).
- [3] M. N. Leuenberger and D. Loss, *Nature (London)* **410**, 789 (2001).
- [4] W. Wernsdorfer, T. Ohm, C. Sangregorio, R. Sessoli, D. Mailly, and C. Paulsen, *Phys. Rev. Lett.* **82**, 3903 (1999).
- [5] W. Wernsdorfer and R. Sessoli, *Science* **284**, 133 (1999).
- [6] D. Zipse, J. M. North, N. S. Dalal, S. Hill, and R. S. Edwards, *Phys. Rev. B* **68**, 184408 (2003).
- [7] M. Affronte, A. Cornia, A. Lascialfari, F. Borsa, D. Gatteschi, J. Hinderer, M. Horvatić, A. G. M. Jansen, and M.-H. Julien, *Phys. Rev. Lett.* **88**, 167201 (2002).
- [8] O. Waldmann, J. Schülein, R. Koch, P. Müller, I. Bernt, R. W. Saalfrank, H. P. Andres, H. U. Güdel, and P. Al-lenspach, *Inorg. Chem.* **38**, 5879 (1999).
- [9] O. Waldmann, R. Koch, S. Schromm, J. Schülein, P. Müller, I. Bernt, R. W. Saalfrank, F. Hempel, and E. Balthes, *Inorg. Chem.* **40**, 2986 (2001).
- [10] H. Nakano and S. Miyashita, *J. Phys. Chem. Solids* **63**, 1519 (2002).
- [11] D. A. Tennant, S. E. Nagler, A. W. Garrett, T. Barnes, and C. C. Torardi, *Phys. Rev. Lett.* **78**, 4998 (1997).
- [12] H. U. Güdel, *Neutron News* **7**, 24 (1996)
- [13] A. W. Garrett, S. E. Nagler, D. A. Tennant, B. C. Sales, and T. Barnes, *Phys. Rev. Lett.* **79**, 745 (1997).
- [14] D. V. Efremov and R. A. Klemm, *Phys. Rev. B* **66**, 174427 (2002).
- [15] F. Le Gall, F. Fabrizi de Biani, A. Caneschi, P. Cinelli, A. Cornia, A. C. Fabretti, and D. Gatteschi, *Inorg. Chim. Acta* **262**, 123 (1997).
- [16] Y. Shapira, M. T. Liu, S. Foner, R. J. Howard, and W. H. Armstrong, *Phys. Rev. B* **63**, 094422 (2001).
- [17] Y. Shapira, M. T. Liu, S. Foner, C. E. Dubé, and P. J. Bonitatebus, Jr., *Phys. Rev. B* **59**, 1046 (1999).
- [18] K. L. Taft, C. D. Delfs, G. C. Papaefthymiou, S. Foner, D. Gatteschi, and S. J. Lippard, *J. Am. Chem. Soc.* **116**, 823 (1994).
- [19] J. D. Walker and R. Poli, *Inorg. Chem.* **29**, 756 (1990).
- [20] J. A. Bertrand, J. L. Breece, and P. G. Eller, *Inorg. Chem.* **13**, 125 (1974).
- [21] R. Tiron, W. Wernsdorfer, D. Foguet-Albiol, N. Aliaga-Alcalde, and G. Christou, *Phys. Rev. Lett.* **91**, 227203 (2003).
- [22] J. M. North, N. S. Dalal, D. Foguet-Albiol, A. Vinslava, and G. Christou, *Phys. Rev. B* **69**, 174419 (2004).
- [23] O. Waldmann, J. Hassmann, P. Müller, D. Volkmer, U. S. Schubert, and J.-M. Lehn, *Phys. Rev. B* **58**, 3277 (1998).
- [24] J. J. Borrás-Almenar, J. M. Clemente-Juan, E. Coronado, and B. S. Tsukerblat, *Inorg. Chem.* **38**, 6081 (1999).
- [25] D. V. Efremov and R. A. Klemm, *cond-mat/0409168*.
- [26] R. M. White, *Quantum Theory of Magnetism* (McGraw-Hill, New York, 1970), Chapters 1, 5, 8.
- [27] K. Park, M. A. Novotny, N. S. Dalal, S. Hill, and P. A. Rikvold, *Phys. Rev. B* **66**, 144409 (2002).
- [28] R. A. Klemm and J. R. Clem, *Phys. Rev. B* **21**, 1868 (1980); R. A. Klemm, *SIAM J. Appl. Math.* **55**, 986 (1995).
- [29] H. Goldstein, *Classical Mechanics*, (Addison-Wesley, Reading, MA, 1965), p. 109.